CONDITION MONITORING AND FAULT DIAGNOSIS OF ELECTRICAL MOTOR DRIVE SYSTEMS

A THESIS SUBMITTED TO
THE GRADUATE SCHOOL OF NATURAL AND APPLIED SCIENCES
OF
MIDDLE EAST TECHNICAL UNIVERSITY

BY

AYKUT DEMİREL

IN PARTIAL FULFILLMENT OF THE REQUIREMENTS
FOR
THE DEGREE OF MASTER OF SCIENCE
IN
ELECTRICAL AND ELECTRONICS ENGINEERING

SEPTEMBER 2019

Approval of the thesis:

CONDITION MONITORING AND FAULT DIAGNOSIS OF ELECTRICAL MOTOR DRIVE SYSTEMS

submitted by **AYKUT DEMİREL** in partial fulfillment of the requirements for the degree of **Master of Science in Electrical and Electronics Engineering Department, Middle East Technical University** by,

Prof. Dr. Halil Kalıpçılar
Dean, Graduate School of **Natural and Applied Sciences** _____

Prof. Dr. İlkay Ulusoy
Head of Department, **Electrical and Electronics Eng.** _____

Assist. Prof. Dr. Ozan Keysan
Supervisor, **Electrical and Electronics Eng., METU** _____

Examining Committee Members:

Assoc. Prof. Dr. Murat Göl
Electrical and Electronics Eng., METU _____

Assist. Prof. Dr. Ozan Keysan
Electrical and Electronics Eng., METU _____

Assist. Prof. Dr. Emine Bostancı
Electrical and Electronics Eng., METU _____

Prof. Dr. Işık Çadırcı
Electrical and Electronics Eng., Hacettepe University _____

Assist. Prof. Dr. Taner Göktaş
Electrical and Electronics Eng., İnönü University _____

Date: 10.09.2019

I hereby declare that all information in this document has been obtained and presented in accordance with academic rules and ethical conduct. I also declare that, as required by these rules and conduct, I have fully cited and referenced all material and results that are not original to this work.

Name, Surname: Aykut Demirel

Signature:

ABSTRACT

CONDITION MONITORING AND FAULT DIAGNOSIS OF ELECTRICAL MOTOR DRIVE SYSTEMS

Demirel, Aykut
Master of Science, Electrical and Electronics Engineering
Supervisor: Assist. Prof. Dr. Ozan Keysan

September 2019, 108 pages

Increasing utilization of electrical machines results in an increasing demand of high reliability and safety. Especially in mission critical applications, unexpected failures of these machines may bring irrecoverable damages to the systems. Furthermore, such failures may be hazardous to human life in military or aerospace applications. One method to meet the reliability and safety requirement is introducing redundant modules to be used in case of an emergency. However, adding extra modules as substitutes increases overall cost, volume and complexity of the system. A better solution can be monitoring the machine condition continuously or running a test on the machine periodically to predict the failure before it causes a fatal damage to the system or human health. In this thesis, characteristics of possible machine faults are described. Methods for condition monitoring and fault detection are proposed. Different signal processing techniques are analyzed. Theoretical propositions are validated on an experimental test-rig. The results are examined to evaluate the accuracy of the proposed methods and possible further improvements are declared as future work.

Keywords: Permanent Magnet Synchronous Motor, PMSM, Condition Monitoring, Fault Diagnosis, Safety, Reliability, Motor Drive Systems

ÖZ

ELEKTRİK MOTOR SÜRÜCÜ SİSTEMLERİNDE DURUM GÖZLEMLEME VE HATA TANIMLAMA

Demirel, Aykut
Yüksek Lisans, Elektrik ve Elektronik Mühendisliği
Tez Danışmanı: Dr. Öğr. Üyesi Ozan Keysan

Eylül 2019, 108 sayfa

Elektrik makinalarının kullanımında görülen artış, yüksek güvenilirlik isteğini de beraberinde getirmektedir. Özellikle hassas uygulamalarda, beklenmedik anlarda ortaya çıkan hatalar, sisteme telafisi mümkün olmayan hasarlar verebilmektedir. Daha da önemlisi, bu tip hatalar askeri uygulamalar ve uzay uygulamalarında, insan sağlığı açısından da tehlike oluşturabilmektedir. Artan güvenilirlik ihtiyacına bir çözüm olarak; sistemlere, acil ihtiyaç durumunda kullanılmak üzere, yedek üniteler eklemek öne sürülebilir. Fakat sisteme yedek üniteler eklemek, sistemin fiyatını, hacmini ve karmaşıklığını artıracaktır. Bu bakış açısıyla; elektrik makinasının durumunu sürekli olarak gözlemleyerek veya makina üzerinde periyodik testler yaparak, hata durumunu sisteme veya insan sağlığına zarar vermeden önce tahmin etmek daha iyi bir çözüm olacaktır. Bu tezde, olası makina hatalarının karakteristikleri tanımlanarak durum gözlemleme ve hata tespiti için yöntemler önerilmiştir. Farklı işaret işleme teknikleri analiz edilmiştir. Önerilen yöntemler bir test düzeneği üzerinde doğrulanmıştır. Test sonuçları, önerilen metotların başarısının değerlendirilmesi için incelenmiş, tez kapsamı dışında kalacak olası iyileştirme ve geliştirmeler beyan edilmiştir.

Anahtar Kelimeler: Kalıcı Mıknatıslı Senkron Motor, KMSM, Durum Gözlemleme, Hata Tanımlama, Güvenlik, Güvenilirlik, Motor Sürücü Sistemleri

To my beloved family, without whom I could have never come so far…

ACKNOWLEDGEMENTS

I would like to thank my supervisor, Assist. Prof. Dr. Ozan Keysan, for his valuable support and guidance throughout my studies. He led me for performing the necessary work in an organized and efficient way. Thanks to the technical support and the motivation he gave to me, I have completed my thesis successfully. I also would like to thank Assist. Prof. Dr. Taner Göktaş for his valuable support and guidance for the simulations and participating as an examining committee member in my thesis defense.

I would like to thank Aselsan for giving the opportunity to perform the experiments and the simulations at motor test laboratory. I also would like to thank my colleagues at Aselsan for their support throughout my studies. I am very grateful to Ümit Büyükkeleş and Hüseyin Meşe for their help and leadership. I learned much from them since the day we met. I am the person who I am today thanks to the inspiration they have given me in challenging the problems and adding meaning to life, as well as their engineering perspective and skills. I would like to thank our manager, Murat Ertek, for his valuable time and support on the project management. I also would like to thank Erdinç Güneş, Onur Cem Erdoğan, and Okan Arpacık for their help on dealing with the problems I had encountered while building the software. I also thank our technicians for their support on preparing the experimental setup and the test motors.

I would like to thank Seren Oğuz for her support on organizing the thesis and Büşra Timur for her help and support at the defense day. I am also grateful to Mesut Dur for serving fresh fruits while I was studying. Success is the well-balanced mixture of studying hard and enjoying the life. Over the past 9 years of my life, I have met lots of friends who make my life more meaningful and boost my confidence. I would like to thank Oğuzhan Üstündağ, Berk Yaşyerli, Gözde Bulut Dönmez, Burak Dönmez, Ezgi Atçakan Akca, Melih Akca, Furkan Ünlü, Tolga Dağdelen, Jülide Arzu Uluçay,

Melike Bayana, Mustafa Eren Bük, Oğuz Kerem Şengöz and Özge Önceler for enjoying the life together.

As a person for whom the family comes first, I would like to thank my mother and my sister for becoming irreplaceable parts of my life. They have always encouraged me on the way that goes to the success. They have always believed me. They have always loved me the most. Without them, I could have never come so far. I also would like to thank Yeşim Toydaş for making the life easier for me since the day we met and for believing and supporting me while I was struggling to write my thesis.

Dear God, thank you for this beautiful life and forgive me if I do not love it enough.

TABLE OF CONTENTS

LIST OF TABLES

TABLES

LIST OF FIGURES

FIGURES

LIST OF ABBREVIATIONS

ABBREVIATIONS

CM	:	Condition Monitoring
DTFT	:	Discrete-time Fourier Transform
EMF	:	Electro Motive Force
FD	:	Fault Diagnosis
FDB	:	Fault Detection Block
FEA	:	Finite Element Analysis
FEM	:	Finite Element Method
FFT	:	Fast Fourier Transform
FOC	:	Field-oriented Control
IPMSM	:	Interior Permanent Magnet Synchronous Motor
ITSC	:	Inter-turn Short Circuit
MCSA	:	Motor Current Signature Analysis
PM	:	Permanent Magnet
PMSM	:	Permanent Magnet Synchronous Motor
PWM	:	Pulse Width Modulation
RMS	:	Root Mean Square
SMPMSM	:	Surface Mount Permanent Magnet Synchronous Motor
STFT	:	Short-time Fourier Transform
WT	:	Wavelet Transform

LIST OF SYMBOLS

SYMBOLS

f_e	:	fundamental frequency of the phase currents
f_f	:	fault frequency
f_m	:	mechanical frequency
$fi_{eccentricity}$	:	fault indicator for static eccentricity fault
$ft_{eccentricity}$	:	fault threshold for static eccentricity fault
fi_{magnet}	:	fault indicator for demagnetization fault
ft_{magnet}	:	fault threshold for demagnetization fault
$fi_{shortcircuit}$	:	fault indicator for short circuit fault
$ft_{shortcircuit}$	:	fault threshold for short circuit fault
i_a	:	current of phase A
i_{abcf}	:	current vector for the faulty PMSM in ABC reference frame
i_b	:	current of phase B
i_c	:	current of phase C
i_d	:	direct axis current
i_f	:	fault current
i_q	:	quadrature axis current
L_m	:	mutual inductance between phases
pp	:	number of pole pairs
R_f	:	fault resistance

v_a	:	voltage of phase A
v_{abcf}	:	voltage vector for the faulty PMSM in ABC reference frame
v_b	:	voltage of phase B
v_{base}	:	common voltage phasor for the healthy phases
v_c	:	voltage of phase C
v_d	:	direct axis voltage
v_q	:	quadrature axis voltage
w_{rotor}	:	electrical speed in deg/s
w_{max}	:	maximum electrical speed
$w_{average}$	:	average electrical speed
$\lambda_{m,abcf}$	:	permanent magnet flux vector for the faulty PMSM

CHAPTER 1

INTRODUCTION

Electrical machines have been used for decades in power plant systems and industrial applications. Recently they have started to be widely used in medical, military and aerospace applications because of their easy and precise speed and position control.

Increasing in use of electrical machines results in an increasing demand of high reliability and safety.

- Industrial plants cannot tolerate any failure occurred in one of the electrical machines installed. In such plants, the entire system including electrical machines should be periodically checked. These periodic controls bring extra costs and yet some failures might never be anticipated before they happen.
- Another sector in which electrical machines play an important role is renewable energy sector. The generators are placed outside of the cities or off-shores. Any possible failure of the modules in those systems is impossible to know without continuously or periodically checking for it. Periodic maintenance and repair can be supplied by technicians however this could cost much because the plants are hard to reach generally. Therefore, a more intelligent, automatic and detailed condition monitoring is needed.
- Medical, military and aerospace applications are other important areas that use electric motors as actuators making use of their capability of sensitive speed and position control. In such areas, operating conditions are much more coercive therefore demand of high reliability and safety increases further. Especially in mission critical applications, unexpected failures of the electrical machines may bring irrecoverable damages to the systems. Furthermore, such failures may even be hazardous to human life. Systems may not always be

available for periodic maintenance and repair to prevent such unexpected failures.

One method to meet the reliability and safety requirement is introducing redundant modules to be used in case of an emergency. The system can be constructed in a modular way such that it includes one or more redundant modules for each critical part. Although adding extra modules as substitutes can be a proper solution for small systems with low cost components, for more sophisticated systems this method increases overall cost, volume and complexity. Especially for electrical machines, adding redundant machines to the systems almost impossible because not only electrical but also mechanical changes are needed in the systems to replace the faulty machine. To do this replacement automatically, even a more complex mechanism than the actual machine might be needed. This brings maintenance and repair requirement to the substitution mechanism and the reliability level of the whole systems may become even worse. From this point of view, a better solution to increase reliability and safety of an electrical machine can be watching the machine's condition continuously or running a test on the machine periodically to predict the failure before it causes a fatal damage to the system or human health.

Condition monitoring and fault diagnosis of electrical machines, as its name implies, is to check the health status of the machine and diagnose any abnormalities in the operation of the machine. Together with the fact that condition monitoring is applicable to almost any electronic and mechanic device, it has been used for electrical machines for more than 30 years [1]. As different types of machines are constructed and the computational power of the microprocessors grows significantly, condition monitoring and fault diagnosis concepts have remained popular among researchers who wants to apply new techniques on new machines in order to achieve more accurate and reliable diagnosis and classification of faults that may occur in electrical machines.

1.1. The Motivation

The demand for high reliability and safe operation of electrical motors is higher for military applications. Military systems are supposed to operate in mission-critical applications under more coercive conditions. Motor drivers in such systems should have fault detection capabilities to track the health of the motors and warn the users before the system encounters with an emergency.

Figure 1.1. HERKUL-04D Servo Controller

HERKUL-04D, which is shown in Figure 1.1 is a motor driver used in military systems of ASELSAN. It is used in remote controlled weapon and electro-optic tracking systems shown in Figure 1.2. There are total of 3000 systems that uses HERKUL-04D as the servo controller driving 6000 PMSMs. Robustness of these widely-used systems is a necessity and unexpected failures are intolerable.

Figure 1.2. Remote Controlled Weapon System and Electro-optic Tracking System of ASELSAN

The motivation of this thesis is to construct a CM and FD algorithm for PMSMs to increase reliability of the military systems.

- The algorithm will be implemented in the motor control software.
- The focus of the thesis is to build a software that can evaluate the motor signals and decide whether the motor is healthy or faulty. Training data for the healthy motors can be collected in a further study to determine the motor behavior and fault thresholds.
- The users will be informed about the health status of the PMSMs periodically.
- In case of an abnormality, the algorithm will warn the users before the fault create a catastrophic consequence.

By this way, waste of resources and economical cost caused by unplanned shut downs can be avoided. Furthermore, knowing the fault type and severity, root cause of the fault can be determined and necessary precautions can be taken to prevent repetition of the same fault and increase the reliability of the system.

1.2. The Objectives and the Scope of the Thesis

Although there are various faults that can be seen on PMSMs, in the scope of this thesis, stator inter-turn short circuit faults, non-uniform demagnetization of permanent magnets and static rotor eccentricities will be covered as they are the most common

failure types on PMSMs [2]. The application will be on a low power PMSM drive system with field-oriented control fed by a voltage source inverter. The general specifications of the drive system are given in Table 1.1.

Table 1.1. *General Specifications of the Drive System*

Property	*Value*
Servo Controller	HERKUL-04D
Voltage	28-32V
Power	400W
Motor	Surface Mounted PMSM
Control	Voltage Source Inverter
Software	Embedded Code Composer

The objectives of the thesis are:

- To mathematically model the faults that are in the scope of this thesis
- To verify mathematical models by simulations and experiments
- To detect the fault types and severities accurately to give a correct estimation of the health status of the motor
- To build a CM and FD algorithm that achieves the objectives above and
    - Runs real-time and gives online information to the users
    - Uses only built-in sensors of the servo controller and does not need any external source of information
    - and stays in the memory and speed limits of the digital signal processor used in the servo controller.

The thesis is organized and the work is conducted to achieve these objectives. There are six chapters in the thesis:

- The first chapter focuses on the motivation for conducting this research and the scope of the thesis. Objectives and methodology of the thesis are described.

- The second chapter focuses on research carried out so far on CM and FD of PMSMs. Fault types are listed and the FD methods are expressed.
- In the third chapter, PMSM faults are described in detail. Mathematical models of the faulty machines are given. Effects of these faults on the machine variables are explained. Simulations results for each fault are shared.
- The fourth chapter starts with the description of the experimental setup. Technical specifications of test equipment are given. Creation of the artificial faults on the test motors is explained. Experimental results are compared with analytical and simulation results.
- In the fifth chapter, an online CM and FD algorithm is built to detect and categorize the faults. The servo controller detects PMSM faults by using built-in sensors and software without using any external source.
- The work conducted in the thesis is summarized in the sixth chapter. Remarks on the topics are shared. The ideas and the research that are beyond the scope of this thesis are declared as future work.

CHAPTER 2

CONDITION MONITORING AND FAULT DIAGNOSIS OF PMSMS IN THE LITERATURE

Permanent magnet synchronous motors have been increasingly used in industrial, automotive, medical, military and aerospace areas because of their small volume, high power density, precise position and speed control performance and high efficiency [3]–[5]. They are irreplaceable components of robotic and automation systems. Because of their wide usage, researchers have made a significant effort for years to increase reliability of PMSMs and the systems they are used in. Applying condition monitoring and fault diagnosis is the latest and current challenge in PMSM drive systems [2], [3], [6]. In this chapter, faults that may occur in a PMSM are investigated. Condition monitoring techniques for each of these faults are introduced.

2.1. Types of Faults in PMSMs

Faults in PMSMs can be categorized into two main groups as stator related faults and rotor related faults. Stator related faults that are studied by the researchers are stator phase unbalances, inter-turn short circuits, inter-phase short circuits, open circuits and breaking of insulation from the chassis. Rotor related faults are rotor mass unbalances, rotor misalignments, also known as static or dynamic eccentricities, local or uniform demagnetizations of the permanent magnets and bearing failures. Although there are many types of faults, stator short circuit faults, permanent magnet demagnetizations and rotor eccentricity faults are the main interests of this thesis because they are seen more often.

Stator related faults are one of the most common failures in electrical machines. 30-40% of motor faults are stator related faults [2]. The most common type of stator related faults is inter-turn short circuit faults. PMSMs have high power density and

they are high performance motors which are usually driven by inverters. Because of the high switching frequency, high voltage stresses are present on the windings. Especially when the motor is connected to the driver with a long cable, high rate of change of voltages may have negative impacts on the insulation between adjacent conductors. This is one of the reasons why inter-turn short circuits are the most common faults in PMSMs [7]. If such faults are not detected at early stages, the insulation between winding conductors may be damaged further because of high circulating currents and thermal hotspots. Therefore, inter-turn short circuit faults may evolve to phase-to-phase or phase-to-chassis short circuit faults if necessary precautions are not taken.

Another common failure type of PMSMs is local or uniform permanent magnet demagnetizations. A local permanent magnet demagnetization is a failure where one or more permanent magnets placed on the rotor surface are partially or fully demagnetized. Demagnetization can be caused by local heating due to excessive stator current, strong magnetic field opposing the magnet flux due to extremely high negative d-axis current or mechanical stresses [8], [9].

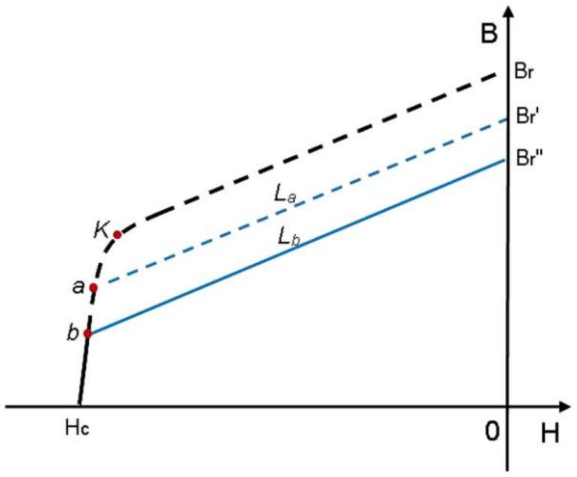

Figure 2.1. B-H Curve of a Permanent Magnet and Recoil Lines [10]

Figure 2.1. shows B-H curve of a permanent magnet and demagnetization lines due to strong external magnetic excitation. If the operating point goes below the knee point K, after the external effect is removed, the permanent magnet cannot reach to its original magnetic flux density. Instead it follows the recoil line L_a. If the external field is strong enough, permanent magnet may be demagnetized irreversibly. This strong external field may be caused by an uncontrolled current or a short circuit [10].

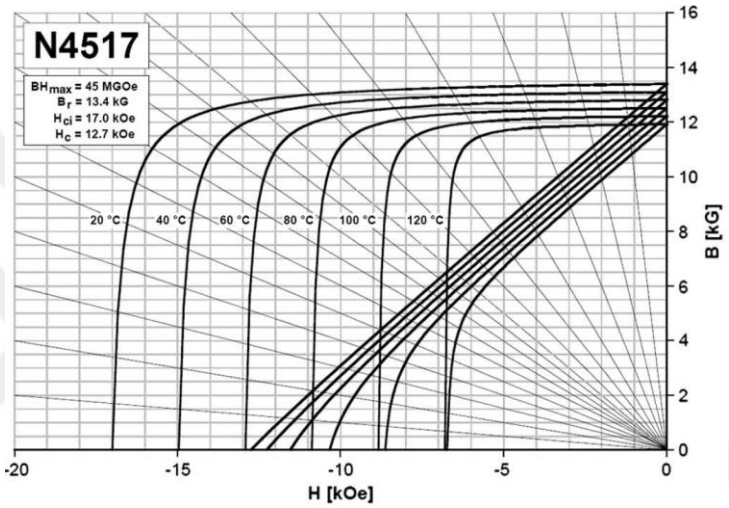

Figure 2.2. Temperature Dependence of B-H Curve of a Permanent Magnet [10]

B-H curve of a permanent magnet changes with the temperature as shown in Figure 2.2. As the temperature rises, the area enclosed by the B-H curve gets smaller. Further increase in the temperature may result in irreversible demagnetization [10].

If demagnetization occurs in a PMSM, the torque output decreases for the same amount of current. In a closed loop system, either machine performance becomes inadequate for the operation or the applied current magnitudes increase to get the same torque performance with the healthy motor. Higher currents mean higher losses and temperature of the motor increases eventually. Increase of the temperature in the motor can cause further demagnetization of the magnets. Sequence of events that starts with

a slight magnet fault and ends up with total failing of PMSM is called as demagnetization catastrophe [11], [12]. Therefore, condition monitoring of permanent magnets to detect any abnormalities is crucial to improve reliability of the PMSM and drive system.

One of the most common mechanical failures in electric motors is eccentricity faults. Once an eccentricity fault occurs in a motor, air-gap flux distribution is disturbed and hence radial forces between rotor and stator grows up causing vibration, noise and possible damage to bearings [13]. Therefore, early detection of eccentricity faults is important to support reliability of the drive system. There are three types of eccentricity faults which are static, dynamic and mixed eccentricity faults. In static eccentricity case, center of rotor is displaced from center of stator but center of rotation is still is the same with center of rotor. Air-gap uniformity is disturbed but it does not change as the rotor rotates. However, in dynamic eccentricity, center of rotor is displaced and it rotates around the center of stator. Air-gap uniformity is disturbed again and it also changes as the rotor rotates. In mixed eccentricity, static and dynamic eccentricities are combined in the same motor. Because of their nature, two eccentricity faults create different signatures on the phase currents and they should be handled separately.

2.2. Condition Monitoring and Fault Diagnosis Techniques

There are number of methods for condition monitoring and fault diagnosis of permanent magnet synchronous motors. Each technique can be considered as a combination of two components.

- The first component is variable to be used for fault diagnosis. This variable is physical measurement that gives the information on the health of the machine. In a survey on condition monitoring and fault diagnosis of wind turbines, it is stated that temperature, vibration, acoustic emission, torque, strain, oil parameters and electrical signals such as phase voltages and currents, air-gap flux density and speed feedbacks are the most commonly used variables for

condition monitoring and fault diagnosis of PMSM drive systems. Each variable has its advantages and disadvantages. Among these variables, those do not need extra sensors on the system are favorable [14]. Phase currents and speed feedbacks are such variables. In a motor drive system, current sensors and position & speed feedback hardware like resolvers and encoders are already installed for commutation. By using those sensors, a valid condition monitoring algorithm can be implemented with no hardware cost on the system. Therefore, motor current signature analysis is the most common technique for condition monitoring and fault diagnosis in literature.

- The second component is feature extraction method. Feature extraction method is the technique that is used to extract necessary information from the first component, i.e., physical measurements. This technique can be in time domain or in frequency domain. Frequency domain signal processing techniques are particularly useful for condition monitoring and fault diagnosis purposes because in rotating machines, mechanical or electrical faults affect the power spectrum of many physical variables the most obvious one of which is phase currents. A brief comparison of signal processing techniques is given [14].

Depending on the fault type, the method which gives the best result to distinguish between healthy and faulty motors can change. For stator and rotor related faults different modeling and simulation techniques may result in different accuracy and computational load. For stator related faults, electrical equivalent circuit approach is generally sufficient to simulate effects of the faults whereas for rotor related faults, which are directly connected with the permanent magnet and air-gap flux density, magnetic equivalent circuit approach gives more accurate results however it brings more computational load than electrical equivalent circuit approach [4]. As in the case that different methods can detect different faults more easily, for one fault different methods can be applied depending on the severity of the fault to get more accurate fault detection. For instance, stator inter-turn short circuit faults can be accurately

detected in early stages using voltage and current residual components [15]; however, the very same method cannot give correct results when a severe short circuit is present in the stator.

Condition monitoring and fault diagnosis techniques applied by the researchers to distinct types of faults are listed and explained in the following sections.

2.2.1. Stator Short Circuit Faults

Small inter-turn short circuit faults may lead to weakening of insulation at some point on the motor. This fault creates damping effect on the rotor and shows itself on currents, torque and speed measurements. A model of internally shorted stator winding can be used to predict behavior of faulty motor by mathematical equations. Fault signatures are searched through power spectrum of phase currents based on mathematical predictions [16].

In [17], stator winding is considered as series of inductances, mutual inductances and resistances in a simplified and efficient model (Figure 2.3). Shorted stator windings are connected to each other in the model and matrix equations are rewritten to show the effect of the fault on electrical parameters of the motor. Torque ripple is taken as a fault indicator and simulation results are verified by experimental measurements [17].

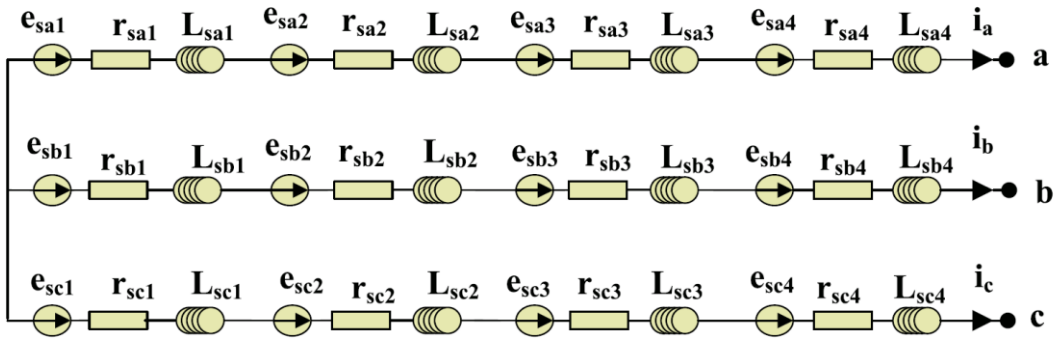

Figure 2.3. Simplified Faulty Model of a Permanent Magnet Synchronous Machine [17]

Motor current signature analysis is the most used technique in stator short circuit fault diagnosis. In [18], authors presented a simple approach for inter-turn fault model. It focuses on stator current harmonics. Harmonic spectrum of the stator currents changes beginning from the 3rd harmonic content in an open loop control system. The paper shows the differences between two models one of which takes the spatial harmonics into consideration while the other does not. The experimental results show that even for a healthy motor, there are even and fractional harmonics in the current spectrum due to inherent rotor misalignments and eccentricities [18].

2D FEM modeling is an especially useful technique to understand a machine's behavior under fault conditions. Theoretical claims can be proven by 2D FEM simulations. In two different research, Air-gap magnetic field and stator currents are inspected as two separate methods. Stator current method is favorable because it does not need additional sensors [18], [19]. PMSM is fed by sinusoidal voltage supply and current frequency pattern for inter-turn short circuit fault is given as in equation (2.1). Frequency pattern of magnetic flux density is given in equation (2.2). K_{cu} is a coefficient introduced by the voltage source and it is equal to unity for sinusoidal voltage supply. K_{sa} is a coefficient which changes with the winding configuration.

$$f_f = f_e \left(K_{cu} \pm \frac{2K_{sa} + 1}{pp} \right) \tag{2.1}$$

$$f_f = f_e \left(K_{cu} \pm \frac{2K_{sa}}{pp} \right) \tag{2.2}$$

In [20], it is claimed that 3rd harmonic content of the phase currents increases in case of inter-turn short circuit fault but this is valid only if motor is supplied by 3 phase balanced voltage source. When a short circuit occurs, phases are not balanced anymore and as they are supplied by balanced voltage source, 3rd harmonic current flows. The effects of SC appear on I_q, I_d and torque output as 2nd harmonic content. They also explain the phenomena behind the fact that ITSC fault behavior changes as number of shorted turns and speed changes. This is because resistance of the shorted turns is dominant in reactance at low speeds while inductance of the shorted turns become

more effective at high speeds. Fault characteristics of a machine highly depend on the machine variables. Interactions between phases are affected by mutual inductances which are determined by winding configuration. Distributed winding machines are more vulnerable to short circuit faults as their mutual inductances are higher because this increases the d-axis current which may cause permanent magnet demagnetizations in case of a short circuit fault. Rotor topology is another important design parameter. When surface mounted PMSMs and interior PMSMs are compared, SMPMSMs have higher phase and short circuit peak currents and higher torque ripple than IPMSMs in fault cases [20].

Depending on the severity of the short circuit fault, it may not be possible to extract correct information from harmonic analysis. In such situations, wavelet transform can be effective. A wavelet is a short period of signal that is used as a basis. The original signal is decomposed into shifted and scaled versions of this basis wavelet. In faulty mode, the total energy of the decompositions changes and this can be used as the indicator [21].

Although MCSA is the mostly used technique in stator short circuit fault analysis, there are other methods which brings less computational load. Analysis of positive, negative and zero sequence current and voltage components is one of these methods. In [22], a novel fault indicator is defined by using negative sequence voltage and current components. [15] and [23] gives a general faulty winding model. This generic model is changed in a way that the new model considers multi-pole structure of the stator windings. Faulty winding model estimates the faulty phase and fault severity by calculating voltage residual component for severe faults and residual component of I_q for early stage faults [15], [23]. Residual component is the difference between the healthy motor data and the measurements taken for faulty cases. Residual component method is generally good for early stages and slightly severe faults. For more severe faults, they cannot provide a good accuracy. Different methods can be combined to obtain a full-range fault detection.

[24] presents a simple model of PMSM with stator inter-turn short circuit fault. A fault indicator whose value is not affected by the rotor speed in slight short circuit faults is defined. Fault indicator is calculated by negative sequence component of phase voltages. Zero sequence and negative sequence component methods are compared and it is proven both analytically and experimentally that the negative sequence method is more accurate when the fault is not severe. Zero sequence component method may not distinguish the fault signal from the measurement noise when leakage inductance is low and the short circuit is not severe [24].

Another method for detecting short circuit faults is to estimate phase resistances. When a short circuit occurs, depending on the severity of the fault, phase resistances decrease. An accurate estimate of the 3 phase resistances is a simple and good fault indicator [25].

Linear and non-linear magnetic equivalent circuit models reflect the behavior of faulty PMSMs best; however, such models bring heavy computational loads. Therefore, these methods are used for offline evaluations rather than online fault detection [7], [26].

Being the most common fault type on electrical machines, stator inter-turn short circuit fault has been investigated by researchers. A small portion of studies on the topic is presented in this section in order to give an insight about the problem and the solutions applied so far.

2.2.2. Permanent Magnet Demagnetization Faults

[27] is an overview on demagnetization fault detection. They summarize 17 indexes and compare them from 19 distinct aspects in their study. Some of these indexes are:

- Harmonic spectrum of stator phase currents
- Instantaneous back EMF
- Estimated or measured torque constant
- D-axis flux of PM

- Injected d-axis current at standstill

Each of the indexes have their own advantages and disadvantages. For example, harmonic analysis of phase currents does not need additional sensors and is not affected much by the load change; however, it cannot distinguish between dynamic eccentricity fault and demagnetization fault. Uniform demagnetization faults cannot be detected by this method also. To detect uniform demagnetization, measuring the torque constant is a good method; however, it needs additional torque sensor to measure produced torque. One should know about pros and cons of a fault detection index and choose the most suitable for the application [27].

As in the case of stator short circuit faults, motor current signature analysis is a common technique to detect demagnetization faults in PMSMs. A non-uniform demagnetization is a rotor related fault and creates disturbances on motor associated with mechanical rotating frequency. [28] states that local magnet demagnetization and dynamic eccentricity faults create harmonics in ABC frame stator current waveforms. These two faults can be separated from each other by estimating the permanent magnet flux although they create the same harmonic effect in current spectrum. A rotor magnet is drilled partially to create an artificial fault and verify the theory (Figure 2.4). Measurements through this study are taken when motor is controlled in speed reference mode by vector control algorithm. If the motor is driven in torque or current control mode, those harmonics may not be seen in current signals but in speed or actual torque signals measured by a torque transducer. In a motor drive system that does not include a torque sensor, it is necessary to drive in speed control mode to extract information from current signals [28].

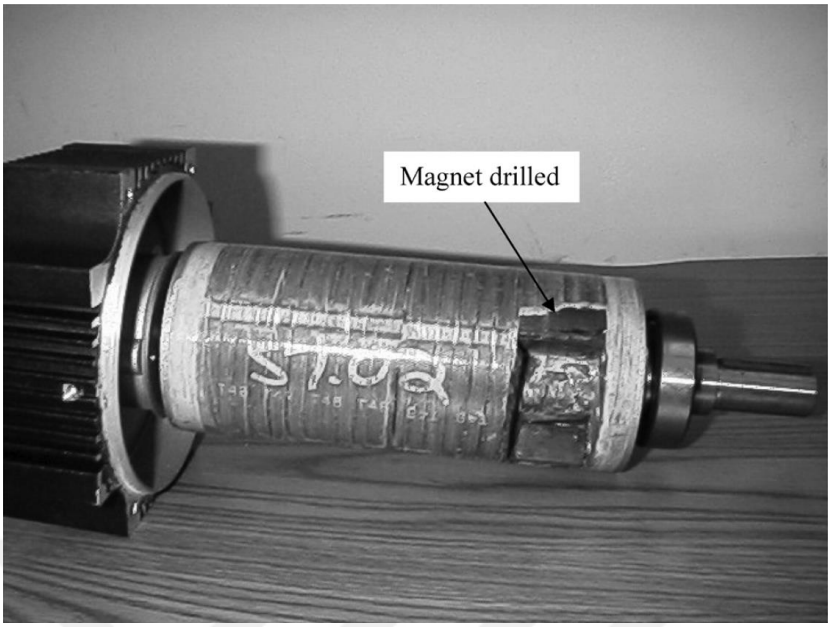

Figure 2.4. A Rotor Magnet Fault Created for Experimental Purposes [28]

Application of wavelet transform on phase currents is another fault diagnosis method. In [3], the authors studied on detection of broken rotor magnet and eccentricity faults using adaptive filtering and wavelet transform. Adaptive filtering removes fundamental component of the phase current from measured signal to eliminate shadow of it on the harmonics by using an estimation and optimization algorithm. Then, wavelet transform does the feature extraction which gives 97% accuracy in detection and classification of faults [3].

Change in the motor inductances is another indicator of demagnetization fault. In [27], direct axis inductance and direct axis differential inductance of the machine are measured by applying d axis current at standstill. Demagnetization index is how much current needed to saturate the core and decrease the direct axis inductance. If demagnetization is present, more d axis current is needed to saturate the core. Proposed method has the disadvantage that an extra inverter is needed. One is for applying direct axis current while other is for measuring the inductance. On the other hand, method can distinguish magnet demagnetization faults from rotor eccentricity

faults. Moreover, as the measurements are taken at standstill, there are no problems related to change in rotor speed and load torque [27].

Harmonic content of stator current at frequencies specified by equation 2.3 are also indicators of demagnetization fault. The amplitude of certain harmonics changes as demagnetization level changes. Frequency analysis should be done under steady-state conditions therefore this method is sensitive to load and speed changes. Uniform demagnetizations cannot be detected by this method because it detects the harmonics induced by the asymmetric structure of the air-gap flux [27].

$$f_f = f_e\left(1 \pm \frac{k}{pp}\right), \qquad k = 1,2,3 \ldots \tag{2.3}$$

In [11], a zero-sequence current based method for delta connected PMSMs is introduced. Magnet flux is estimated from synchronous frame equations utilizing the fact that sum of three phase voltages is zero in a delta connected winding. Phase currents are defined as branch currents therefore extra current sensors inside the motor are needed to implement this method. Research includes only mathematical equations and simulations. When one considers applying this method to a Y connected motor, zero sequence current cannot flow because the neutral point is not connected to ground. When there is an unbalance in the phases, potential voltage of the neutral point changes. In this case, the method may be changed by evaluating zero sequence voltage components instead of current [11].

V_d, V_q and their inverse transforms also have the same harmonics with the measured phase currents in a wide bandwidth controller [13]. The highest frequency content that can be observed in commanded voltages due to the current harmonics is limited by the bandwidth of the controller. Back EMF voltages are not available in an inverter fed PMSM however current feedbacks are always available. Therefore, obtaining the voltage feedbacks from V_q and V_d is a convenient way. In [13], sample and compare method is used. Sample data set is formed by FEA and experimental results are compared with those obtained from FEA and two linear discriminant analysis

classifiers are used to detect the type and severity of the fault. Besides demagnetization, eccentricity and stator short circuit faults are analyzed [13].

[1] used a model-based approach to detect magnet faults. Three phase voltages are generally not available for inverter-fed PMSMs. However, for PMSMs controlled by FOC, commanded V_d and V_q voltages are available for control purposes. Changes in commanded voltages can be tracked to detect several faults including demagnetization, rotor eccentricity and stator short circuit faults. Researchers create a database of machine parameters from FEA simulations of faulty models and estimate V_d and V_q voltages from the machine parameters. Comparisons between the estimated and measured parameters give information about health status of the machine [1].

Flux density of a magnet is a direct measure of demagnetization. [29] analyzed speed harmonics and extracted magnetic flux density by using particle filter estimation. Speed harmonics are created by harmonic current injection. Harmonic current creates torque oscillations causing disturbances in motor speed. These disturbances have a relation with air-gap magnetic flux density [29]. The method needs system inertia information as an input.

[30] used the ripple on produced torque as a fault indicator. Torque measurements are finite, non-periodic and non-stationary signals and continuous wavelet transform is a good signal processing method for such signals. The reference waveform is chosen as a space vector whose real and imaginary parts are original (noisy) torque signal and Hilbert transform of it, respectively. Afterwards, energies stored in each wavelet component are calculated to estimate the rotor demagnetization level [30].

Different methods used for detection of permanent magnet demagnetization fault in PMSMs are mentioned in this section. Methods differ from each other in terms of observed motor variables and feature extraction methods. The most common variable that is observed for fault detection is phase currents while the most common feature extraction method is frequency domain analysis.

2.2.3. Rotor Eccentricity Faults

As in the case of stator short circuit and demagnetization faults, motor current signature analysis is the most common technique for diagnosis of rotor eccentricity faults. [31] presented reference frame approach to detect static and dynamic eccentricity faults on an induction motor. Reference frame theory transforms sinusoidal current components into DC for a given frequency (Figure 2.5). Fault frequencies are calculated and compared with predetermined threshold values. Threshold values are assigned as a function of speed and torque. Dynamic and static eccentricity faults are created artificially on the test motor (Figure 2.6) and proposed method is confirmed experimentally [31].

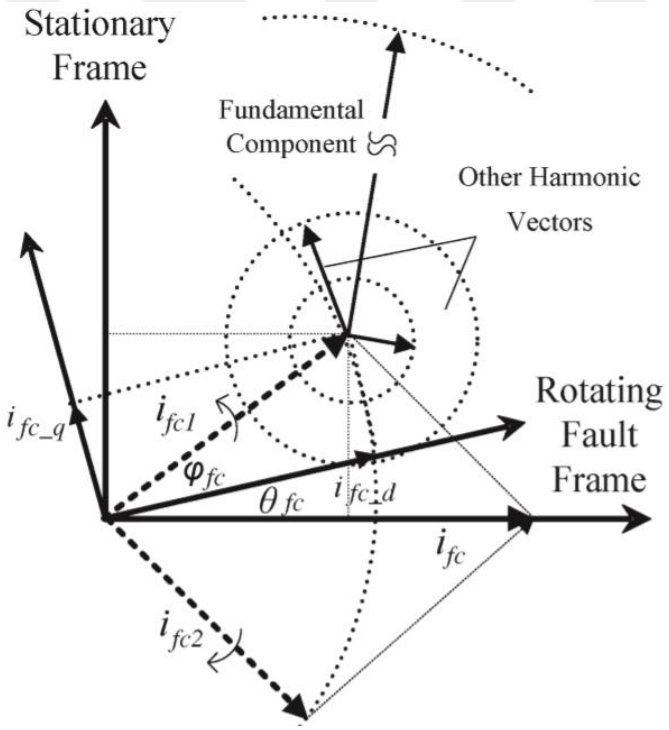

Figure 2.5. Rotating Reference Frame Approach for Eccentricity Fault Detection [31]

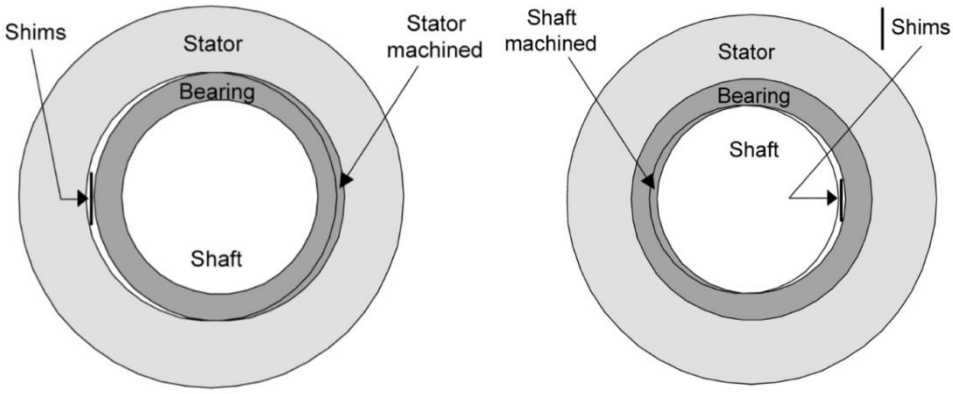

Figure 2.6. Creation of Dynamic and Static Eccentricity Faults [31]

[28] performed classical FFT analysis on motor current signals to show that rotor related faults like eccentricity faults increase the amplitude of frequency component at mechanical rotation frequency and integer multiples of it. Authors use an offline evaluation to see effects of faults on motor current signals instead of building an online fault detection algorithm [28].

[3] used Wavelet transform to extract information on health status of motor. Before application of Wavelet transform, fundamental components of motor current signals are found and extracted from the original signal by using adaptive filtering. Residual signals are transformed and compared with each other. Measurements taken from healthy and faulty motors are used as training data. After training and learning sessions, algorithm successfully detects and classifies 3 distinct types of faults as given in Figure 2.7. The drawbacks of this method are the requirement for training data for each separate motor and lack of information about fault severity [3].

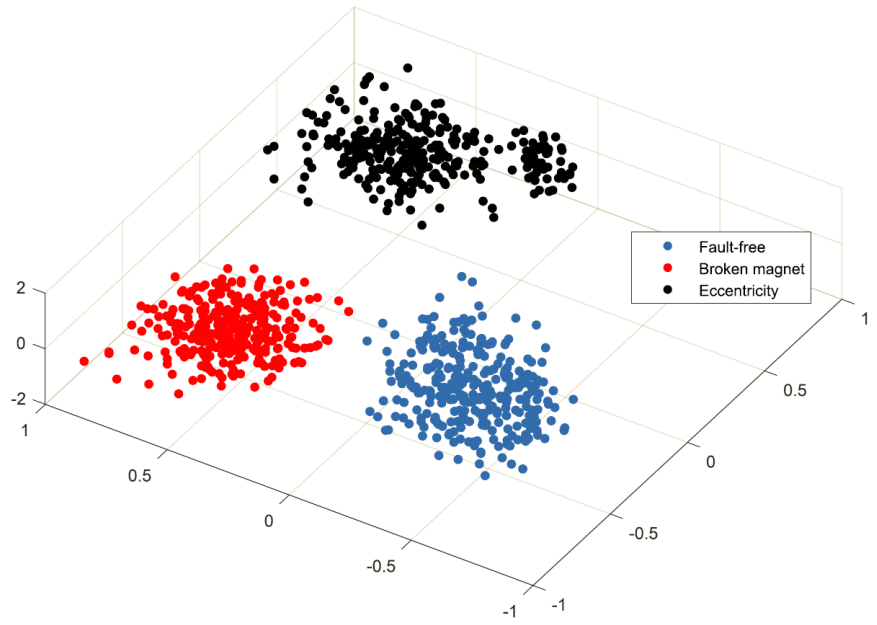

Figure 2.7. Scatter Plot of Training Data for 3 Fault Types [3]

[32] states that although rotor related faults are associated with mechanical rotation frequency, broken magnet and static eccentricity faults differ from each other as they create harmonics at different multiples of mechanical frequency. Broken magnet fault shows itself at once and twice the mechanical frequency while static eccentricity increases amplitude of three times the mechanical frequency [32].

[33] studied on separation of rotor eccentricity faults from partial demagnetization faults. The key feature that creates difference is fluctuation of high frequency d-axis inductance and rotor flux. Mathematical equations are given and simulation results that confirm proposed behavior are shared [33].

Researchers have been studying rotor eccentricity faults since the beginning of application of condition monitoring and fault diagnosis approach to electrical motors and generators. Some of those studies that form a basis to understand eccentricity faults and some that are recently published are presented in this section to give an idea about current situation of research focused on rotor eccentricity faults.

2.3. Feature Extraction Methods

Feature extraction from a real time signal can be realized in different ways each having its advantages and disadvantages.

Bilal et al. uses synchronous frame transformation to get information on the amplitude of a certain frequency in phase currents of an induction machine [31]. It has the advantage that there is no need to a buffer stage and results are updated cycle by cycle. Algorithm does not need extra memory therefore it is suitable for low-cost motor drive systems. However, synchronous frame transformation searches only one frequency at a time. Different faults may yield different harmonics so a proper polling should be done to search every fault frequency in the spectrum. Moreover, if fundamental component of the observed signal is very high, it creates very high oscillations in the resulting waveform that do not attenuate rapidly. The time needed to get exact average value of the selected frequency component may increase and the algorithm may even trigger a false alarm.

[34] explained and compared classical methods like FFT, STFT and WT for feature extraction.

- FFT can be the best choice for stationary signals because of its simplicity. However, for non-stationary signals, STFT and WT are more suitable than FFT because FFT does not have a time resolution, i.e., happening times of events cannot be known [34].
- While using WT, a proper reference function should be chosen to adjust the trade-off between time and frequency resolution. [35] applied WT to stationary frame phase current signals to detect demagnetization faults in PMSMs running under non-stationary conditions. Accuracy in calculation of frequency components in non-stationary signals being the main advantage of it, selecting the reference function, determining appropriate coefficients for the transform and extracting information from raw signals (current, voltage, speed etc.) are challenging parts of WT [35]. Besides, computational load of WT is high

which makes it difficult to implement on a motor driver having a limited memory.

- STFT is also applicable to non-stationary signals while it is easier to implement than WT. STFT can be considered as an optimized version of FFT which has time and frequency resolution at the same time. The signal is windowed before applying Fourier transform. Window length and the sampling frequency determine time and frequency resolutions and computational load. By selecting a proper window length, computational load can be decreased compared to WT while a sufficient frequency resolution is maintained to calculate desired amplitudes of power spectrum. Applying windowing enhance the performance of the STFT by cutting high frequency noise and sidebands caused by DTFT [35].

Although the actual signal of interest can be windowed with any type of function, there are certain types of windowing functions that supply advantages in the spectrum analysis. Hamming, Hanning, Kaiser-Bessel, Blackman-Harris and Rectangular windows are examined and compared. Among these, Hanning window is suitable for smoothing noisy signals including high frequency components. It has high peak and low side-lobes touching zero at both ends of the window eliminating all discontinuity. Windowing helps to discriminate the amplitudes of frequencies that are close each other. It is important especially when frequency resolution is low and the frequencies of interests are close to each other.

Depending on the application and the capabilities of the platform which performs the transformation, a suitable feature extraction method should be chosen to achieve the best solution.

In Chapter 2, most common fault types that are seen on PMSMs are declared and each fault type is described. Reasons behind stator and rotor related faults are given. Condition monitoring and fault diagnosis techniques applied on PMSM drives are introduced. Most informative and most recent research on stator short circuit faults,

permanent magnet demagnetization faults and rotor eccentricity faults are shared. Comparisons between researchers' approach to the topic are made. Advantages and disadvantages of different methods are listed. In the following chapter, analytical basis of condition monitoring and fault diagnosis of stator short circuit, demagnetization and static eccentricity faults will be presented.

CHAPTER 3

ANALYTICAL MODELING AND SIMULATIONS OF PMSM FAULTS

In this study, the faults that are investigated can be listed as:

- Stator inter-turn short circuit faults
- Non-uniform permanent magnet demagnetization faults
- Rotor static eccentricity faults

The effect of failure mode is modeled analytically and simulation results are presented in this chapter. Simulation environment is ANSYS Maxwell (Release 19.2).

Figure 3.1. The Test Motor (400W PMSM)

Table 3.1. *Electrical and Mechanical Parameters of Test Motor*

Property	*Value*
Winding	3-Phase Y-connected
Rated input voltage	18-32 V
Rated phase current	18.67 A_{rms}
Rated torque	1.68 Nm
Rated speed	2300 rpm
Rated power	400 W
Number of pole pair	4
Number of stator slots	27
Torque constant	0.09 Nm/A_{rms}
Back EMF constant	0.073 V_{peak}/(rad/s)
Moment of inertia	0.374 kg.cm2
Stator and rotor length	40 mm
Stator outer diameter	68 mm
Rotor outer diameter	33 mm
Air-gap length	1.8 mm

The test motor is shown in Figure3.1. Electrical and mechanical parameters of the motor are given in Table 3.1. Experiments will be carried out on the same motor. The test motor will run under different speed and load conditions. HERKUL-04D servo controller will be used. The CM and FD algorithm will be implemented on the servo controller.

The motor is first modeled in ANSYS RMxprt using these parameters. Therefore; stator, rotor, slots and permanent magnet geometries are exported from three-dimensional model of the motor to create an exact replica in simulations. Real winding scheme of the motor is also used in RMxprt design.

RMxprt model of the motor is verified by running steady-state analysis. Then, 2D model of the motor is created for healthy case. 2D healthy motor model is modified and simulated for each fault type separately.

3.1. Stator Inter-Turn Short Circuit Faults

3.1.1. Analysis of Stator Inter-turn Short Circuit Faults

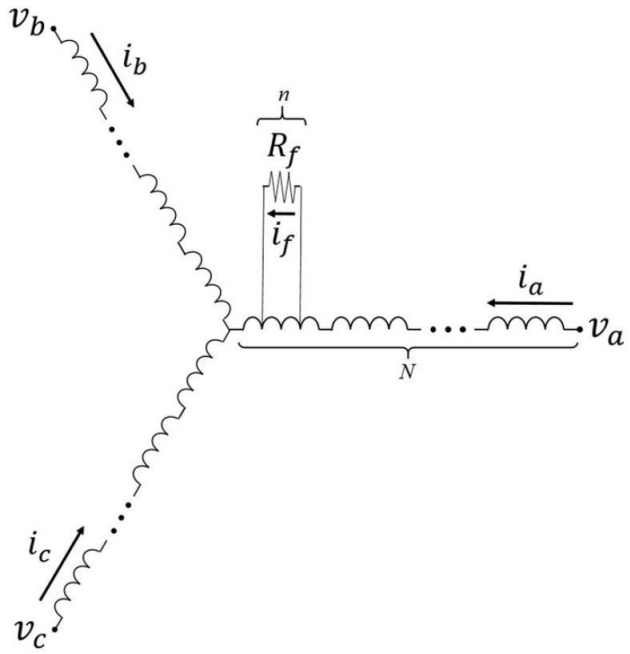

Figure 3.2. Electrical Equivalent Representation of Stator Windings of a PMSM [24]

A simple electrical equivalent representation of stator windings for a Y-connected PMSM with short circuit fault is given in Figure 3.2. In this figure, it is assumed that fault occurred in phase-A without loss of generalization. Stator voltage equation in stationary ABC reference frame can be written in matrix form as:

$$v_{abcf} = Ri_{abcf} + L\frac{d}{dt}i_{abcf} + \frac{d}{dt}\lambda_{m,abcf} \tag{3.1}$$

where;

$$v_{abcf} = \begin{bmatrix} v_a \\ v_b \\ v_c \\ 0 \end{bmatrix}, i_{abcf} = \begin{bmatrix} i_a \\ i_b \\ i_c \\ i_f \end{bmatrix}, \lambda_{m,abcf} = \begin{bmatrix} \lambda_m \cos(\theta) \\ \lambda_m \cos\left(\theta - \frac{2\pi}{3}\right) \\ \lambda_m \cos\left(\theta + \frac{2\pi}{3}\right) \\ u\lambda_m \cos(\theta) \end{bmatrix} \tag{3.2}$$

$$R = \begin{bmatrix} R_s & 0 & 0 & -uR_s \\ 0 & R_s & 0 & 0 \\ 0 & 0 & R_s & 0 \\ uR_s & 0 & 0 & -uR_s - R_f \end{bmatrix} \tag{3.3}$$

$$L = \begin{bmatrix} 2L_m & -L_m & -L_m & -u2L_m \\ -L_m & 2L_m & -L_m & -uL_m \\ -L_m & -L_m & 2L_m & -uL_m \\ u2L_m & -uL_m & -uL_m & -u^2 2L_m \end{bmatrix}, u = \frac{n}{N} \tag{3.4}$$

Phase voltage equations can be written separately to see the effect of the fault on each phase.

$$v_a = R_s i_a + 2L_m \frac{d}{dt} i_a - L_m \frac{d}{dt}(i_b + i_c) + \frac{d}{dt}\lambda_m \cos(\theta) - uR_s i_f - u2L_m \frac{d}{dt} i_f \tag{3.5}$$

$$v_b = R_s i_b + 2L_m \frac{d}{dt} i_b - L_m \frac{d}{dt}(i_a + i_c) + \frac{d}{dt}\lambda_m \cos\left(\theta - \frac{2\pi}{3}\right) - uL_m \frac{d}{dt} i_f \tag{3.6}$$

$$v_c = R_s i_c + 2L_m \frac{d}{dt} i_c - L_m \frac{d}{dt}(i_a + i_b) + \frac{d}{dt}\lambda_m \cos\left(\theta + \frac{2\pi}{3}\right) - uL_m \frac{d}{dt} i_f \tag{3.7}$$

According to phase voltage equations above, faulty motor equations differ from those for a healthy motor by the terms including i_f. It is consistent in a way that when fault is not present i_f is equal to zero and the equations hold for healthy motors. Considering RMS values of phase voltages, equations can be rearranged as:

$$V_{a,RMS} = V_{base,RMS} - uR_s I_{f,RMS} - u2X_m I_{f,RMS} \tag{3.8}$$

$$V_{b,RMS} = V_{base,RMS} - uX_m I_{f,RMS} \tag{3.9}$$

$$V_{c,RMS} = V_{base,RMS} - uX_m I_{f,RMS} \tag{3.10}$$

$V_{base,RMS}$ is the common term for all phases. The difference between RMS voltages of faulty and healthy phases is given by the equation (3.11).

$$V_{f,RMS} - V_{h,RMS} = uI_{f,RMS}\sqrt{(R_s^2 + X_m^2)} \tag{3.11}$$

When an inter-turn short circuit occurs in phase A, change in the RMS voltage of phase A is greater than other two phases. According to equation (3.11), this voltage difference depends on motor speed and fault characteristics.

- As u increases, voltage difference increases directly and indirectly because increase in u leads to increase in induced voltage on faulty turns, which causes more $I_{f,RMS}$ to flow.
- Voltage difference increases with the severity of the fault. If R_f is small, i.e., fault is severe, $I_{f,RMS}$ increases which is positively related with voltage deviation.
- Increase in motor speed also leads to increase in induced voltage on faulty turns, which causes more $I_{f,RMS}$ to flow.

The difference between RMS values of phase voltages is an indicator of stator inter-turn short circuit faults. Faulty phase is the phase for which the deviation from the base value is bigger than others. Moreover, fault severity can be estimated from the amplitude of the deviation given by equation (3.11). However, the effect of motor speed on fault signal should be eliminated for a proper fault diagnosis.

3.1.2. Electromagnetic Simulations

PMSM is modeled in RMxprt using 3D motor model of the motor and the parameters given in Table 3.1. Then, this model is imported to Maxwell 2D design tool. An overall look of the resulting design is given in Figure 3.3.

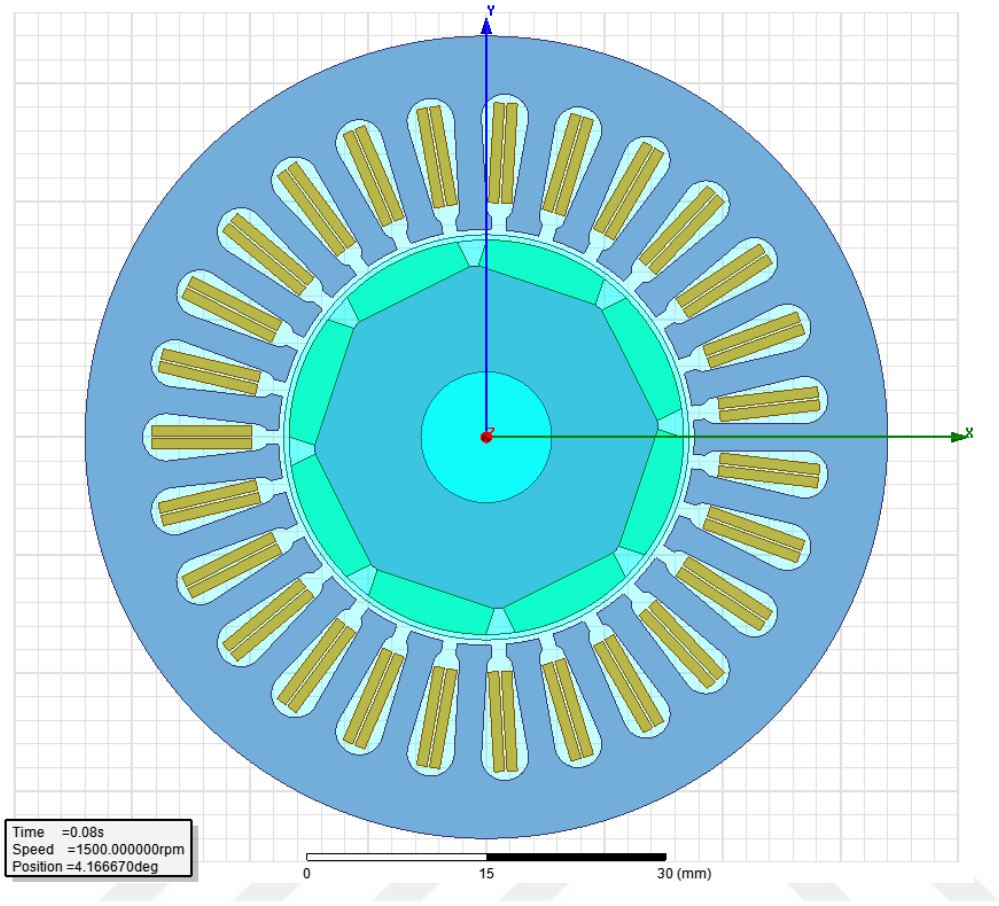

Figure 3.3. PMSM Model in Maxwell 2D Design

The healthy motor is simulated in Maxwell. Winding diagram of the healthy motor is given in the left side of Figure 3.4.a. To create a short circuit, winding between 11T and 14B is removed and it is directly connected to 11B. Faulty winding can be inspected in the right side of Figure 3.4.b.

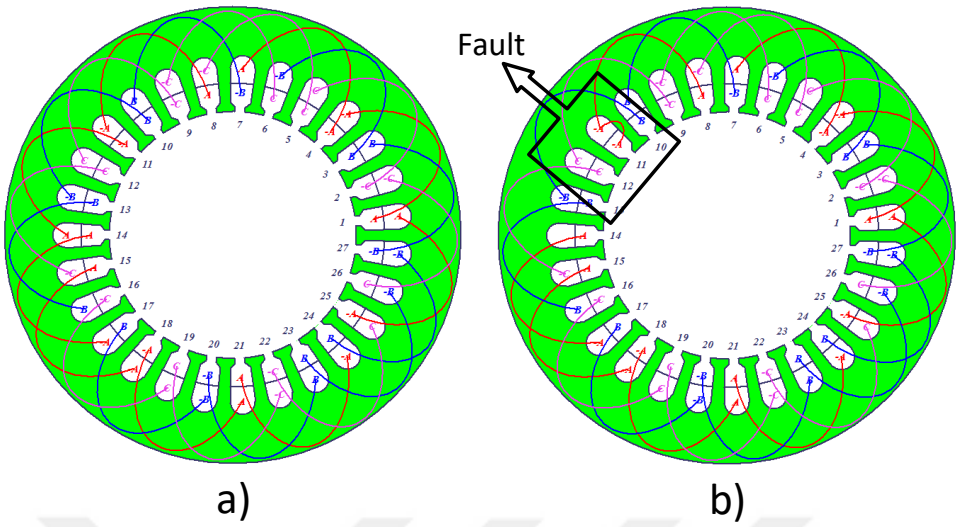

Figure 3.4. Healthy (a) and Faulty (b) Windings in 2D Model

Transient analysis is performed on both healthy and faulty motors which are running at 1500 rpm and loaded at nominal torque. The first observation is that the balance between flux linkages of the phases is disturbed because of the ideal short circuit fault created on phase A. Flux linkages of healthy and faulty motors are shown in Figure 3.5.

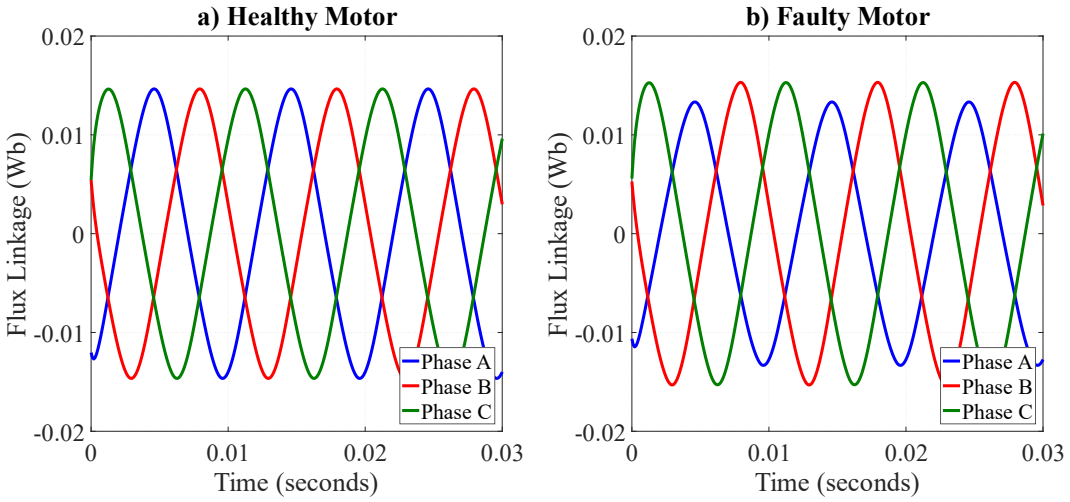

Figure 3.5. Flux Linkages of Stator Windings of PMSMs, a) Healthy Motor, b) Faulty Motor

Short circuit fault creates disturbances on electromechanical variables such as produced torque and motor speed in a non-ideal environment. Since the motor speed is set to 1500 rpm in simulations, the effect of short circuit can only be seen on the produced torque. Torque output of healthy and faulty motors are given in Figure 3.6.

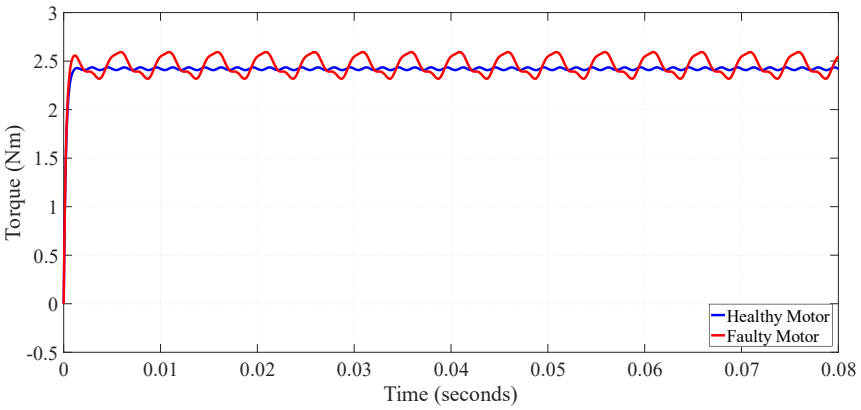

Figure 3.6. Electromagnetic Torque Produced by Healthy and Faulty PMSMs

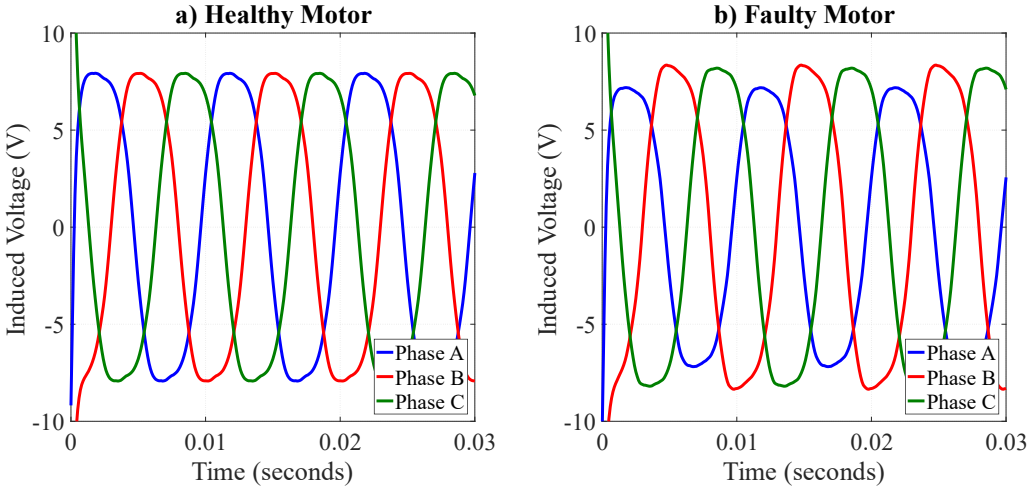

Figure 3.7. Induced Phase Voltages of PMSMs, a) Healthy Motor, b) Faulty Motor

According to equations 3.8, 3.9 and 3.10, induced phase voltages should show the same characteristics with the flux linkages. Peak or RMS value of induced voltage on

phase A is expected to be smaller than those of phase B and C. Simulations verify the expectations. Induced voltages on three phases of healthy and faulty motors are given in Figure 3.7. Three phase balance of the motor is disturbed. Therefore, the effect of the short circuit fault can be seen on V_q as second harmonic. Amplitude spectrum of V_q for healthy and faulty PMSMs are shown in Figure 3.8. In the figure, f_e is 100 Hz. The harmonic at 600 Hz is caused by voltage source inverter and PWM switching. The fault frequency is 200 Hz.

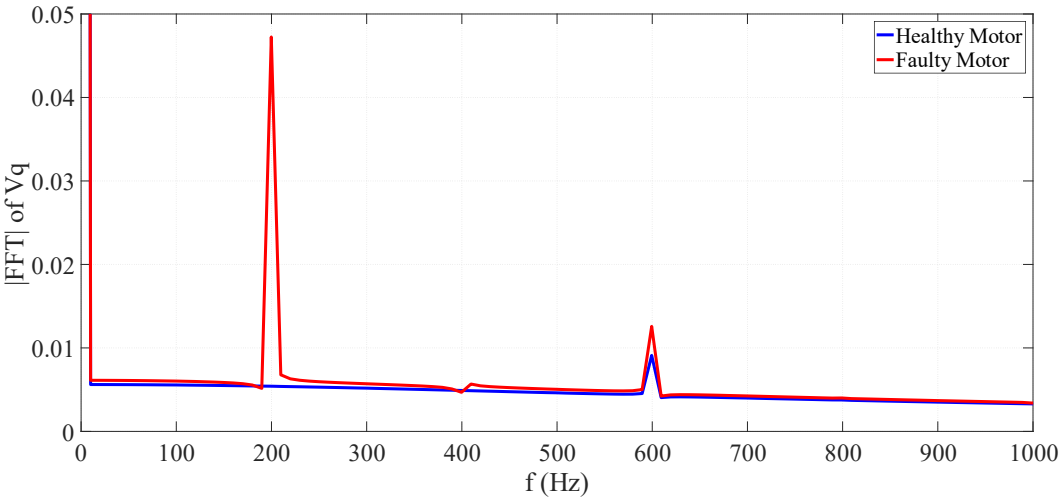

Figure 3.8. Amplitude Spectrum of V_q at The Second Harmonic (200 Hz), 1500 rpm, 2.5 Nm

It is clearly seen from Figure 3.7 that the faulty phase voltage decreases by a certain amount verifying the equation 3.11. The difference between peak or RMS values of phase voltages can be a measure of stator inter-turn short circuit faults as expected from mathematical expressions given in the previous section.

3.1.3. Remarks

Mathematical modelling and simulation results for stator inter-turn short circuit faults are presented in this section. The difference between peak or RMS values of the induced phase voltages is the signature of the short circuit fault. For the fault detection,

RMS values of the phase voltages will be calculated and compared with their average value. If a phase voltage deviates from the average value more than a pre-determined threshold value, the fault alarm is set.

Although the simulation was performed for ideal short circuit case only, it showed the effect of the fault on the phase voltages clearly. Short circuit fault current could not be measured in simulations but these fault currents are never available for real fault scenarios also.

Detecting short circuit faults by looking at phase voltages has some advantages and disadvantages. It has the advantages that:

- It is easy to implement on a motor drive. Even though the phase voltage measurements are not available in a drive, they can easily be obtained by transforming V_d and V_q voltages. Therefore, it does not need extra sensors.
- Calculation of peak or RMS value of a signal is much easier than performing a spectrum analysis. Therefore, this method does not need a high-performance processor and can be implemented on most of the micro-controllers. Although RMS calculation is more vulnerable to speed and load changes and may trigger a false alarm during transients, it performs well in the steady state.
- Besides the type and presence of the fault, fault severity can also be estimated from the voltage differences. The bigger the voltage difference in a phase is, the more severe the short circuit fault is.

It has the disadvantages that:

- The source of the fault severity cannot be detected. Number of faulty turns and fault resistance affects the voltage difference in the same way therefore the user does not know the exact source and location of the fault. However, the exact information on the fault may not be necessary for the most cases. The user should be informed about the presence of the fault and its severity to decide whether to continue or stop the operation.

- The fault indicator gives correct results only in steady state operation of the motor. Evaluation on transient regions may trigger false alarms. As long as the condition monitoring and fault diagnosis algorithm is aware of this fact, decisions can be made in steady state operation to overcome this disadvantage.

3.2. Permanent Magnet Demagnetization Faults

3.2.1. Analysis of Non-uniform Demagnetization Faults

Whether it is caused by missing a piece of magnet or excessive heat that causes a structural demagnetization, in a permanent magnet demagnetization fault, spatial flux distribution of air gap is disturbed. Fundamental magnetic flux density through the air-gap for healthy and faulty motors are shown in Figure 3.9. Due to a non-uniform magnet defect in one pole, flux density decreases in that area, which is represented by green line in the figure. Resultant magnetic flux density function is given by equation (3.12) where K_{dem} is the distortion factor representing fault severity [36].

$$B(\theta) = B_f cos(pp * \theta) + K_{dem} \sum_{k=1}^{\infty} \sin(\frac{\pi k}{2pp}) cos\left(\theta(1 \pm \frac{k}{pp})\right) \quad (3.12)$$

Disturbance of magnetic flux is not expected to bring new spectral content on phase currents because relative permeability of the magnets is almost equal to unity and phase inductances do not change. Instead, because of the step change in flux density at the fault location, frequency components at the rotating frequency and its integer multiples increase for all three phase currents [28]. Therefore, by using equations (3.1) and (3.12), fault frequencies on phase currents can be represented by equation (3.13).

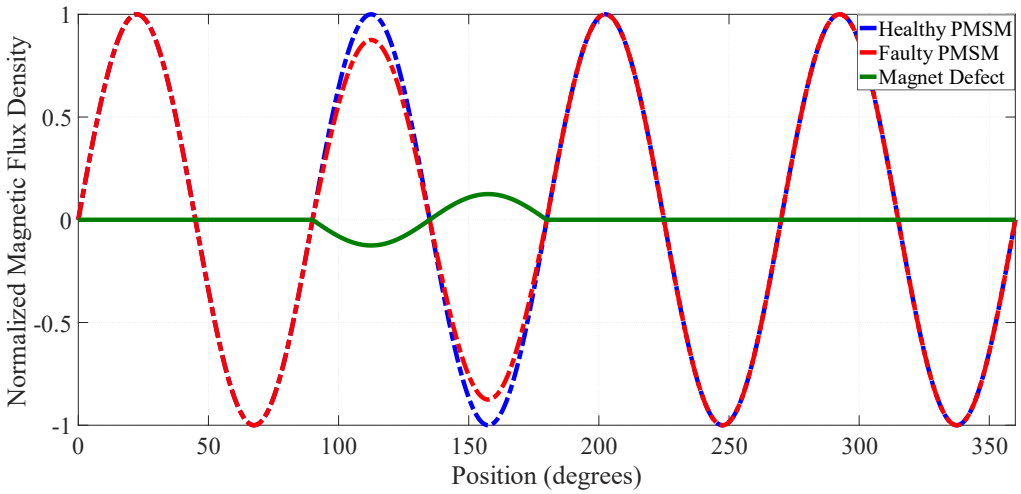

Figure 3.9. Magnetic Flux Density Through the Air-gap for Healthy and Faulty PMSMs

$$f_{demag} = f_e\left(1 \pm \frac{k}{pp}\right), \qquad k = 1, 2, 3 \ldots \tag{3.13}$$

Note that, demagnetization fault affects three phase currents in the same way. Therefore, phase currents can be represented as below.

$$i_A(t) = Icos(2\pi f_e t) + I_f \sum_{k=1}^{\infty} \sin(\frac{\pi k}{2pp})\, cos\left(\frac{k2\pi f_e t}{pp}\right) \tag{3.14}$$

$$i_B(t) = Icos\left(2\pi f_e t - \frac{2\pi}{3}\right) + I_f \sum_{k=1}^{\infty} \sin(\frac{\pi k}{2pp})\, cos\left(\frac{k2\pi f_e t}{pp} - \frac{2\pi}{3}\right) \tag{3.15}$$

$$i_C(t) = Icos\left(2\pi f_e t + \frac{2\pi}{3}\right) + I_f \sum_{k=1}^{\infty} \sin(\frac{\pi k}{2pp})\, cos\left(\frac{k2\pi f_e t}{pp} + \frac{2\pi}{3}\right) \tag{3.16}$$

Since the fault frequency components given by equation (3.13) exist in all three phases, they also exist in i_q. When rotational frame transformation is applied to a signal having frequency of f_s with the reference frame having frequency of f_r, the resulting waveform has the frequency of $|f_s - f_r|$. By applying synchronous reference frame

transformation to phase currents which are given by the equations above, i_q has the form of:

$$i_q(t) = I_q + I_f \sum_{k=1}^{\infty} \sin(\frac{\pi k}{2pp}) \cos\left(\left(1 \pm \frac{k}{pp}\right) wt\right) \quad (3.17)$$

Equation (3.17) shows the effect of demagnetization fault on I_q. In the equation, fundamental (DC) component is I_q of healthy motor while harmonics (AC) are the fault currents. Common factor of all harmonics is I_f which is dependent on the demagnetization level. Amplitudes of the harmonics given by the equation (3.17),

- increases as severity of the fault increases, i.e., as I_f increases
- increases as the speed of the motor increases, which also leads to increase in I_f
- does not change as the load torque increases because load torque only changes the fundamental component I_q.

Harmonics on I_q at rotational frequency and integer multiples of it are indicators of non-uniform demagnetization faults in PMSMs. An accurate fault detection can be achieved by monitoring these harmonics in steady-state operation.

3.2.2. Electromagnetic Simulations

First, a healthy 2D motor model is created from RMxprt design of the test motor. Then one of the eight magnets is selected and material for that magnet is set to be vacuum. This action simulates total demagnetization of one magnet.

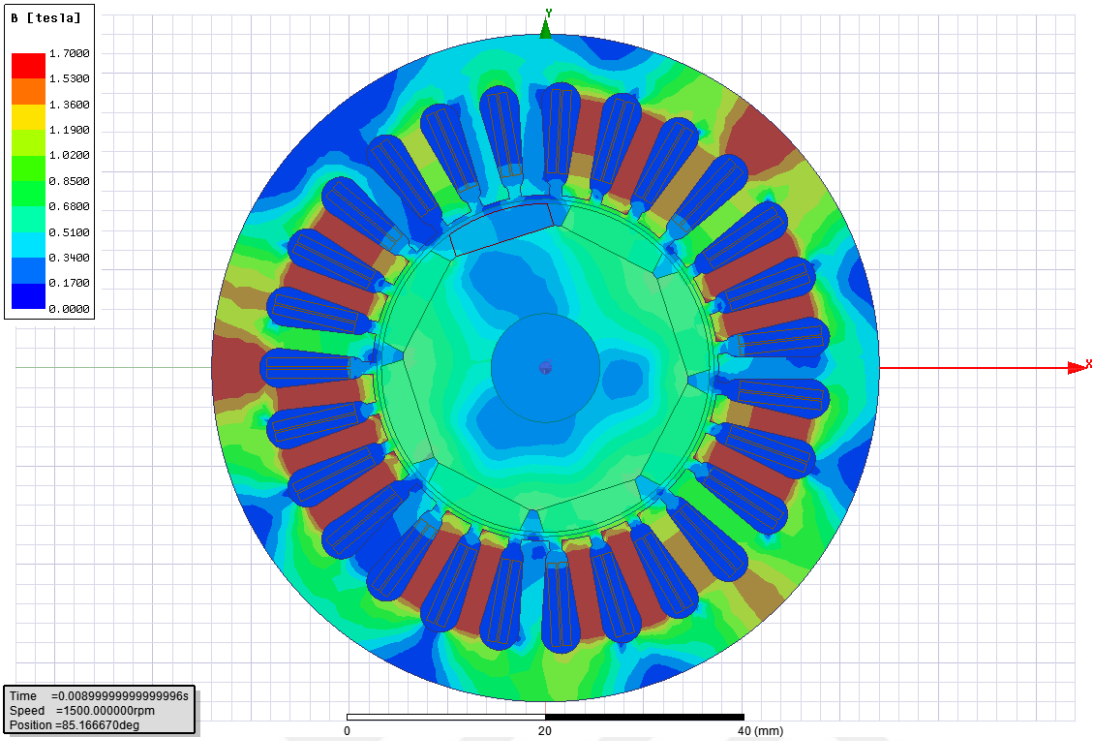

Figure 3.10. 2D Flux Density Distribution of PMSM with Demagnetization Fault

Transient analysis is performed on both healthy and faulty motors which are loaded at nominal torque for speed values of 750 rpm and 1500 rpm. Magnetic flux density distribution of the faulty motor is shown in Figure 3.10. Magnetic flux density of stator teeth is 0.5 T near the faulty magnet while it reaches 1.7 T near the healthy magnets. As the motor rotates, the asymmetry moves along all three phases therefore demagnetization fault affects all three phases in the same way.

The first observation is that phase currents are affected and some harmonics are introduced for faulty cases. Current waveforms for healthy and faulty motors are shown in Figure 3.11. Harmonic contents of these currents at critical frequencies are given in Table 3.2.

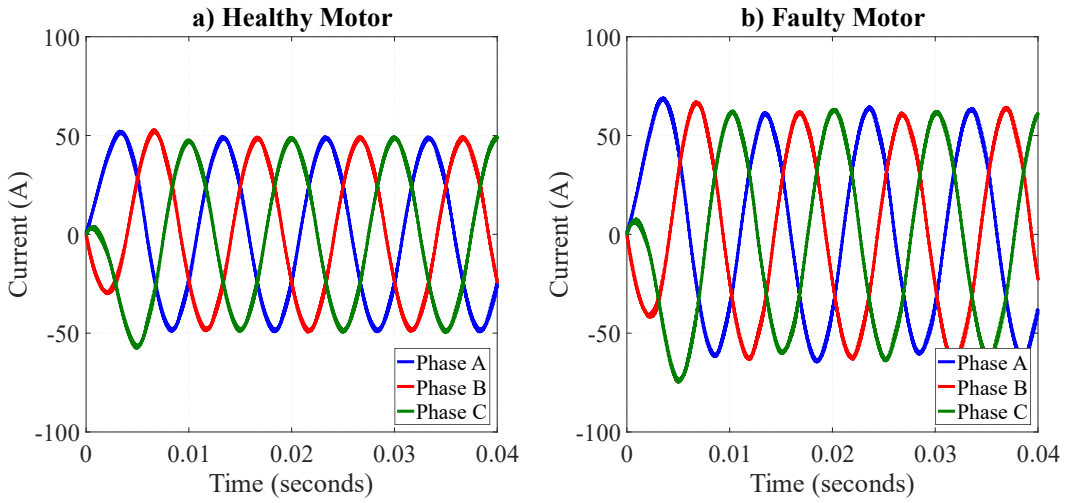

Figure 3.11. Phase Current Waveforms of PMSMs, a) Healthy Motor, b) Faulty Motor

Table 3.2. *Harmonic Content of Phase Currents for Healthy and Faulty PMSMs*

Harmonic	*Healthy (1500 rpm, f_e=100 Hz)*	*Faulty (1500 rpm, f_e=100 Hz)*
$\frac{f_e}{4}$	4.43%	6.14%
$\frac{2f_e}{4}$	3.76%	5.22%
$\frac{3f_e}{4}$	2.78%	3.78%
f_e	100%	100%

Values given in Table 3.2 verifies the mathematical expressions given by equations 3.14, 3.15 and 3.16. Harmonic content at mechanical frequency and its integer multiples increases due to demagnetization fault.

The change in the phase currents is reflected to q-axis current and the produced torque also. Figure 3.12 shows electromechanical torque output of healthy and faulty motors.

The oscillation is due to magnet fault and the frequency of the oscillation is proportional to the motor speed.

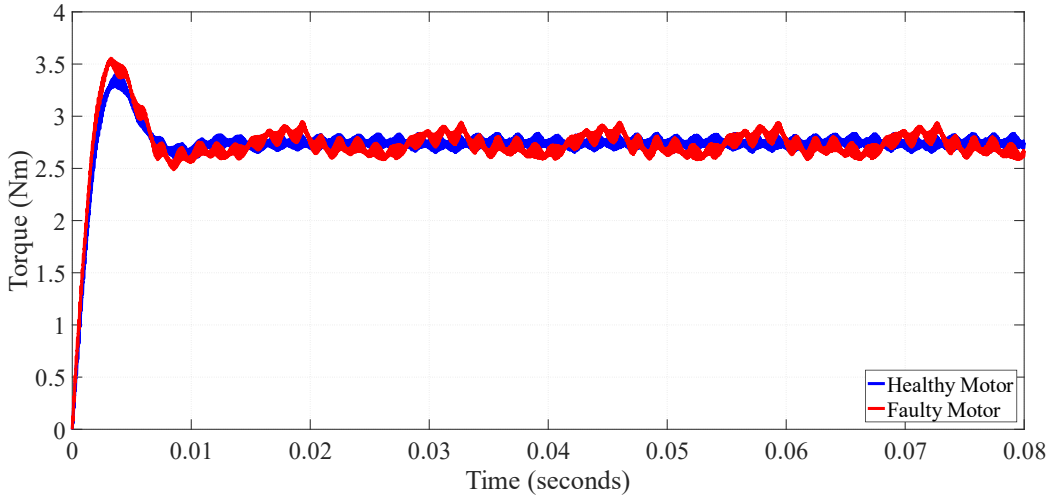

Figure 3.12. Electromagnetic Torque Produced by Healthy and Faulty PMSMs

Q-axis current waveforms of healthy and faulty motors are given in Figure 3.13. The average value of the current increases to obtain the same amount of torque. The frequency of the oscillations are the indications of demagnetization fault. According to equation 3.17, an increase in the harmonic content of i_q at mechanical frequency and its integer multiples is expected. From Table 3.2, harmonic content at $\frac{f_e}{4}$ is greater than others for phase currents. When rotational frame transformation is applied to calculate i_q, this harmonic content shifts to $\frac{3f_e}{4}$. Therefore, maximum disturbance on i_q is expected at that frequency. Table 3.3 shows the harmonic content of i_q of healthy and faulty motors, which confirms the mathematical approach to the effect of demagnetization.

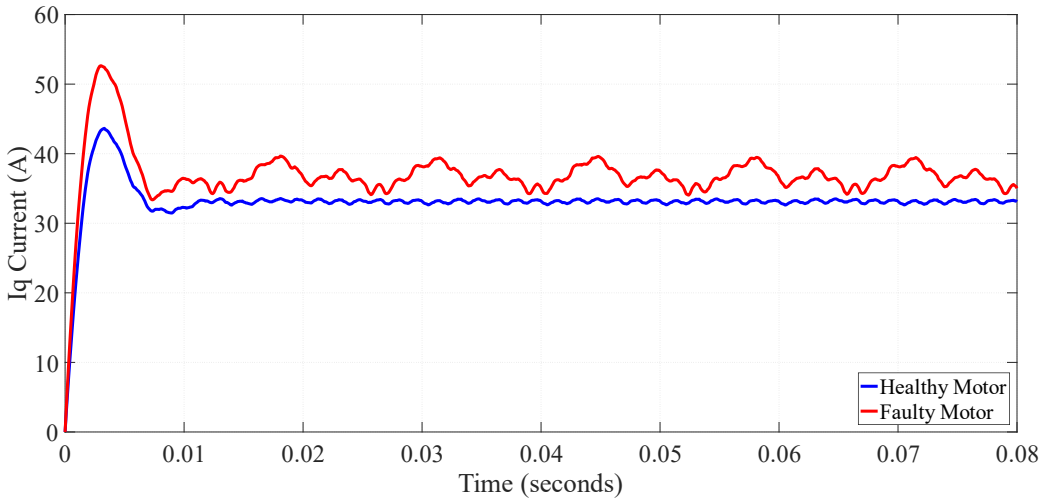

Figure 3.13. Q-axis Current Waveforms of Healthy and Faulty PMSMs

Table 3.3. *Harmonic Content of I_q for Healthy and Faulty PMSMs*

Harmonic	*Healthy (1500 rpm, f_e=100 Hz)*	*Faulty (1500 rpm, f_e=100 Hz)*
$\frac{3f_e}{4}$	0.07%	3.73%
$\frac{6f_e}{4}$	0.08%	3.16%

3.2.3. Remarks

Mathematical modeling and simulation results of demagnetization faults in PMSMs are given in this section. Harmonic content of I_q at $\frac{3f_e}{4}$ is selected to be fault indicator where f_e is the fundamental frequency of phase currents.

Simulations were performed in different speed values but the load torque was the nominal torque in both cases. Therefore, speed dependence of the effects of the fault is observed but the load dependence could not be examined. However, the torque and

I_q is proportional to each other and change in the load only changes the fundamental component of I_q.

The fault detection algorithm will perform FFT on I_q and compare the harmonic content at $\frac{3f_e}{4}$ with a predefined fault threshold value. If it is greater, fault alarm will be set.

Performing harmonic analysis on I_q to detect demagnetization faults has advantages and disadvantages. It has the advantages that:

- It can provide an accurate fault detection for all motor speed and load torque conditions.
- It does not need extra sensors to measure a motor variable. I_q is already available in motor drives with vector control algorithm.

It has the disadvantages that:

- Spectrum analysis brings computational load to the controller. Extra memory fields and time intervals for computations should be spared in the algorithm.
- The method is valid for steady state operation only. The algorithm should wait for a suitable time to monitor the health of the motor to prevent false alarms.

3.3. Rotor Static Eccentricity Faults

3.3.1. Analysis of Rotor Static Eccentricity Faults

In static eccentricity faults, which is shown in Figure 3.14, position of minimum air gap length does not change as the rotor rotates. Therefore, machine variables are in a steady condition. Since they are steady, they do not create harmonic components at the frequency of rotation as in the case of demagnetization fault. Hence it can be concluded that a pure static eccentricity fault cannot be detected by looking at the fault harmonics in the current spectrum at the rotational frequency [28].

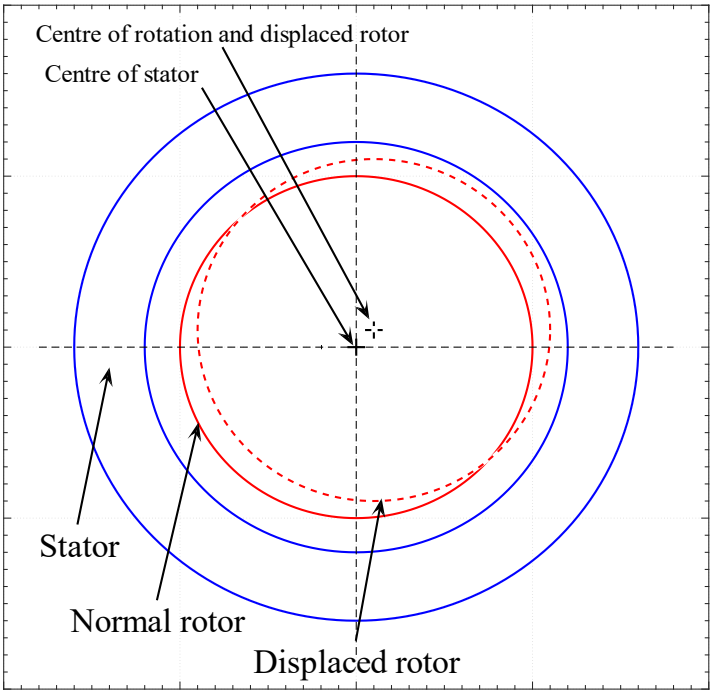

Figure 3.14. Static Eccentricity Fault

Although the motor variables are steady in time, there are differences between phase inductances. Inductance is defined as magnetic flux linked per ampere and motor inductances are given by the equation (3.18) where L_x is inductance, N_x is number of turns, r is rotor radius, l is rotor length and g is the air-gap length. As the equation shows, motor inductances are inversely proportional to air-gap length between stator and rotor.

$$L_x = \mu_0 N_x^2 \frac{\pi}{4}\left(\frac{rl}{g}\right) \tag{3.18}$$

In case of a static eccentricity, center of rotor and rotation is displaced a certain amount such that air-gap length increases for an arbitrary phase while it decreases for others. The displacement and the change in the air-gap length result in differences between inductance values of each phase. Phase voltage equations for a PMSM can be written

in terms of instantaneous voltage and current vectors and resistance and inductance matrices as follows:

$$\begin{bmatrix} v_a \\ v_b \\ v_c \end{bmatrix} = R \begin{bmatrix} i_a \\ i_b \\ i_c \end{bmatrix} + \frac{d}{dt} \begin{bmatrix} L_a & -L_a/2 & -L_a/2 \\ -L_b/2 & L_b & -L_b/2 \\ -L_c/2 & -L_c/2 & L_c \end{bmatrix} \begin{bmatrix} i_a \\ i_b \\ i_c \end{bmatrix} + \frac{d}{dt} (\lambda_m \begin{bmatrix} \cos(\theta) \\ \cos(\theta - \frac{2\pi}{3}) \\ \cos(\theta + \frac{2\pi}{3}) \end{bmatrix}) \tag{3.19}$$

If (3.19) is written for each phase:

$$v_a = R_s i_a + L_a \frac{d}{dt} i_a - \frac{1}{2} L_a \frac{d}{dt} (i_b + i_c) + \frac{d}{dt} \lambda_m \cos(\theta) \tag{3.20}$$

$$v_b = R_s i_b + L_b \frac{d}{dt} i_b - \frac{1}{2} L_b \frac{d}{dt} (i_a + i_c) + \frac{d}{dt} \lambda_m \cos\left(\theta - \frac{2\pi}{3}\right) \tag{3.21}$$

$$v_c = R_s i_c + L_c \frac{d}{dt} i_c - \frac{1}{2} L_c \frac{d}{dt} (i_a + i_b) + \frac{d}{dt} \lambda_m \cos\left(\theta + \frac{2\pi}{3}\right) \tag{3.22}$$

Considering the steady state RMS values of currents and voltages, equations can be rewritten as:

$$\widehat{V_a} - jw\widehat{\lambda_m} = R_s \widehat{I_a} + jwL_a \left(\widehat{I_a} - \frac{1}{2} (\widehat{I_b} + \widehat{I_c}) \right) \tag{3.23}$$

$$\widehat{V_b} - je^{-j\frac{2\pi}{3}} w\widehat{\lambda_m} = R_s \widehat{I_b} + jwL_b \left(\widehat{I_b} - \frac{1}{2} (\widehat{I_a} + \widehat{I_c}) \right) \tag{3.24}$$

$$\widehat{V_c} - je^{+j\frac{2\pi}{3}} w\widehat{\lambda_m} = R_s \widehat{I_b} + jwL_c \left(\widehat{I_c} - \frac{1}{2} (\widehat{I_a} + \widehat{I_b}) \right) \tag{3.25}$$

According to (3.23, 3.24 and 3.25), left sides of the equations have equal amplitudes when 3 phase excitations and permanent magnet flux are the same. Hence, it can be concluded from the right side that there is an inverse relationship between phase inductances and phase currents. At high speeds, impedance for inductances get higher and resistive terms become negligible. Therefore, the difference between the phase currents is more distinguishable at high speeds.

Rotor static eccentricity faults can be detected by monitoring peak or RMS values of phase currents. Since the fault is asymmetric, it affects one phase more than the others. Therefore, the faulty condition can be distinguished from the instantaneous speed and load changes because all three phases are affected in the same way in such cases. However, one should be aware of the following facts:

- The bigger the eccentricity is, the bigger the unbalance between the phase currents is.
- The method is valid for steady state operation of the motor.
- The method gives more accurate results for higher motor speeds.

3.3.2. Electromagnetic Simulations

2D model of the healthy PMSM is created from RMxprt design of the test motor. Then a new coordinate system is defined and named as "Eccentricity SC". Origin of this coordinate system is set to three different positions to create three degrees of static eccentricity fault, which are 0.3 mm, 0.5 mm and 0.8 mm, respectively. The process is shown in Figure 3.15. Note that the figure is for reference only and not to scale. Then the centers of rotor, magnets, shaft and rotation are moved to the origin of "Eccentricity CS". By this way, three separate 2D model for static eccentricity fault is created. A zoomed picture of one of the faulty PMSMs is given in Figure 3.16.

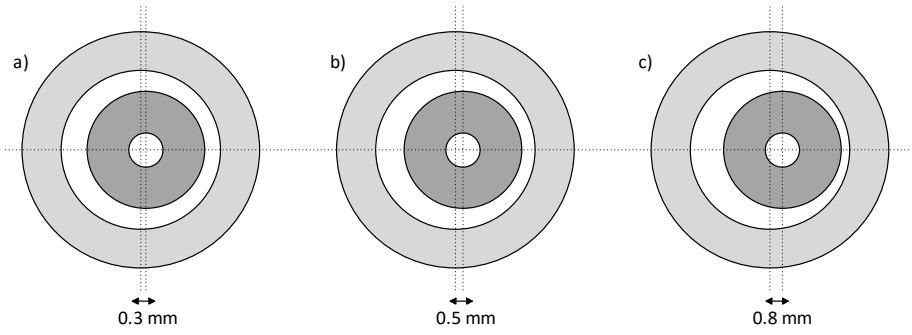

Figure 3.15. Three Different Static Eccentricity Faults, a) 0.3 mm, b) 0.5 mm, c) 0.8 mm

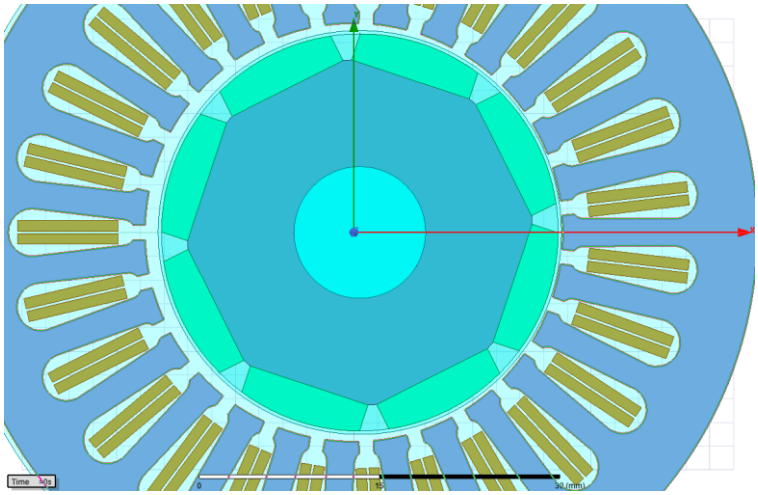

Figure 3.16. Zoomed Picture of The Faulty PMSM (0.5 mm Static Eccentricity)

Transient analysis is performed on all machines to observe the effects of the fault on motor variables. First observation is that magnetic flux density is higher on the side where the air gap length is smaller (Figure 3.17). As shown in Figure 3.18, flux density is 1.7 T on the right while it is 1.35 T on the left because the center of rotor is shifted to right by 0.5mm. Since the eccentricity is static, right side always experiences more flux density while the motor is rotating. Therefore, depending on the position of the static eccentricity, inductances of phases are affected by the fault by different amounts.

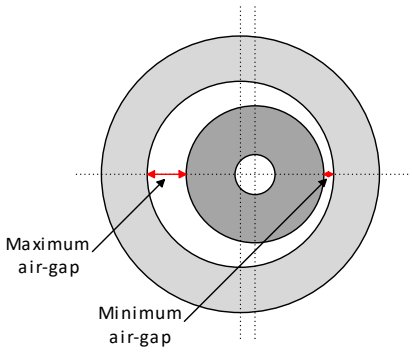

Figure 3.17. Change in the Air-gap Length in Case of Static Eccentricity Fault

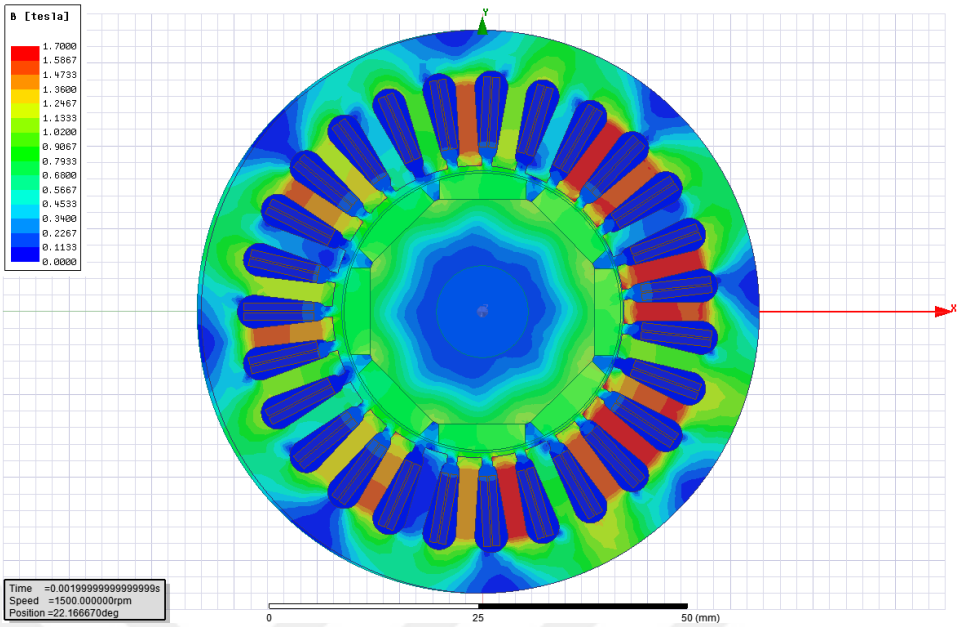

Figure 3.18. 2D Flux Density Distribution of PMSM with 0.5mm Static Eccentricity Fault

Phase currents for healthy and faulty PMSMs are given in Figure 3.19. There are differences between the peak values of phase currents which are numerically given in Table 3.4.

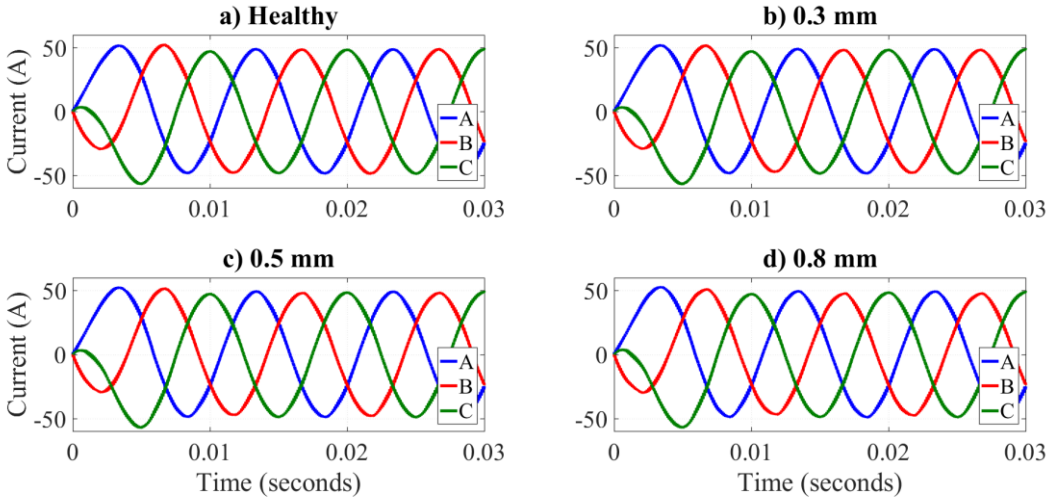

Figure 3.19. Phase Current Waveforms of Healthy and Faulty PMSMs, a) Healthy Motor, b) Faulty Motor with 0.3mm Static Eccentricity, c) Faulty Motor with 0.5mm Static Eccentricity, d) Faulty Motor with 0.8mm Static Eccentricity

Table 3.4. *Peak Values of Phase Currents and Their Difference for Healthy and Faulty PMSMs Running at 1500 rpm and 2.5 Nm*

	$I_{a(peak)}$	$I_{b(peak)}$	$I_{c(peak)}$	*Maximum Difference*
Healthy Motor	49.36A	49.55A	49.42A	0.23A
Faulty Motor (0.3 mm)	49.48A	49.01A	49.45A	0.47A
Faulty Motor (0.5 mm)	49.70A	48.82A	49.55A	0.88A
Faulty Motor (0.8 mm)	49.76A	48.28A	49.63A	1.48A

The relations between phase currents for the same voltage excitations are given by equations 3.23, 3.24 and 3.25. The results given in Table 3.4 confirms the mathematical expressions. As the degree of the static eccentricity increases, difference between peak values of the phase currents increases. Amplitude of the deviation of phase currents from their average value is a measure of static eccentricity fault for PMSMs as expected.

3.3.3. Remarks

Mathematical model and simulation results for static eccentricity faults in PMSMs are presented in this section. The difference between peak or RMS values of phase currents is selected to be fault indicator. Simulations were performed for three degrees of eccentricity fault.

Detecting static eccentricity fault by observing phase currents has advantages and disadvantages. It has the advantages that:

- It is easy to implement. Phase current feedbacks are already available for motor control purposes in a motor drive. It does not need additional sensors to perform condition monitoring.

- Calculating peak or RMS values of currents is easier than performing a spectrum analysis. Therefore, the method does not bring much computational load and can be run on a standard micro-processor used for motor control purpose.
- Fault severity can also be detected from the difference between phase currents.

It has the disadvantage that:

- It makes accurate decisions only for steady state operation of the motor. In transients, the method may trigger false alarms. Therefore, the fault detection algorithm should be run in steady state operation.

In this chapter, PMSM faults that are in the scope of this thesis are mathematically modelled and each fault type is simulated in ANSYS Maxwell. Mathematical models are verified by simulations and fault indicators are determined based on these results. Advantages and disadvantages of each fault indicator are given. In common, fault detection algorithm has the disadvantage that it works only in steady state operation; however, this disadvantage can be overcome by a proper condition monitoring algorithm which is going to be given in the following chapters.

In the next chapter, experimental work conducted on the test motors are presented. Each fault type is created on the test motors separately and effects of them on motor variables are examined. Experimental results are shared and discussed.

CHAPTER 4

EXPERIMENTAL RESULTS

Analytical modeling and simulation results of healthy and faulty PMSMs with different types of faults are given in Chapter 3. Mathematical models and simulation results are verified with experiments performed on a motor drive system. Properties of the test bench and methodology of the experiments are given in the following sections. Experimental results are compared with the aforementioned theoretical and simulation results.

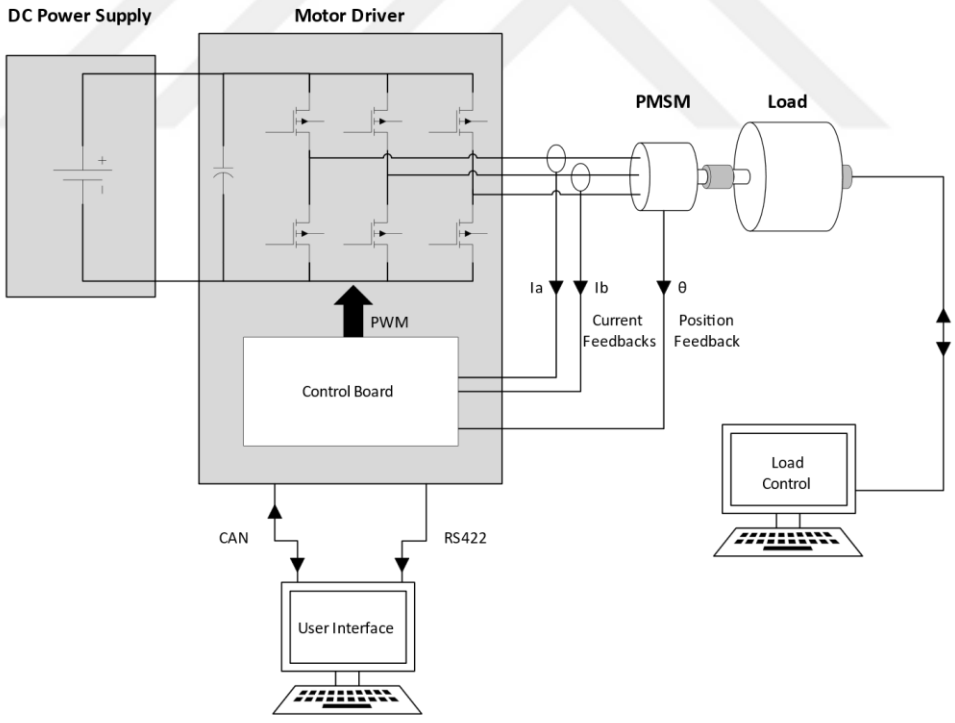

Figure 4.1. Block Scheme of Experimental Setup

4.1. Experimental Setup

The block scheme of the experimental setup is given in Figure 4.1. Each of the components shown in the scheme is described in this section.

3 identical PMSMs are used in the experiments for different types of faults. One of the motors is spared as control specimen which is called as healthy motor while the others are used as experimental specimens. Stators, rotors, bearings and housings of these motors are interchangeable.

Table 4.1. *Electrical Specifications of HERKUL-04D Servo Controller*

Property	*Value*
Rated input voltage	18-32 V
Rated phase current	20 A_{rms} per axis
Number of axes	2
Rated power	700 W per axis

Electrical specifications of HERKUL-04D servo controller are given in Table 4.1. The servo controller consists of control and power stages. It has current sensors to measure phase currents and it is equipped with all required hardware interfaces to read motor position and speed information either from a resolver or encoder. Throughout the experiments, resolver position feedback is used and motor speed is calculated by taking derivative of the motor position. HERKUL-04D uses vector control algorithm with space vector PWM to control the PMSM. A simplified block diagram of such a controller is given in Figure 4.2.

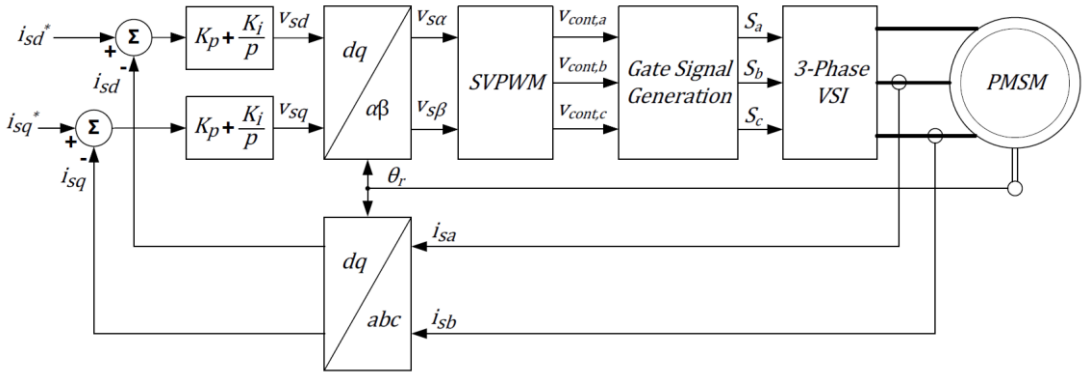

Figure 4.2. Simplified Block Diagram of Vector Control Algorithm with Space Vector PWM [37]

One of RS422 serial communication channels of HERKUL-04D is set as test channel. The signals listed in Table 4.2 are sampled at 1 kHz and sent to the computer via this test channel. Before working on condition monitoring and fault diagnosis algorithm within the servo controller, test channel feedback signals are processed offline using a MATLAB Simulink model. Signal characteristics of healthy and faulty motors are compared with theoretical and simulation results. Once expectations on different signal characteristics are verified by experimental results offline, a proper condition monitoring and fault diagnosis algorithm is implemented on the actual motor drive software.

Table 4.2. *Measurements of the Test Channel*

Number	*Signal (Unit)*	*Explanation*
1	Rotor speed (degree/s)	Mechanical speed of the rotor
2	I_d (A)	Measured I_d current
3	I_q (A)	Measured I_q current
4	θ (rad)	Electrical rotor position
5	I_a (A)	Measured current of Phase A
6	I_b (A)	Measured current of Phase B
7	I_c (A)	Measured current of Phase C
8	V_q (V)	Q-axis voltage
9	V_d (V)	D-axis voltage

Test motors are loaded by MAGTROL Motor Test Equipment. Specifications of MAGTROL and the other test equipment are given in Table 4.3.

Table 4.3. *Specifications of MAGTROL and The Other Test Equipment*

Property	*Value*
Max load torque	14 Nm
Max load speed	10000 rpm
Load type	Hysteresis braking
Power Supply	60V-50A
Control Channel	CAN
Test Channel	RS422
Offline Processing Tool	MATLAB

4.2. Experiments and Results for Permanent Magnet Demagnetization Faults

In order to verify the results found in Chapter 3, one of the eight permanent magnets of a test motor is fully demagnetized. For this purpose, one magnet is separated from the rotor and excessive heat is applied on it. Magnetic flux density near the surface of the magnet was 0.3 T prior to demagnetization. After the heat is applied, flux density decreased to 0.03 T. Demagnetization process of the permanent magnet is summarized in Figure 4.3.

Motor is reassembled after demagnetization and coupled to the test-rig. Experiments are performed in torque and speed control modes separately for healthy and faulty motors.

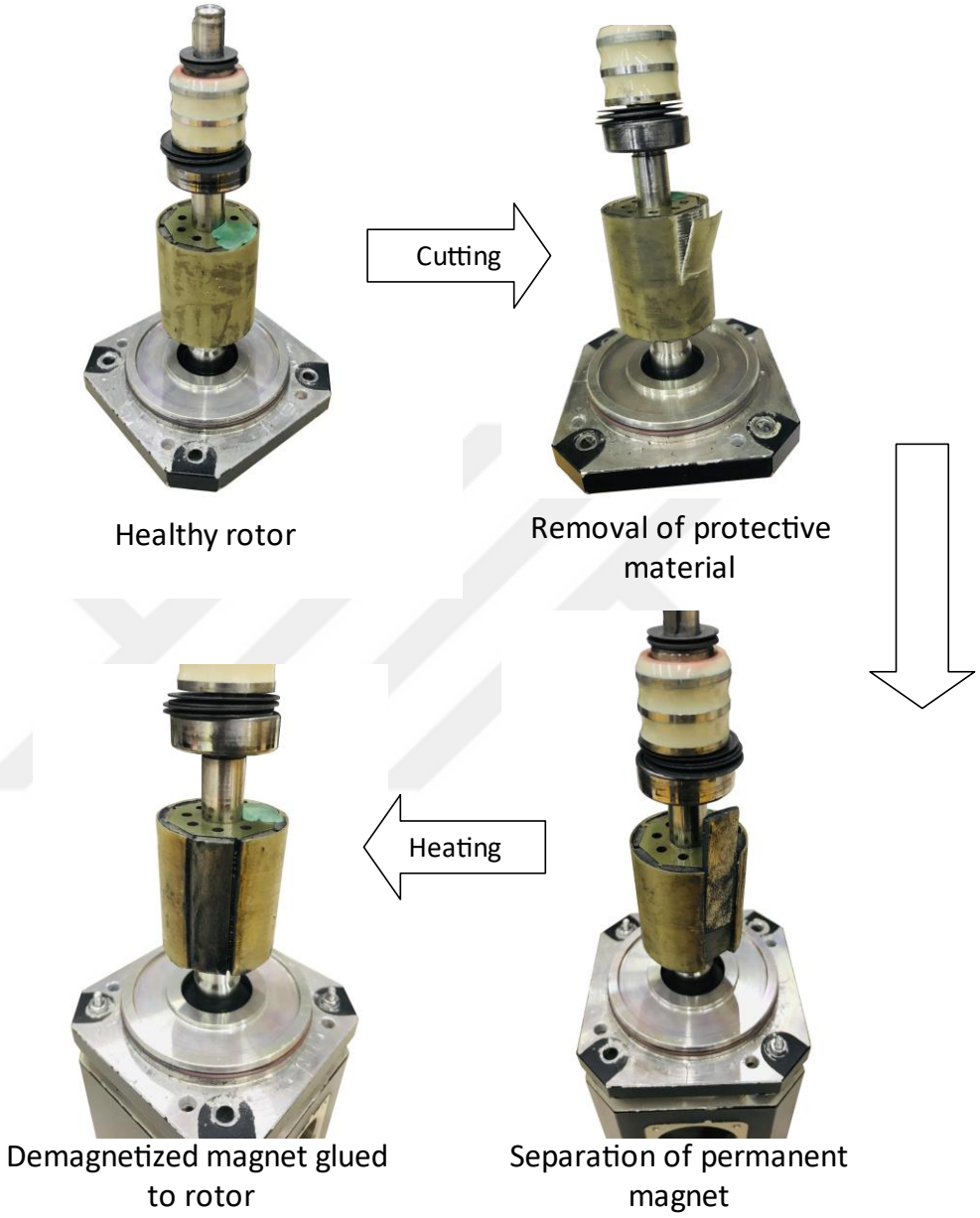

Figure 4.3. Physical Demagnetization of a Permanent Magnet of the Rotor

4.2.1. Experiments in Torque Control Mode of Operation

In torque control mode of operation, a constant torque command is sent to the servo controller and motor speed is regulated by the load side. Motor is run at the conditions given in Table 4.4. Measurements are post-processed in MATLAB. By applying full length FFT, frequency contents of the signals given in Table 4.2 are examined.

Table 4.4. *Test Conditions of the Experiments*

	0.4 Nm	*0.8 Nm*	*1.2 Nm*	*1.6 Nm*
600 rpm	✓	✓	✓	✓
1200 rpm	✓	✓	✓	✓
1800 rpm	✓	✓	✓	✓
2400 rpm	✓	✓	✓	✓

Since torque command is constant during tests, I_q demanded from the controller is also constant. I_d command is always zero if the motor is not working in the field weakening region. Therefore, together with I_q and I_d, all torque and current related signals including phase currents are determined by torque command and they do not change by demagnetization of a magnet. Therefore there is no significant difference between frequency contents of I_q, I_d, I_a, I_b and I_c for healthy and faulty motors. Figure 4.4 shows currents waveforms of phase A for healthy and faulty motors. They are similar to each other and the effect of the fault cannot be seen.

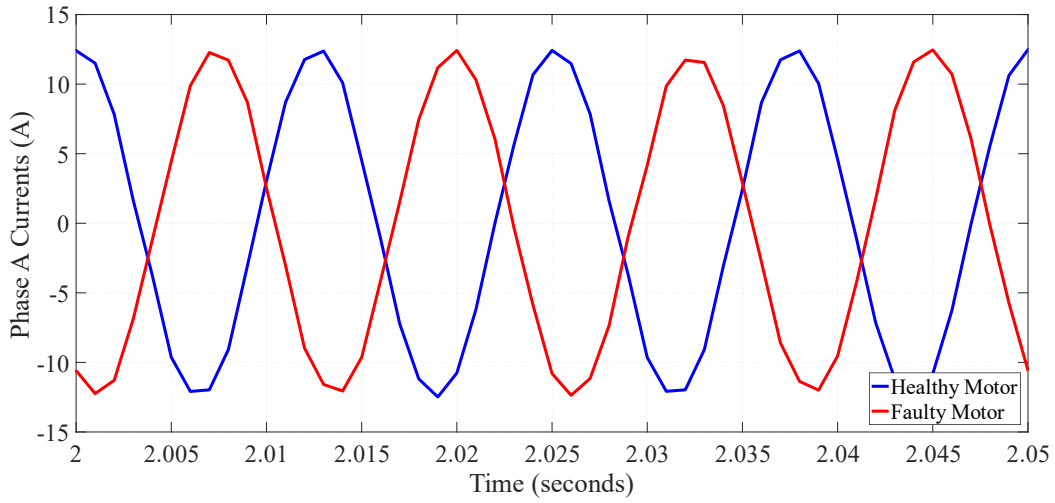

Figure 4.4. Phase A Current Waveforms of Healthy and Faulty Motors Operating in the Torque Control Mode

Although current signals are not affected by magnet fault, the motor cannot produce the same torque for the same current when demagnetization occurs. Since one of the magnets is demagnetized, spatial magnetic flux density distribution is disturbed as given by the equation 3.12. This disturbance travels around air gap as the motor rotates and creates torque oscillations for its every rotation. Therefore, torque produced by the motor has harmonic content at the frequencies given by the equation 3.13. Unfortunately, test setup does not include a torque transducer so that actual torque can directly be measured at the motor shaft. Alternatively, effects of torque oscillations can be seen on the speed measurements. The speed of the motor is regulated by the test equipment and its speed controller bandwidth is 5 Hz which is lower than the frequencies of the expected harmonics. Therefore the motor speed cannot be regulated by the load perfectly and torque disturbances are reflected on the speed of the faulty motor.

Rotor mechanical speed measurements of healthy and faulty motors are examined and compared. Comparisons show that FFT coefficients at f_m and its integer multiples have higher amplitudes as expected.

Figure 4.5 shows the rotor speed measurements of healthy and faulty motors and their normalized spectrums while the motors are running at 600 rpm (3600 deg/s) and loaded with 0.8 Nm. The amplitude of FFT is higher for the faulty motor at 10 Hz (f_m) as shown.

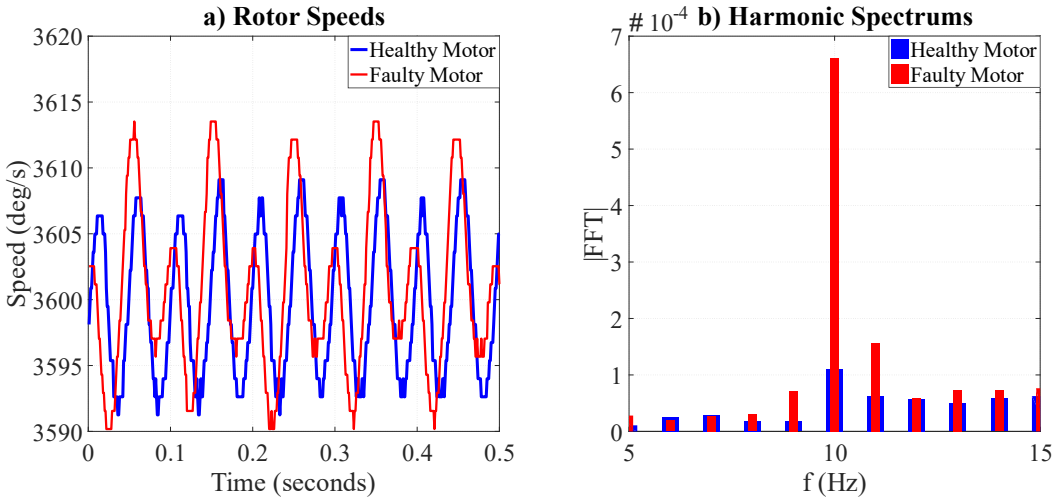

Figure 4.5. Healthy and Faulty Motors Running at 600 rpm (3600 deg/s) and 0.8 Nm Load, a) Rotor Speed Measurements, b) Normalized Harmonic Spectrums of Rotor Speeds

Equivalent results are obtained for all other torque and speed conditions. Normalized amplitude spectrums of rotor speed measurements at f_m are shown in Figure 4.6 for all conditions given in Table 4.4. The amplitudes of FFT coefficients are higher for the faulty motors in all cases. However, as speed of the motor increases, difference between healthy and faulty motor gets smaller which makes fault detection more difficult. The reason behind this fact is that FFT coefficients are normalized by the fundamental component of the rotor speed. As the speed increases, the fundamental component increases and normalized FFT coefficients corresponding to fault frequencies get smaller.

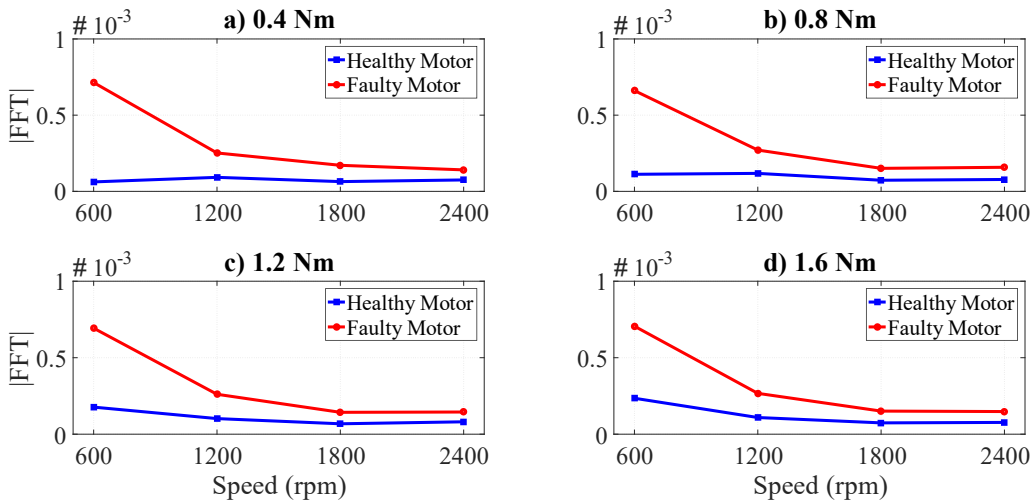

Figure 4.6. Normalized FFT coefficients of Rotor Speed at f_m for Healthy and Faulty Motors, a) 0.4 Nm Load, b) 0.8 Nm Load, c) 1.2 Nm Load, d) 1.6 Nm Load

When FFT coefficients are not normalized by the fundamental component of the rotor speed, the difference between healthy and faulty cases becomes clearer. Figure 4.7 shows amplitudes of FFT coefficients at f_m of each case, which are not normalized.

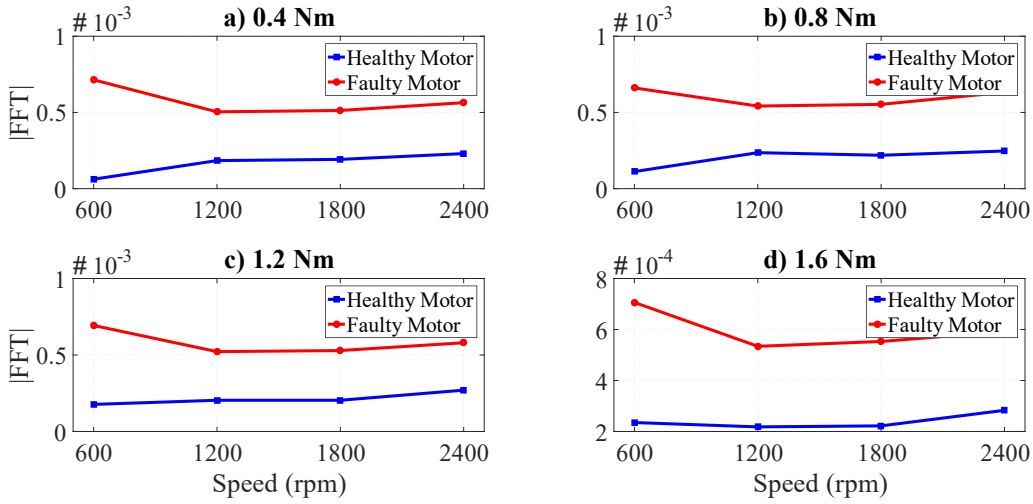

Figure 4.7. FFT coefficients of Rotor Speed at f_m for Healthy and Faulty Motors, a) 0.4 Nm Load, b) 0.8 Nm Load, c) 1.2 Nm Load, d) 1.6 Nm Load

In torque control mode of operation, although there are inherent harmonics in the spectrum of the speed measurements of healthy motors, the harmonics of the motor speeds at f_m increase with the demagnetization fault as shown in Figure 4.6 and Figure 4.7. Inherent oscillations on the speeds may be due to cyclic loading of mechanical misalignments or controller parameters. However, these inherent imperfections can be taken into consideration by a condition monitoring algorithm trained on measurements of the healthy motor in a real application.

4.2.2. Experiments in Speed Control Mode of Operation

In the speed control mode of operation, constant speed commands are sent to the servo controller from the computer. Tests are performed for the speed and torque values given in Table 4.4. By applying full length FFT, frequency contents of the signals given in Table 4.2 are examined.

One faulty magnet on the rotor creates torque oscillations at mechanical rotational frequency as explained in the previous section. In speed control mode, speed controller modifies inner torque commands so that torque oscillations due to faulty magnet do not appear on the speed of the motor. In other words, speed controller compensates torque oscillations by adjusting motor phase currents. Therefore, effects of the fault can be seen not on rotor speed but on phase currents and I_q in this case.

Phase current measurements of healthy and faulty motors are examined and compared. Comparisons show that FFT coefficients of phase currents corresponding to f_m are higher for the faulty motors. When the motors are run at 1200 rpm, harmonic content at 20 Hz is expected to be lower for the healthy motor. Figure 4.8 illustrates amplitude spectrum of phase A current for healthy and faulty motors running at 1200 rpm and no-load condition. Frequency axis is centered around the frequency of interest for a better view. Harmonic content is higher for the faulty motor and measurements meet expectations.

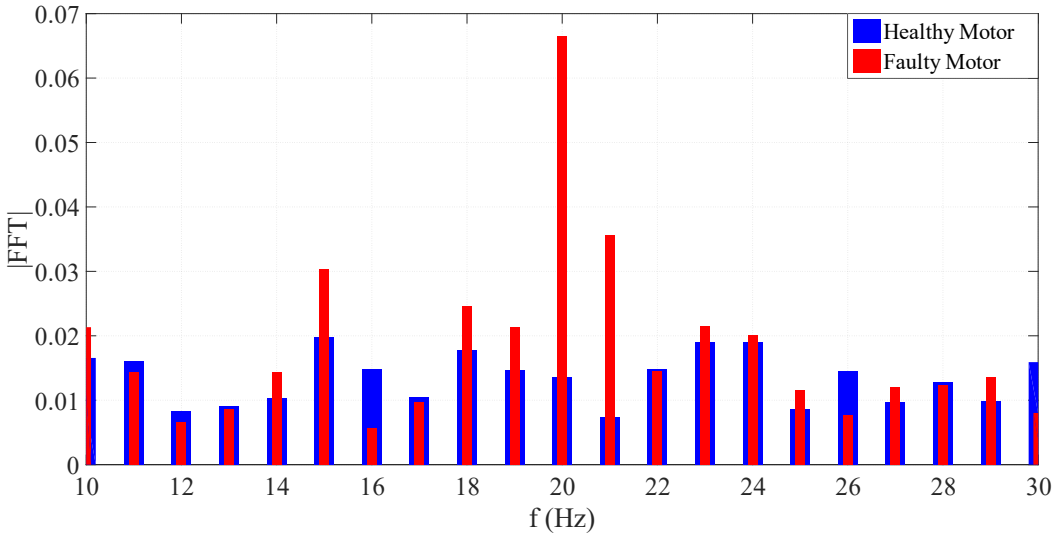

Figure 4.8. Normalized Amplitude Spectrum of Phase Current A for Healthy and Faulty Motors Running at 1200 rpm and No Load

Comparisons on phase currents of the healthy and faulty motors are made for each speed and load value and the same behavior is observed. Permanent magnet demagnetization fault affects all three phases in an equivalent way and does not create any asymmetries between the phases. Therefore FFT coefficient of I_q corresponding to $\frac{3f_e}{pp}$ should be an indicator of demagnetization fault as given in the equation 3.17 and explained in section 3.2.2. Figure 4.9 shows FFT coefficients of I_q at $\frac{3f_e}{pp}$ for the healthy and faulty motors running at different torque and speed conditions. According to the figure, harmonic content is independent from load torque but it increases with speed. FFT coefficients are normalized with the square of the rotor speed per unit to make fault indicator independent from speed. The resulting indicator clearly separates healthy and faulty motors at all operating conditions. It is illustrated in Figure 4.10.

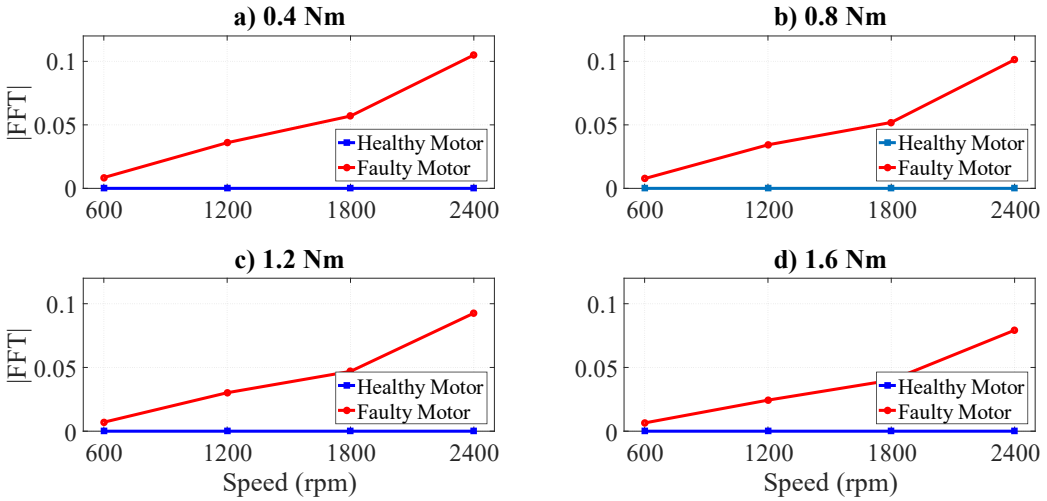

Figure 4.9. FFT Coefficients of I_q at Fault Frequencies for Healthy and Faulty Motors, a) 0.4 Nm, b) 0.8 Nm, c) 1.2 Nm, d) 1.6 Nm

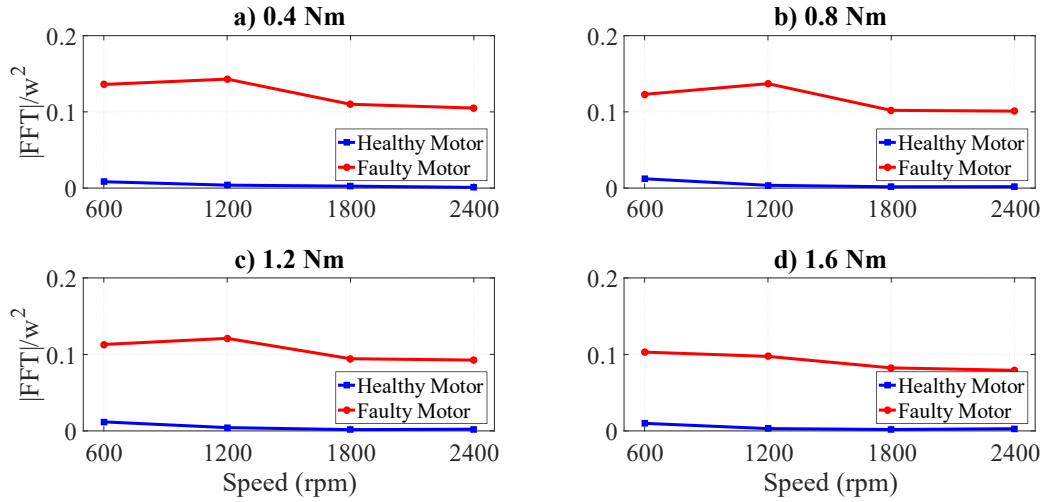

Figure 4.10. FFT Coefficients of I_q at Fault Frequencies Normalized by w^2 for Healthy and Faulty Motors, a) 0.4 Nm, b) 0.8 Nm, c) 1.2 Nm, d) 1.6 Nm

In speed control mode of operation, speed is regulated by the servo controller and the effect of demagnetization show itself on the phase currents and I_q. According to experimental results, harmonic contents of phase currents at f_m and I_q at $\frac{3f_e}{pp}$ are good

candidates to be indicators of permanent magnet demagnetization faults verifying the results given in Chapter 3.

4.3. Experiments and Results for Stator Short Circuit Faults

Effects of stator inter-turn short circuit faults on motor electrical signals are given in Chapter 3. Experiments are performed to verify the results in Chapter 3 on a real PMSM.

Stator winding of the test motor is distributed winding consisting of 16 series turns stranded with 8 conductors having 0.5 mm diameter for each phase.

Artificial short circuit faults for experiments is decided to be created on phase A without loss of generalization. Windings of phase A should be available from outside for this purpose. On a standard motor, windings are placed on stator slots and then they are molded with epoxy. Therefore, it is impossible to reach desired positions of a winding and connect them together to create a short circuit on a standard motor. Hence, a special design stator is needed.

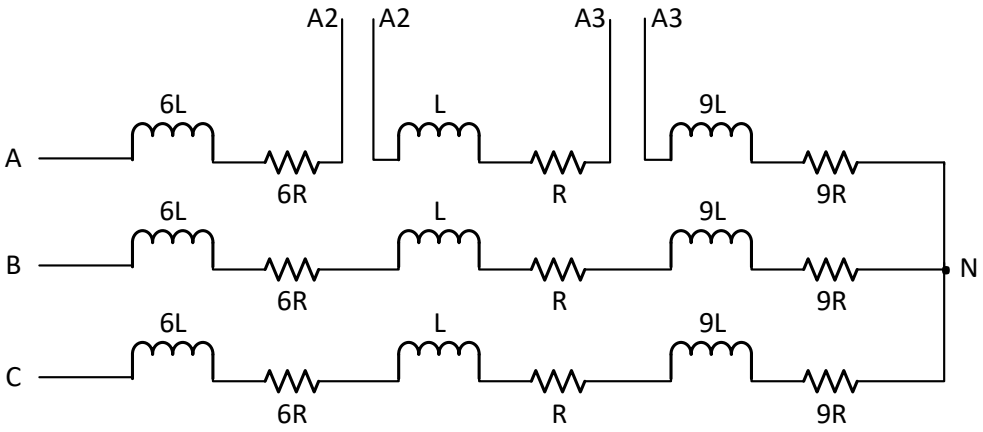

Figure 4.11. Winding and Output Terminals of the Special Design Stator

Winding scheme, inductance and resistance of the special design stator is the same with the standard motor except that it both ends of a single turn on phase A. Figure 4.11 illustrates windings and output terminals of the special design stator winding. Each terminal shown in the figure consists of 8 thin conductors which are electrically isolated from each other. A detailed look of the conductors between the terminals A2 and A3 are given in Figure 4.12.

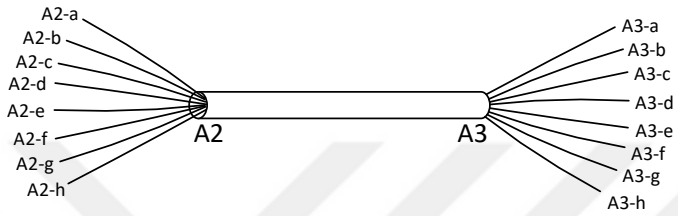

Figure 4.12. Detailed Look of the Conductors Between the Terminals A2 and A3

Required special stator is manufactured and assembled together with other standard motor components like rotor and bearing. Appearance of the actual motor is shown in Figure 4.13.

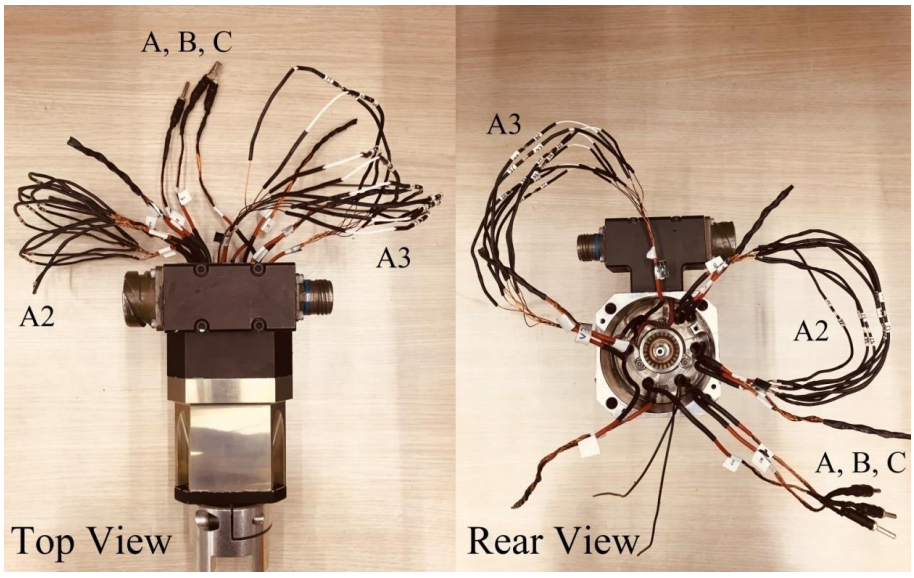

Figure 4.13. Actual Motor with Special Design Stator and Terminals

First, all of the terminals are connected in a standard way so that the test motor acts like a healthy motor. The torque and back EMF constants of the motor are determined by applying a series of tests. Resistances and inductances of the windings are measured. It is verified that the special stator is an exact replica of the healthy stator.

Short circuit faults are created artificially on Phase A as follows:

- A2-a and A3-a terminals (Figure 4.10 and 4.11) are connected over 4 different resistance to simulate faults: 26.1 Ω, 5.1 Ω, 2.4 Ω and 0 Ω (short circuit). This configuration is called as one-conductor fault.

Tests are performed for the conditions given in Table 4.4 for each fault resistance. Measurements are recorded for the signals listed in Table 4.2. Additionally, short circuit currents through the fault resistance are measured for each case with an oscilloscope for reference. They are not used in fault detection because it is not possible to measure such fault currents under normal conditions.

- Then, A2-b and A3-b terminals are also connected to each other and the same test procedure is repeated for two-conductors fault.

Table 4.5. *Short Circuit Currents for Different Fault Conditions and Fault Resistance*

	26.1 Ω	*5.1 Ω*	*2.4 Ω*	*0 Ω*
One-conductor fault	0.4 A	0.9 A	2.2 A	18 A
Two-conductor fault	0.5 A	1.1 A	2.6 A	28 A

The first observation is that short circuit current measured by current probe increases with the decrease of fault resistance at the same speed. Table 4.5 shows change of short circuit current with fault resistance for one-conductor and two-conductor faults at full speed. Short circuit current reaches dangerous amplitudes only when the conductors are directly connected simulating an ideal short circuit .

- The same test procedure is repeated for three-conductor and four-conductor faults which are created by connecting A2-c, A2-d, A3-c and A3-d conductors (Figure 4.12).

The second observation is that short circuit current increases as the motor speed and number of shorted conductors increase. Figure 4.14 shows fault current vs motor speed for four faulty cases. On the other hand, fault current does not change with the load torque, which is shown in Figure 4.15. Therefore, amplitude of the short circuit current can be considered as a direct measure of fault severity.

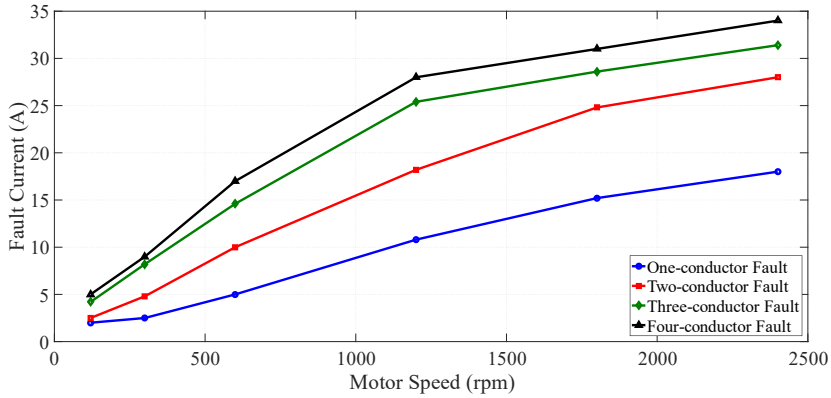

Figure 4.14. Short Circuit Fault Current vs Motor Speed at No Load

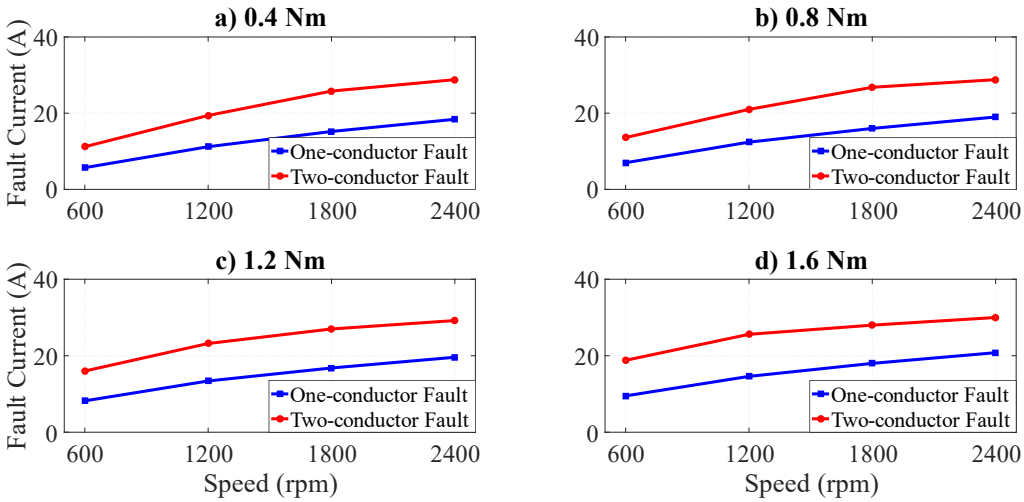

Figure 4.15. Short Circuit Fault Current vs Motor Speed, a) 0.4 Nm, b) 0.8 Nm, c) 1.2 Nm, d) 1.6 Nm

Recorded measurements are post-processed in MATLAB. Since experimental setup does not include voltage sensors to measure phase voltages directly, V_a, V_b and V_c are calculated applying inverse Park Transformation to V_d and V_q signals, which are already available from Table 4.2. The results show that V_a has lower amplitudes than V_b and V_c in faulty cases. In a healthy motor, although there can be differences between applied phase voltages due to inherent asymmetries of stator windings, phase voltages differ a negligible amount from their average value. For faulty motors, the deviation from the average value increases and the faulty phase has the maximum deviation. RMS values of phase voltages are calculated and their deviations from the average values for healthy and faulty motors are shown in Figure 4.16.

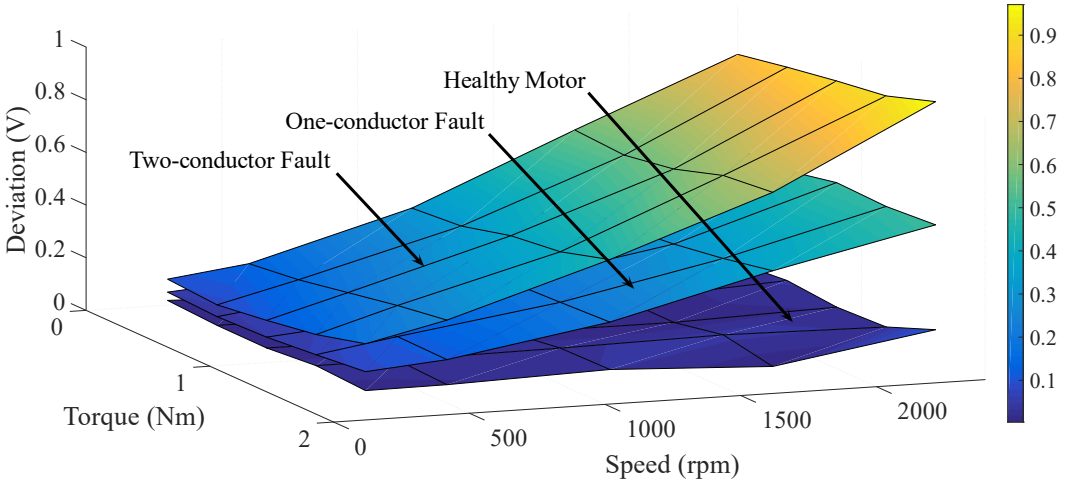

Figure 4.16. Deviation of V_a from the Average vs Motor Speed and Load

According to Figure 4.16, for faulty motors, the difference between voltages does not change with load torque and it increases with motor speed (Figure 4.17). To set a proper fault indicator independent from the speed, the differences are divided to average values of RMS phase voltages. Normalized deviations are shown in Figure 4.18. The normalized deviation is almost independent from the motor speed and it

increases as the number of shorted conductors increase. Fault indicator also gives information about fault severity.

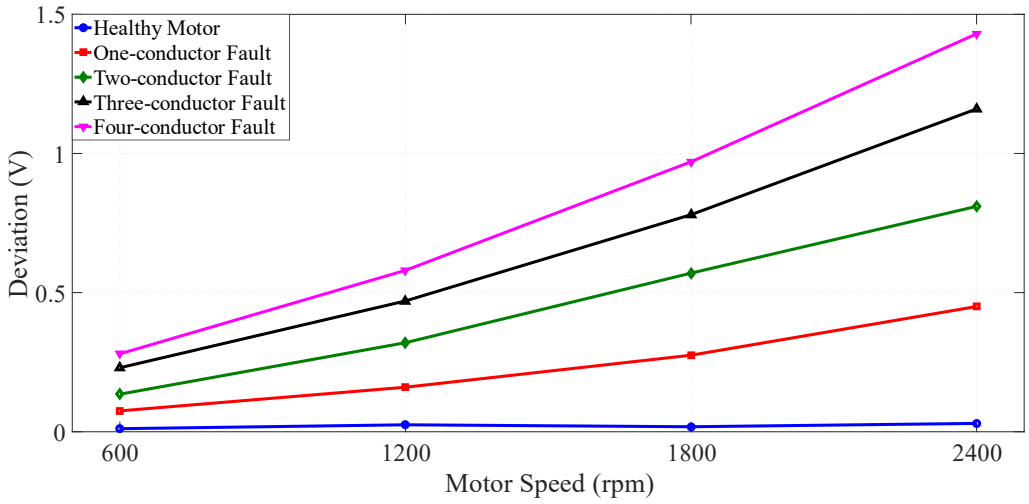

Figure 4.17. Deviation of V_a from the Average vs Motor Speed at No Load

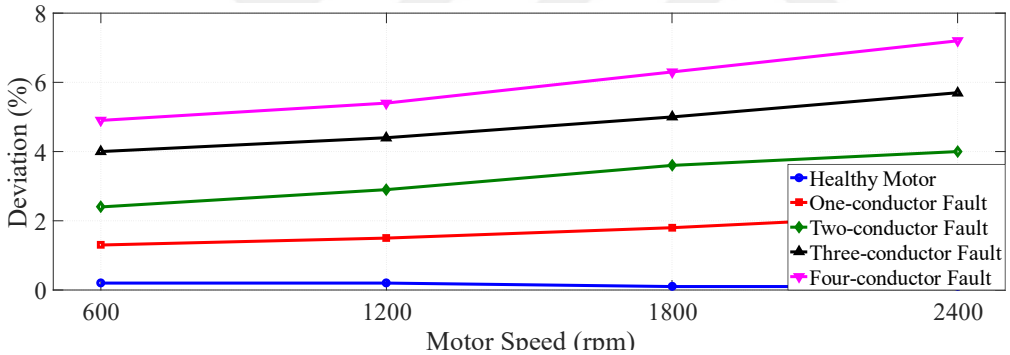

Figure 4.18. Normalized Deviation of V_a from the Average vs Motor Speed at No Load

The results show that difference between RMS phase voltages is an indicator of short circuit faults. It does not show only if the motor is healthy or faulty but also gives an insight about the faulty severity. Experiments on inter-turn stator short circuit faults verified analytical and simulation results given in Chapter 3.

4.4. Experiments and Results for Rotor Static Eccentricity Faults

Effects of static eccentricity faults on the motor signals are observed experimentally in this section to verify theoretical and simulation results presented in Chapter 3. Static eccentricity fault is the one where center of rotor is displaced from center of stator and rotor still rotates around its own axis (Figure 3.14). In other words, center of rotation is still the center of rotor.

The fault is artificially created on rotor of one of the test motors. For this purpose, rotor and bearing are taken out of motor. Inner part of motor cage is machined 0.5 mm from one side only. Rotor and bearing are placed on the machined side of the cage and a shim is placed to other side to prevent bearing sliding to its original place. Figure 4.19 shows the static eccentricity fault on created the test motor. As the air gap is 1.8 mm, displacement of 0.5 mm corresponds to 28% static eccentricity fault.

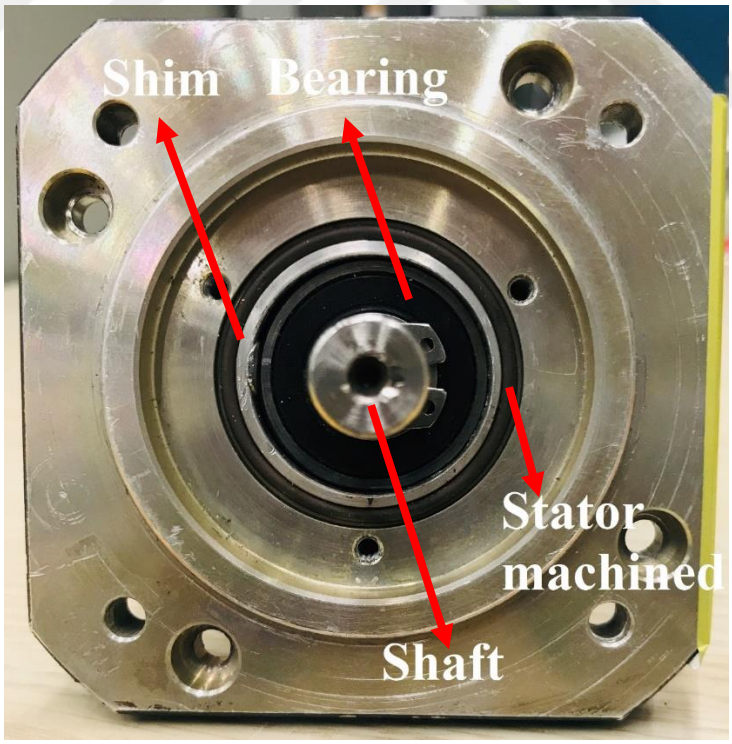

Figure 4.19. Static Eccentricity Fault on the Test Motor

After artificial static eccentricity fault is created on the bearing, test motor is assembled and experiments are performed for the conditions given in Table 4.4. Signals given in Table 4.2 are post-processed in MATLAB.

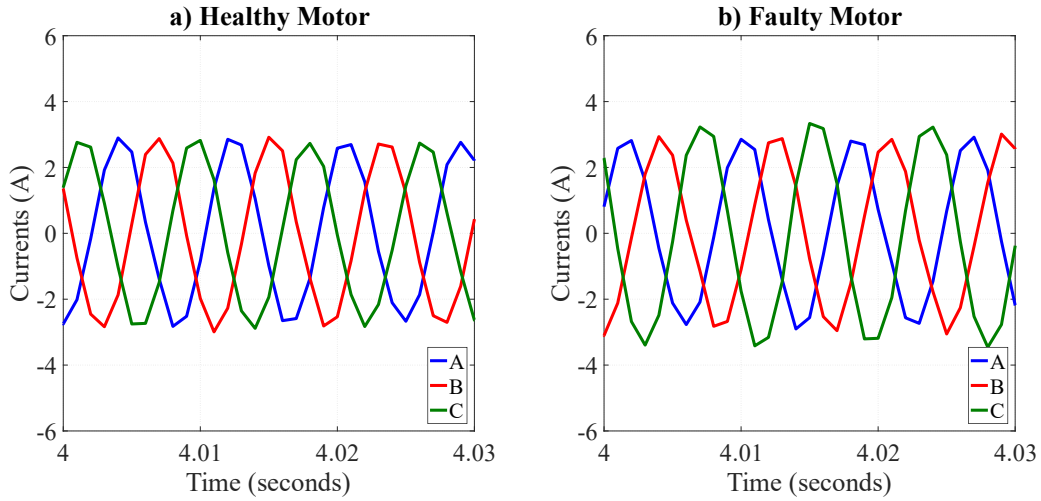

Figure 4.20. Phase Current Measurements of Healthy and Faulty PMSMs Running at 1800 rpm with 0.4 Nm Load, a) Healthy Motor, b) Faulty Motor

Displacement of rotor from center of stator breaks uniformity of the air-gap. As given by the equation 3.18 and explained in Chapter 3, inductances of phases have a direct relationship with the air-gap length. Non-uniform air-gap distribution results in differences between inductances of phases. Change of inductances disrupts three phase balance of the motor; therefore, phase currents differ from each other in case of a static eccentricity fault. Figure 4.20 shows phase currents of healthy and faulty motors running at 1800 rpm with 0.4 Nm load. As shown in the figure, peak value of the phase current C is higher for the faulty PMSM.

The results show that even though there are slight differences between RMS phase currents of the healthy motor, deviations of phase currents from the average increases clearly for the faulty motor in all operating conditions. Results are shown in Figure 4.21.

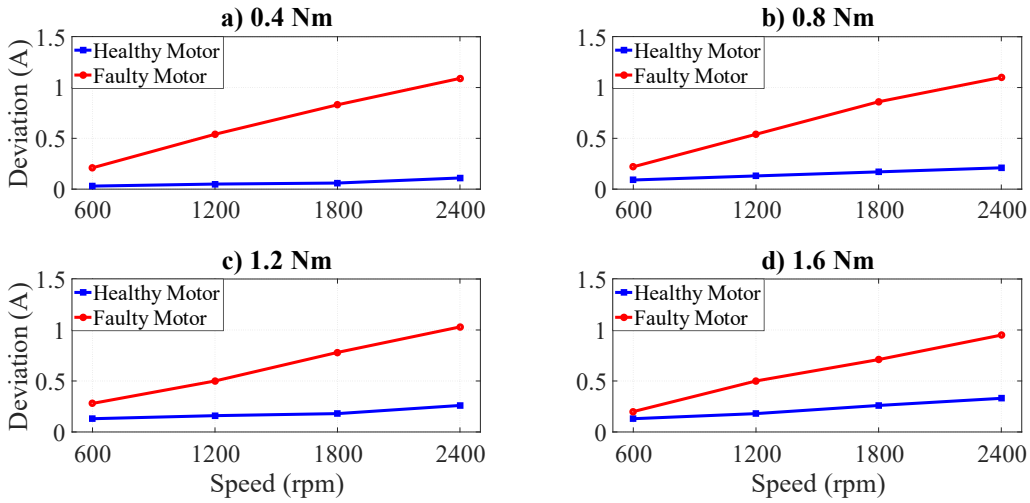

Figure 4.21. Deviation of Phase Currents from the Average for Healthy and Faulty Motors, a) 0.4 Nm, b) 0.8 Nm, c) 1.2 Nm, d) 1.6 Nm

As Figure 4.21 shows, the deviation is independent from the load torque while it increases linearly with the speed. If the deviation is normalized by motor speed, fault indicator becomes speed independent as shown in Figure 4.22.

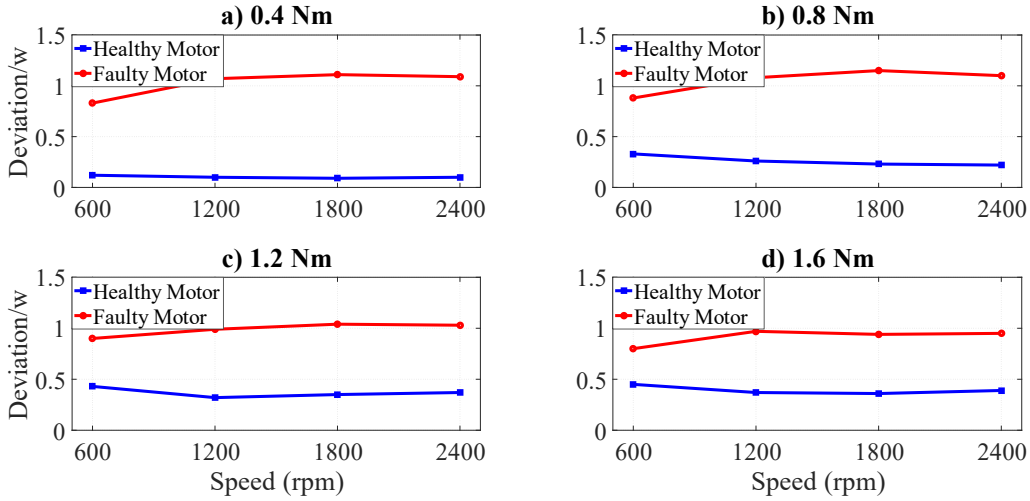

Figure 4.22. Normalized Deviation of Phase Currents from the Average for Healthy and Faulty Motors, a) 0.4 Nm, b) 0.8 Nm, c) 1.2 Nm, d) 1.6 Nm

Experimental results show that static eccentricity fault breaks three phase balance of motor windings and creates differences in RMS values of phase currents. This difference gets higher as motor speed increases. A proper fault detection indicator can be employed by normalizing the differences in phase currents by motor speed. Theoretical expectations are verified by experimental work.

4.5. Remarks

Experiments are performed for 3 types of faults which are partial demagnetization of permanent magnet, stator inter-turn short circuit and rotor static eccentricity faults. Throughout all the experiments, general theoretical approaches are verified. There are explanations and comments on the accuracy of the experiments in this section.

- First, there can be inherent mechanical imperfections like rotor misalignments and rotor mass imbalances in healthy PMSMs. Moreover, stator windings may not have the same inductances and resistances which creates disturbances in electrical signals. Because of all these inherent imperfections, healthy PMSMs give non-zero values when the fault indicators are investigated.
    - As shown in Figure 4.22, the normalized deviations of phase currents reach up to 0.5 A for healthy PMSMs.
- Besides natural imperfections of the test motors, measurement technique also affects the accuracy of fault detection. In the experiments, the major information sources are phase currents I_a, I_b and I_c and rotor electrical position. Each measurement has a certain amount of resolution in the software and carries noise inevitably. Therefore, if the amplitudes of the signals are small, fault may not be detected and categorized accurately. To avoid false alarms, a safe fault detection region should be determined and the signals should be evaluated where the difference between the healthy and faulty motors are clear.
    - In Figure 4.8, Figure 4.15 and Figure 4.21, healthy and faulty lines get closer as the motor speed approaches to 600 rpm. Below 600 rpm, fault detection may trigger false alarms.

- Effects of distinct types of faults on the same signal may also create confusion on fault detection algorithm. In such cases, fault detection algorithm should check multiple signals to categorize the fault accurately.
    - Figure 4.22 shows that motor with static eccentricity fault can be clearly distinguished from healthy motor by looking at deviations of phase currents normalized by motor speed. However, the very same fault indicator cannot distinguish between faulty magnet and static eccentricity faults especially in low torque operation (Figure 4.23). Therefore, by looking at only one variable, faults may not be distinguished from each other.

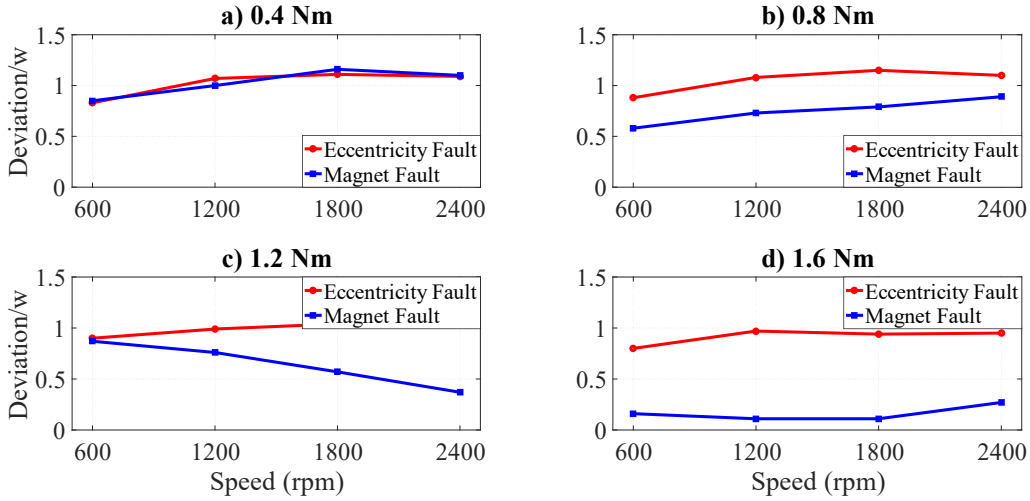

Figure 4.23. Normalized Deviation of Phase Currents from the Average for Demagnetization and Static Eccentricity Faults, a) 0.4 Nm, b) 0.8 Nm, c) 1.2 Nm, d) 1.6 Nm

    - When the fault indicator adopted for detection of demagnetization faults described in section 4.2 is also included in the decision process of static eccentricity faults, algorithm can decide whether the abnormality seen in the motor is the signature of a static eccentricity fault or a demagnetization fault. As shown in Figure 4.24, static

eccentricity fault does not show up in the amplitude spectrum of I_q at $\frac{3f_e}{pp}$.

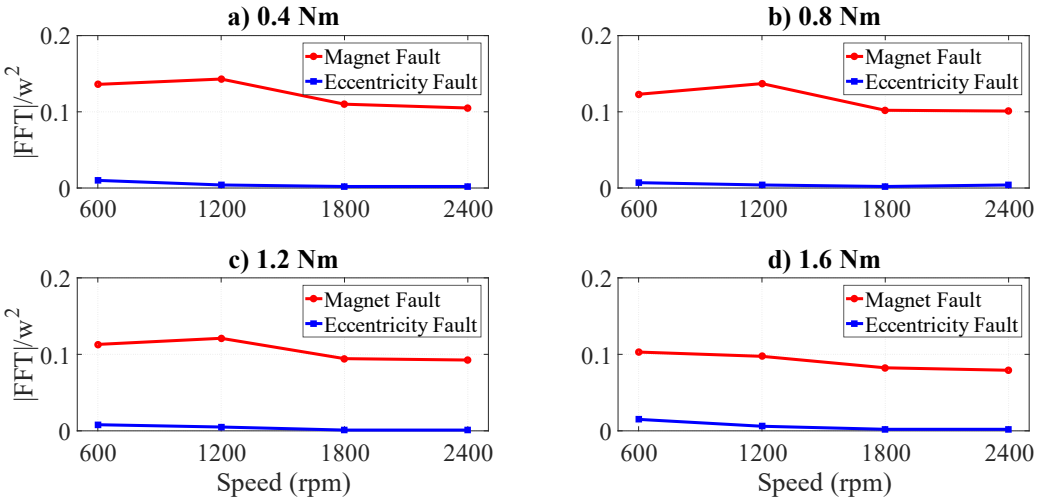

Figure 4.24. FFT Coefficients of I_q corresponding to Fault Frequencies Normalized by w^2 for Demagnetization and Static Eccentricity Faults, a) 0.4 Nm, b) 0.8 Nm, c) 1.2 Nm, d) 1.6 Nm

Electrical and mechanical faults of PMSMs that are in the scope of this thesis are modeled and simulated in Chapter 3. In Chapter 4:

- Mathematical models and simulations are verified by experimental work and the results are given.
- Experimental setup is described. Specifications of test motors, mechanical load, servo controller and power supply are shared. Creation of artificial faults on test motors is explained in detail. Operation conditions are defined.
- For each fault, fault indicators defined in Chapter 3 are investigated for healthy and faulty PMSMs. Results show that the experimental work is consistent with the theory and simulations.
- The effects of operating conditions on the fault indicators are discussed.

- Moreover, the effects of different faults on a certain fault indicator are discussed and the necessity of checking multiple parameters for an accurate fault detection is emphasized.

In Chapter 4, evaluations are made from offline calculations. RMS calculations and harmonic analysis are performed in MATLAB. In the next chapter:

- An online CM and FD algorithm will be built. This algorithm will run on the built-in processor of the servo controller.
- CM and FD will be performed without any computational aid from outside. Only built-in sensors of the motor driver will be used to take measurements.
- Application details of fault detection algorithm such as fault indicator equations, threshold values, real-time monitoring of the results will be presented.
- The test results of graphical user interface of the real-time CM and FD algorithm will be given.

CHAPTER 5

IMPLEMENTATION OF CONDITION MONITORING AND FAULT DETECTION ALGORITHM

Stator inter-turn short circuit faults, non-uniform demagnetization of permanent magnets and static eccentricity faults are analytically modeled and supported by simulations in Chapter 3. Chapter 4 is dedicated to verifying analytical models and simulations by controlled experiments. In Chapter 5, a real time algorithm that samples the required signals and evaluates them while the motor is running is presented.

Fault signatures are searched through electrical signals of the servo controller itself. Built-in current and position sensors are used. Using external sensors is avoided to achieve the objective of the thesis.

The way in which the PMSM is controlled has an important effect on the fault signatures. The current and speed loop bandwidths of the controller affect observation of the fault signals. For example, if the speed loop bandwidth is 50 Hz and the fault frequency is 150 Hz, the speed controller cannot regulate the currents to compensate 150 Hz harmonics in the speed. Therefore, there will be no fault signature in phase current measurements. Hence, the higher the speed loop bandwidth, the clearer the fault signatures in the current measurements [38].

The speed loop bandwidth of the servo controller (HERKUL-04D) is 200 Hz. Motor mechanical frequency at the nominal speed is 40 Hz, which is below the bandwidth. Therefore, test motors are run in constant speed reference mode for fault detection through algorithm implementation.

5.1. Selecting a Feature Extraction Method

Classical feature extraction methods are stated and compared in section 2.3. As the motor signals are going to be evaluated under stationary conditions, STFT is a suitable method because it gives time and frequency resolution at the same time [35]. Hanning function will be used for windowing. Some important properties of the measurement signals are given in Table 5.1.

Table 5.1. *Properties of Measurement Signals*

Property	*Value*
Communication	RS422
Sampling frequency	1 kHz
Maximum observable frequency (by Nyquist Criteria)	500 Hz
Nominal speed	2400 rpm
Nominal electrical frequency	160 Hz

According to Table 5.1, frequencies up to third harmonic (480 Hz) can be observed at nominal speed which is sufficient to implement fault detection algorithm because fractional harmonics are needed to be calculated only.

Frequency resolution requirements and available memory in the processor should be taken into consideration to determine window length of STFT. A 512-point FFT divides double sided frequency spectrum to 512 equal parts which corresponds to 2 Hz of frequency resolution. Resolution of 2 Hz is sufficient to extract information from the measurements while the motor is running at 120 rpm (5% of the nominal speed)

The variables listed in Table 4.2 are stored in 32-bit registers. These signals should be buffered prior to calculations. Buffer length is 512 samples for STFT calculations and 128 samples for RMS calculations. Memory requirement of these buffers are given in Figure 5.1. Moreover, fault decision blocks need 0.3 kB memory for low-pass

filtering. Therefore approximately 8 kB memory is needed for data storage to implement a real-time fault detection algorithm in HERKUL servo controller.

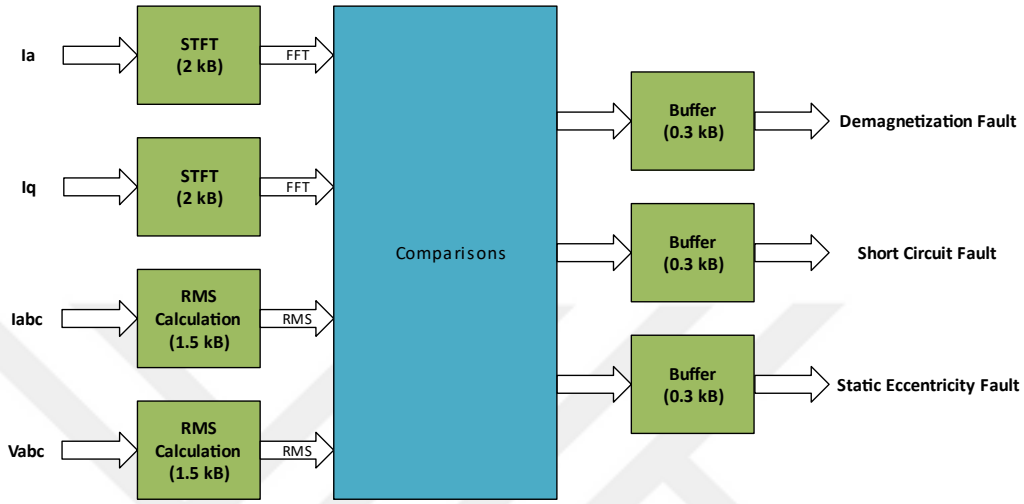

Figure 5.1. Memory Requirement for Data Storage of Fault Detection Algorithm

Based on theoretical and experimental results and abovementioned explanations, feature extraction method is selected to be STFT. Window length and windowing function are determined. Memory requirement for implementation of real-time fault detection on the servo controller is calculated and presented. In the following section, application of the algorithm on a Simulink model is detailed. Then, Simulink model is going to be embedded in the digital signal processor with Embedded Code Generation Tool.

5.2. Implementing the Algorithm on a Simulink Model

Before proceeding to embed the fault detection algorithm on the servo controller, a Simulink model is built to verify the algorithm. Working on a Simulink Model is helpful because debugging and optimizing the algorithm is easier on a computer than a digital signal processor. However, model created should run in similar conditions

with the servo controller software to simulate the real scenario as much as possible. For this purpose,

- A fixed step time of 1 ms is selected for simulations since the feedback signals are collected and evaluated at 1 kHz in the servo controller software.
- All the blocks in the model are selected properly so that they allow C-code generation by Simulink-Coder or Embedded-Coder.
- All the necessary signals are fed into the model from workspaces consisting of arrays of real measurements over time.

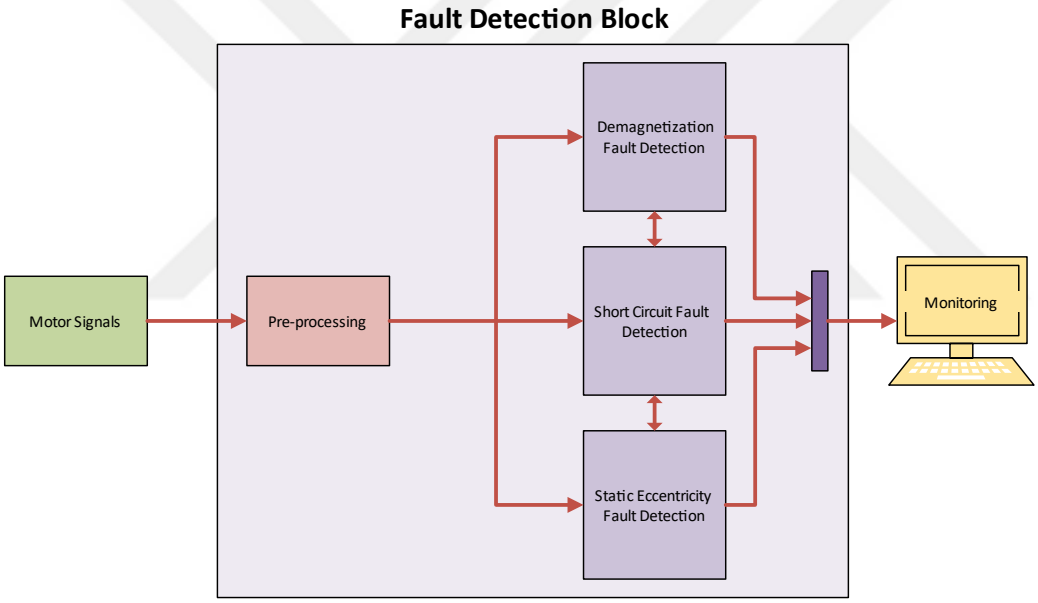

Figure 5.2. A Simplified Block Scheme of the Fault Detection Simulink Model

A simplified block scheme of the Simulink Model is given in Figure 5.2. It takes the measurements sample by sample and searches for different fault signatures on them.

The block named as “Pre-processing” in Figure 5.2 is detailed in Figure 5.3. Electrical frequency of the phase currents is found here. Average speed of the motor is calculated

by filtering the measurement noise out. Moreover, constants like windowing function and maximum speed of the motor are defined in this block.

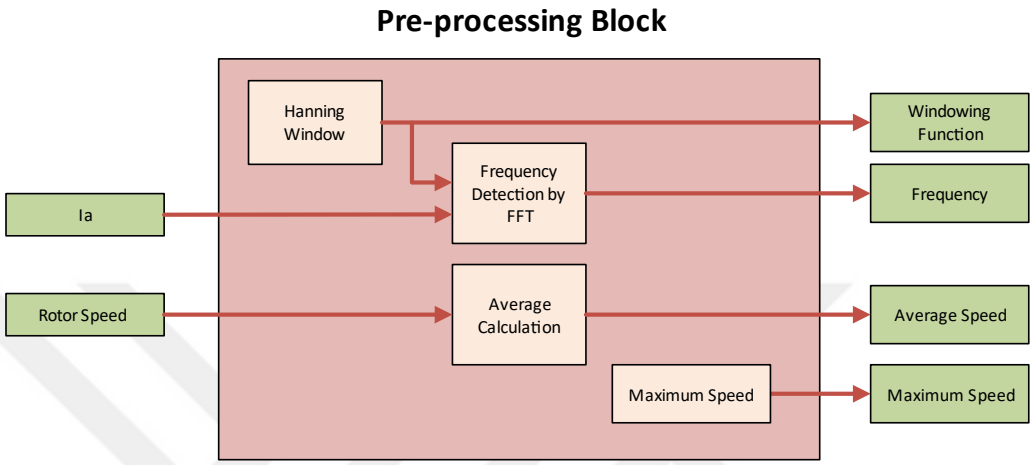

Figure 5.3. Preparing Function Parameter Stage in Fault Detection Block

Other 3 blocks in Figure 5.2. are where demagnetization, short circuit and static eccentricity faults are detected and categorized. Inputs, outputs and other details of these blocks including mathematical definitions of fault indicators are given in the following sections.

5.2.1. Demagnetization Fault Detection Block

Content of the block is shown in Figure 5.4. Inputs of demagnetization detection block are:

- I_q,
- The maximum and the average motor speed,
- pp,
- Windowing function,

- Fundamental frequency and
- The fault threshold.

First, I_q is windowed by Hanning function and 512-point STFT is applied to windowed signal. Then, absolute value of the FFT coefficient corresponding to $\frac{3fe}{pp}$ is found with the help of the fundamental frequency and pp. Absolute value of the coefficient is normalized by the motor speed and fault indicator is created based on the equation 3.17 and experimental results. Explicit equation of the fault indicator is given by the equation 5.1.

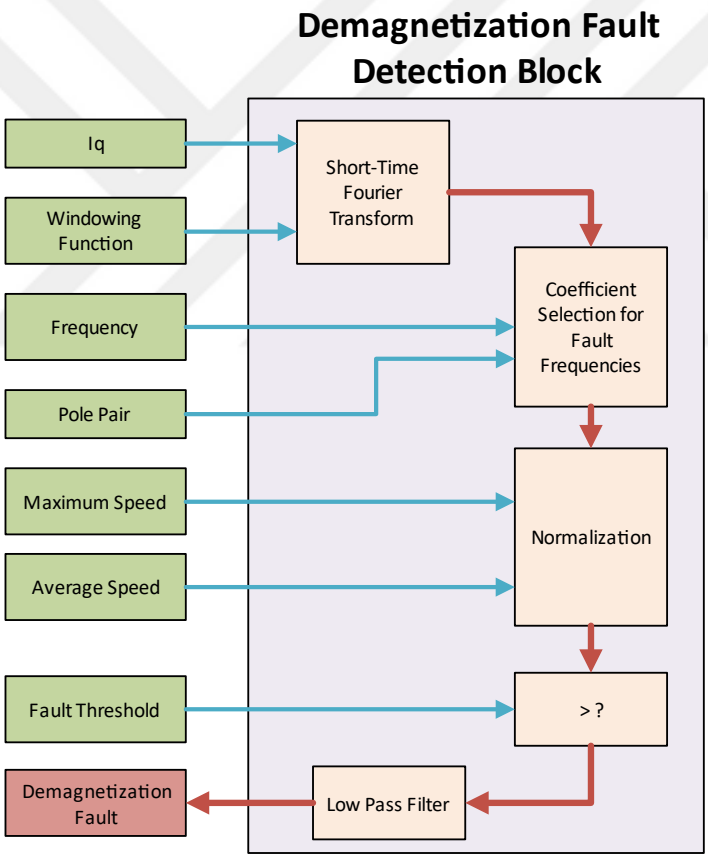

Figure 5.4. Content of Demagnetization Fault Detection Block

Fault threshold is set according to experimental results of healthy and faulty motors. Figure 4.9 shows that the fault indicator:

- Greater than 0.8 for the faulty PMSM and
- Less than 0.2 for the healthy PMSM under all operating conditions.

Therefore, fault threshold for the demagnetization fault is set to 0.06 (Equation 5.2). This value is based on the measured data from healthy and faulty motors. In other words, CM and FD algorithm needs training data to determine a proper fault threshold. Training data can be collected for any PMSM from distributed motor drivers installed on the military systems by using IoT and AI algorithms, which is beyond the scope of this thesis.

$$fi_{magnet} = FFT_{\frac{3f_e}{pp}}(i_q) * (\frac{w_{max}}{w_{rotor}})^2 \quad (5.1)$$

$$ft_{magnet} = 0.06 \quad (5.2)$$

If the fault indicator is greater than the fault threshold, output of the comparator is set. The current measurements are noisy and so is the fault indicator. Therefore, output of the comparator is passed through a low-pass filter. The block output is the sum of last 100 samples. At the end, presence of a demagnetization fault is given as percent probability to the user.

5.2.2. Short Circuit Fault Detection Block

Content of the block is shown in Figure 5.5. Inputs of the short circuit detection block are:

- V_d and V_q,
- Rotor position and
- The fault threshold.

First, three-phase voltages are calculated from V_d, V_q and θ by using standard synchronous frame to stationary frame transformation. Once phase voltages are known, RMS values of them are calculated over last 128 samples. Differences between individual RMS values of the phase voltages and the average of them are found. The deviations are normalized by the average value and fault indicator is created based on the equations 3.8-3.11 and the experimental results. Explicit equation is given by the equation 5.3.

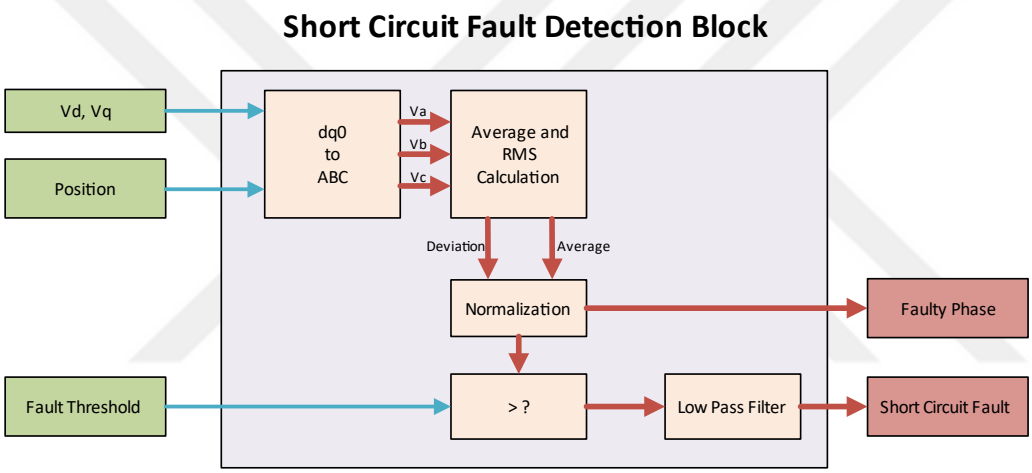

Figure 5.5. Content of Short Circuit Fault Detection Block

Fault threshold is set experimentally as in the case of demagnetization fault. According to Figure 4.17, the fault indicator is:

- Greater than 0.010 for the faulty PMSMs and
- Less than 0.002 for the healthy PMSM under all operating conditions.

Therefore, the fault threshold is set to 0.005 for the short circuit faults (Equation 5.4).

$$fi_{shortcircuit} = \max\left(\frac{|V_b + V_c - 2V_a|}{V_a + V_b + V_c}, \frac{|V_a + V_c - 2V_b|}{V_a + V_b + V_c}, \frac{|V_a + V_b - 2V_c|}{V_a + V_b + V_c}\right) \quad (5.3)$$

$$ft_{shortcircuit} = 0.005 \quad (5.4)$$

If the fault indicator is greater than the fault threshold, output of the comparator is set. A low-pass filter is applied. The block output is sum of the last 100 samples. This action filters out the momentary peaks of the comparator output. Presence of a short circuit fault is given as percentage to the user. The block also detects the faulty phase and inform the user. The faulty phase is the phase for which the voltage deviation is maximum.

5.2.3. Static Eccentricity Fault Detection Block

Content of the block is given in Figure 5.6. Inputs of static eccentricity fault detection block are:

- I_a, I_b and I_c,
- The maximum and the average speed of the motor,
- Presence of demagnetization and short circuit faults and
- The fault threshold.

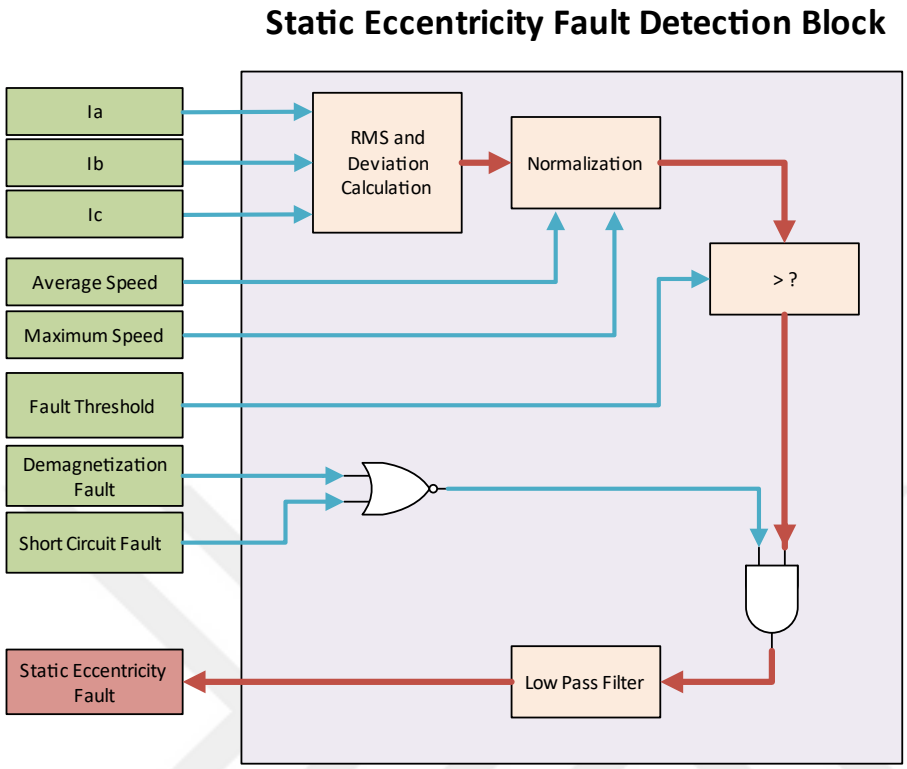

Figure 5.6. Content of Static Eccentricity Fault Detection Block

First, RMS values of the phase currents are calculated over last 128 samples. Deviations of individual phase currents from the average of them are found and normalized by the motor speed. The fault indicator is created based on the equations 3.23-3.25 and the experimental results. It is explicitly defined by the equation 5.5.

Fault threshold is set experimentally as in the case of other fault types. In Figure 4.22, The fault indicator is:

- Greater than 0.85 for the fault PMSM and
- Less than 0.55 for the healthy PMSM under all operating conditions.

Therefore, the fault threshold is set to “0.70” (Equation 5.6).

$$fi_{eccentricity} = \max(|I_b + I_c - 2I_a|, |I_a + I_c - 2I_b|, |I_a + I_b - 2I_c|) * \left(\frac{w_{max}}{w_{rotor}}\right) \quad (5.5)$$

$$ft_{eccentricity} = 0.70 \quad (5.6)$$

Output of the comparator is set the fault indicator is greater than the fault threshold and a demagnetization or short circuit fault is not present. Checking multiple fault indicators prior to decision of static eccentricity fault improves the accuracy of fault detection as explained in Section 4.5. The block output is sum of the last 100 samples, which gives a percent probability of static eccentricity fault to the user.

The Simulink model is built for CM and FD of PMSMs in this section. It is going to be added to the motor control software of HERKUL-04D for a real-time fault detection algorithm operated by motor driver itself. Details are given in the following section.

5.3. Implementing the Algorithm on the Servo Controller

Fault indicators and fault thresholds are defined for demagnetization, short circuit and static eccentricity faults in the previous sections. Details related to the implementation of the algorithm on the servo controller are given in this section.

5.3.1. Memory and Run-time Considerations

Memory requirement for data storage is calculated as 8 kB previously and shown in Figure 5.1. Besides data storage, certain amount of memory is needed to write generated code into digital signal processor. Fault Detection Block (FDB) including STFT blocks, buffers, RMS calculations etc., is added to servo controller software, which increases the generated code size. Increase in the code size cannot be calculated deterministically but it can be measured by compiling the main code with and without FDB and comparing the generated code sizes.

Run-time of the generated code is also important. For proper operation of motor control and condition monitoring at the same time, tasks are sorted and certain amount of time is allowed for each task to be completed. When run-time exceeds the time allowed, sorted tasks cannot be completed sequentially and some data may be lost.

There is a trade-off between the code size and the run-time. Therefore, an optimization is necessary to create a model that runs fast enough to complete all tasks in allowed time and fits in the memory map of digital signal processor.

First, FDB given in Figure 5.2 is directly placed in speed controller loop of the servo controller software. In the speed loop, all the tasks must be completed in 1 ms. Timing diagram of speed control loop is illustrated in Figure 5.7.

- Available time for fault detection is 300 μs.

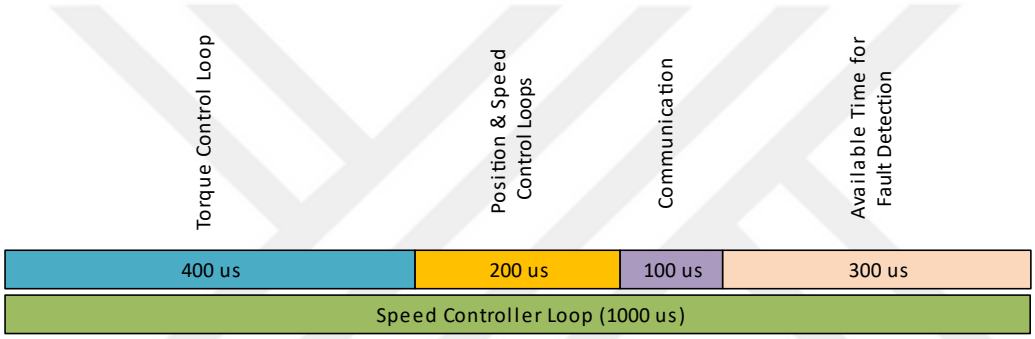

Figure 5.7. Timing Diagram of Speed Control Loop

Code is generated and run on the processor. By using the timer values at the beginning and at the end of the speed controller, elapsed times are measured. When FDB block is enabled, the total time increases to 3.4 ms. It means that FDB is completed in 2.7 ms and cannot be run in the speed controller without making any changes.

Computations that takes much of the time are FFT and RMS calculations. FFT length can be decreased to reduce the run-time; however, decreasing FFT length results in a decrease in the frequency resolution. The same fact is also valid for RMS calculations. Therefore, run-time should be reduced without compromising the performance of the fault detection algorithm. For this purpose, FDB is divided into two separate blocks

which are “Fault Detection Preliminaries” and “Fault Detection”. The data flow between the new blocks are shown in Figure 5.8.

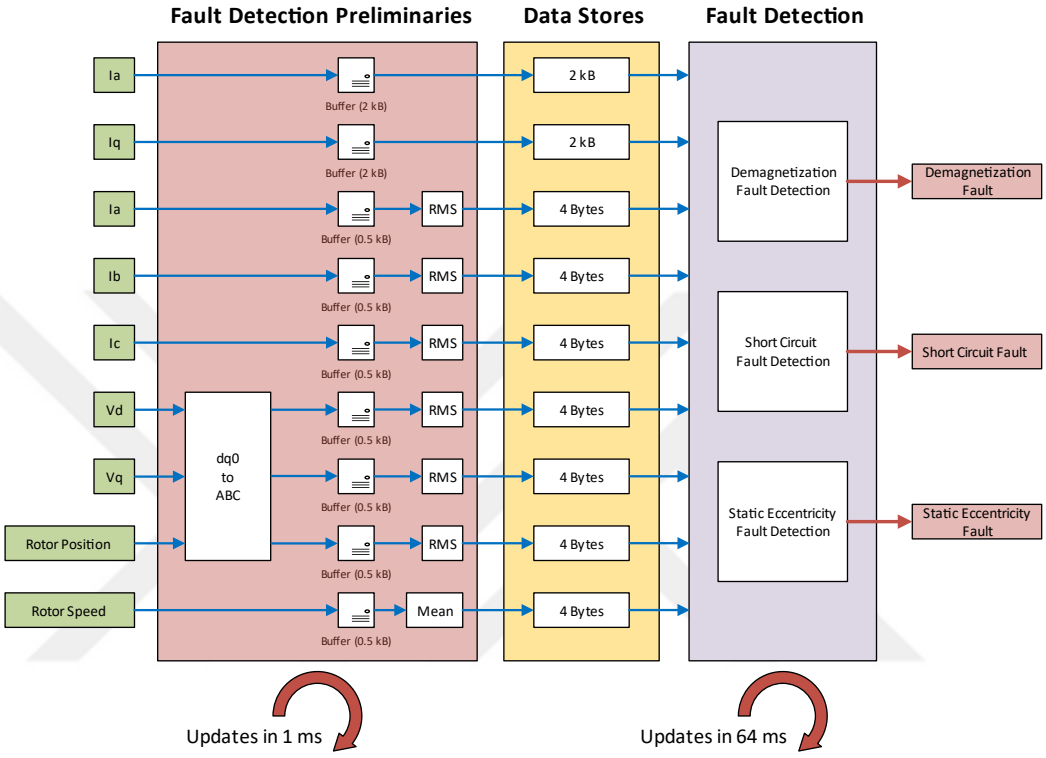

Figure 5.8. Fault Detection Preliminaries and Detection Block Data Flow

“Fault Detection Preliminaries” block runs in the speed controller loop and updates every 1 ms. It includes buffering stages for the signals which are subject to FFT. These signals are sampled and written in the data stores. Sampling and recording frequencies are 1 kHz; therefore, frequency resolution does not change. RMS values of phase currents and voltages are also calculated in this block with 1 kHz sampling frequency. All necessary information is written on the allocated data stores to be used in “Fault Detection” block.

“Fault Detection” block has its own sampling period of 64 ms. FFT computations and decision makings are performed in this block and updated every 64 ms. Since electrical signals are sampled and buffered inside the speed control loop, there is not a loss in the frequency resolution. The trade of is in the time resolution. Fault decisions are made in every 64 ms instead of every 1 ms; however, this does not compromise the overall performance of the CM and FD algorithm because the motor faults occur and evolve with a much slower transition rate.

After separation of Fault Detection Block into two subsystems as described above, the code is generated and run on the processor again. Run-time of the speed controller loop is measured as 900 μs. Details of new timing diagram is given in Figure 5.9. Fault detection preliminaries are completed within 200 μs ensuring the proper operation of the motor control and CM algorithms at the same time.

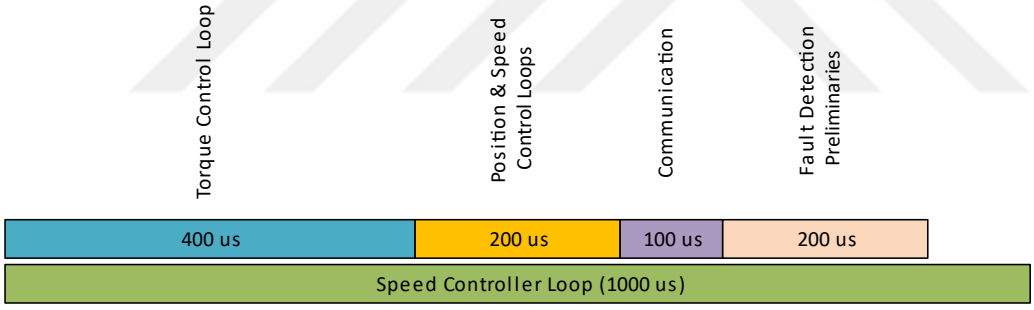

Figure 5.9. Timing Diagram of Speed Control Loop Including Fault Detection Preliminaries

The final version of the software is compiled and code sizes are compared. According to the comparison, fault detection algorithm is built on 36 kB memory, 8 kB of which is for data storage and the rest of which is for the generated C code.

5.3.2. Testing of Motor Driver Software including Condition Monitoring and Fault Detection Algorithm

Being successfully integrated with the servo control software, Real-time CM and FD algorithm is tested on the experimental setup. Tests are performed with the healthy and faulty motors under the conditions given by Table 4.4. Fault signals are sent to the computer and recorded for plotting graphics.

Table 5.2 summarizes the test results of the Real-time CM and FD algorithm. For the given conditions, "✓" sign means accurate decision while "x" means a false alarm. All the tests given in Table 4.4 is performed twice.

Table 5.2. *The Test Results of The CM and FD Algorithm*

Condition	*Healthy PMSM*	*PMSM with Demagnetization Fault*	*PMSM with Stator Short Circuit Fault*	*PMSM with Static Eccentricity Fault*
Number of total tests	32	32	32	32
Accurate decision (✓)	32	31	31	30
Wrong decision (x)	0	1	2	2

According the Table 5.2, total number of cases is 128 and total number of correct decisions is 123. Then, the accuracy of the algorithm is calculated as 96% from this point of view. Some of the test results are shown in the figures as examples. Operating condition for each figure is listed in Table 5.3 for a quick reference.

Table 5.3. *Test Results for Some Cases*

Condition	*Figures*
0.4 Nm, 1200 rpm	Figure 5.10-13
0.8 Nm, 1800 rpm	Figure 5.14-17
1.2 Nm 2400 rpm	Figure 5.18-21

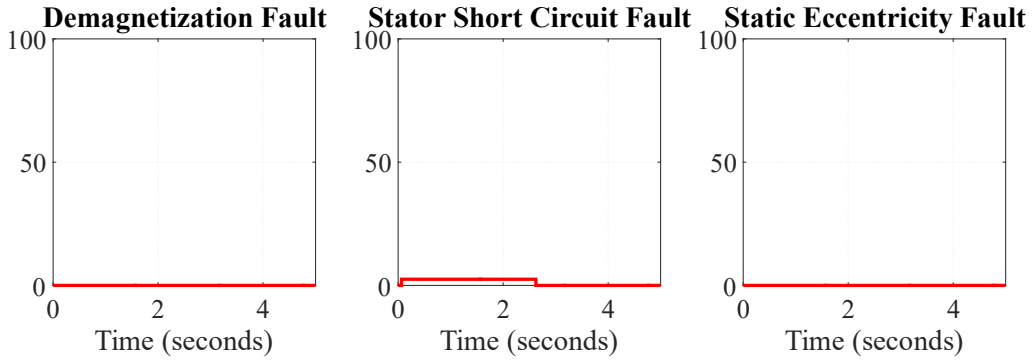

Figure 5.10. CM and FD Results for Healthy PMSM Loaded with 0.4 Nm and Running at 1200 rpm

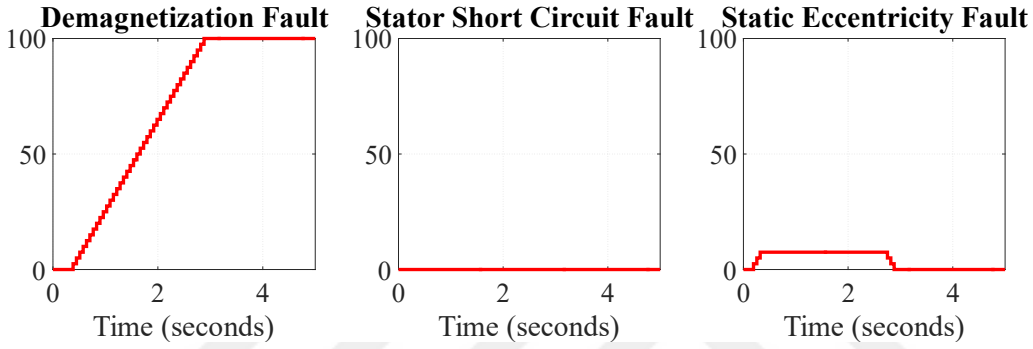

Figure 5.11. CM and FD Results for PMSM with Demagnetization Fault Loaded with 0.4 Nm and Running at 1200 rpm

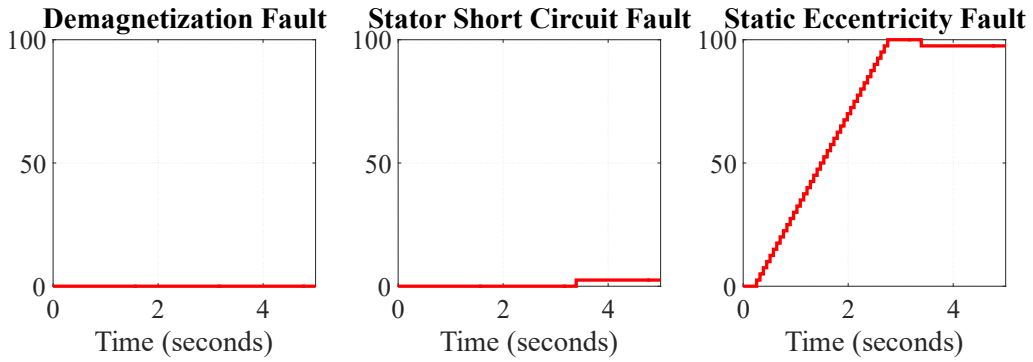

Figure 5.12. CM and FD Results for PMSM with Static Eccentricity Fault Loaded with 0.4 Nm and Running at 1200 rpm

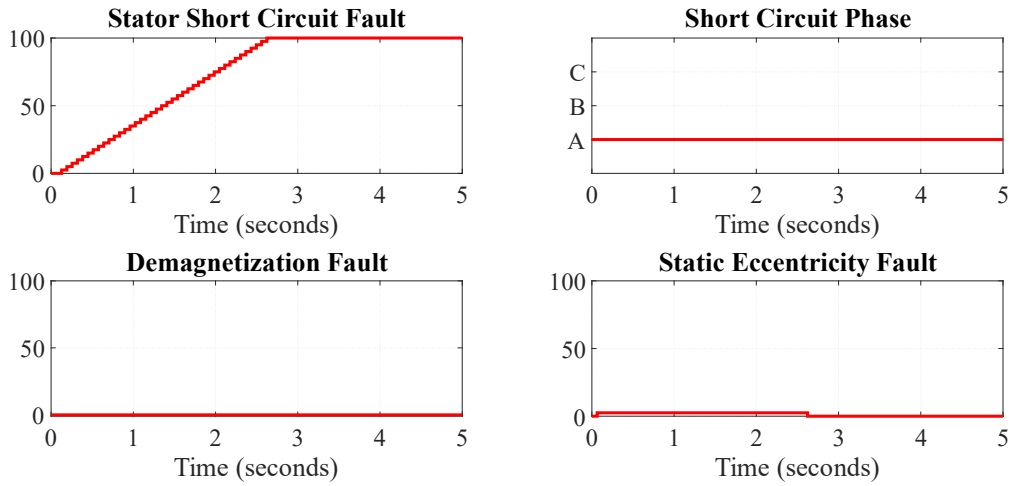

Figure 5.13. CM and FD Results for PMSM with Short Circuit Fault Loaded with 0.4 Nm and Running at 1200 rpm

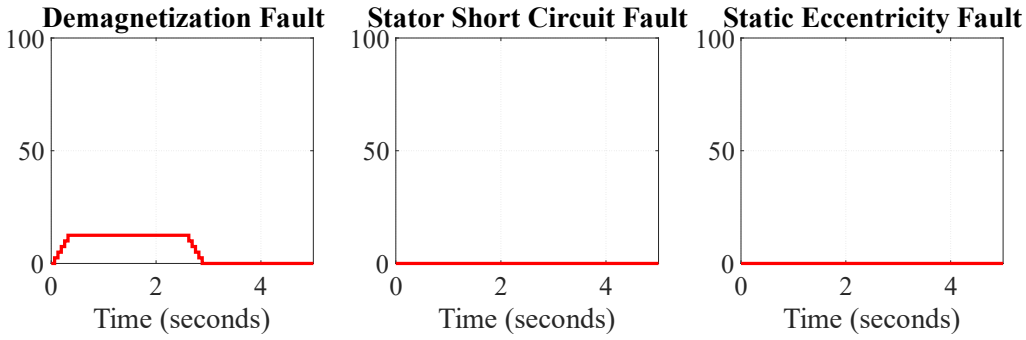

Figure 5.14. CM and FD Results for Healthy PMSM Loaded with 0.8 Nm and Running at 1800 rpm

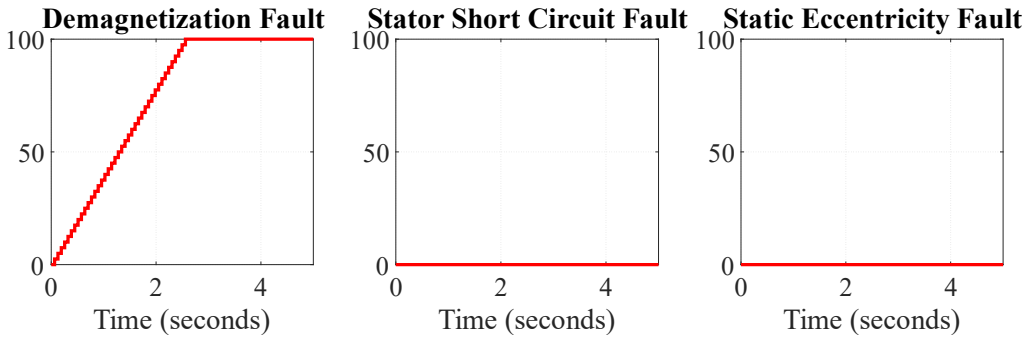

Figure 5.15. CM and FD Results for PMSM with Demagnetization Fault Loaded with 0.8 Nm and Running at 1800 rpm

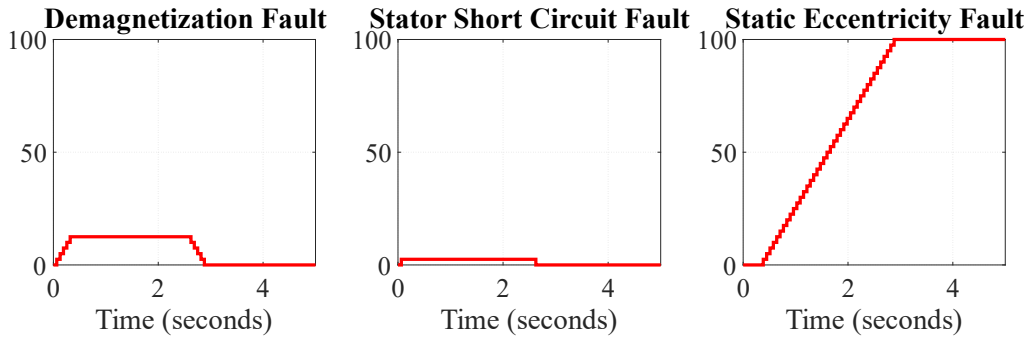

Figure 5.16. CM and FD Results for PMSM with Static Eccentricity Fault Loaded with 0.8 Nm and Running at 1800 rpm

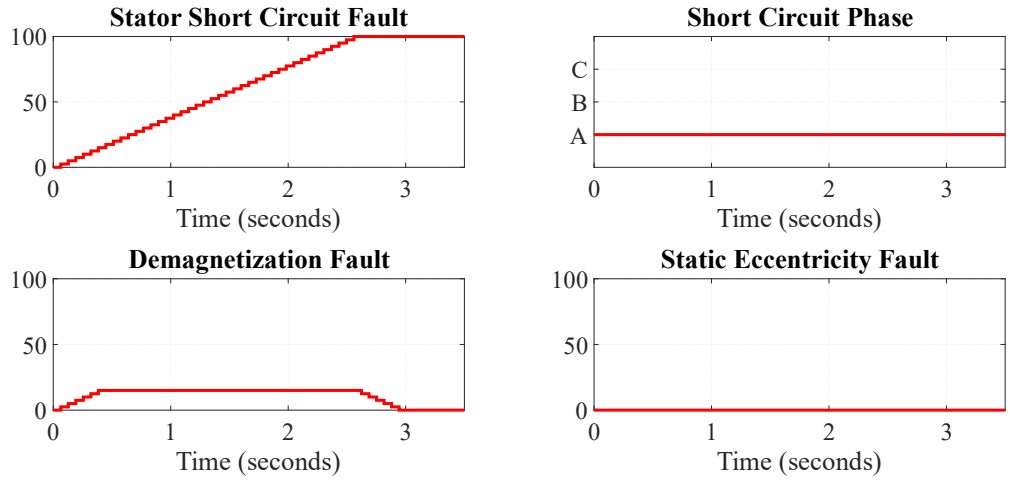

Figure 5.17. CM and FD Results for PMSM with Short Circuit Fault Loaded with 0.8 Nm and Running at 1800 rpm

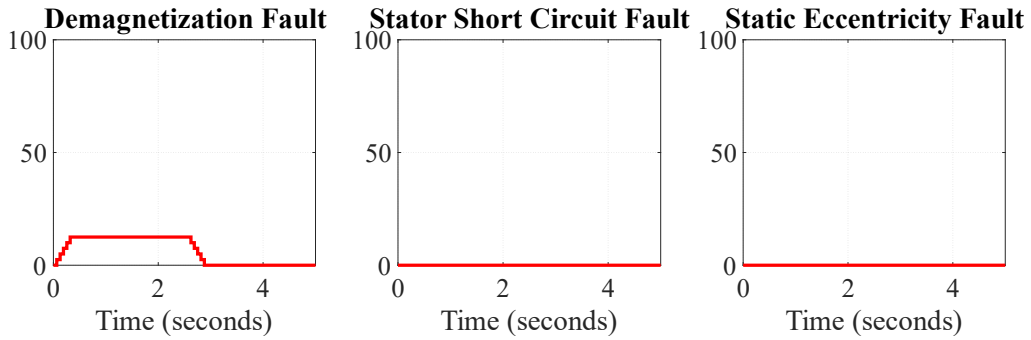

Figure 5.18. CM and FD Results for Healthy PMSM Loaded with 1.2 Nm and Running at 2400 rpm

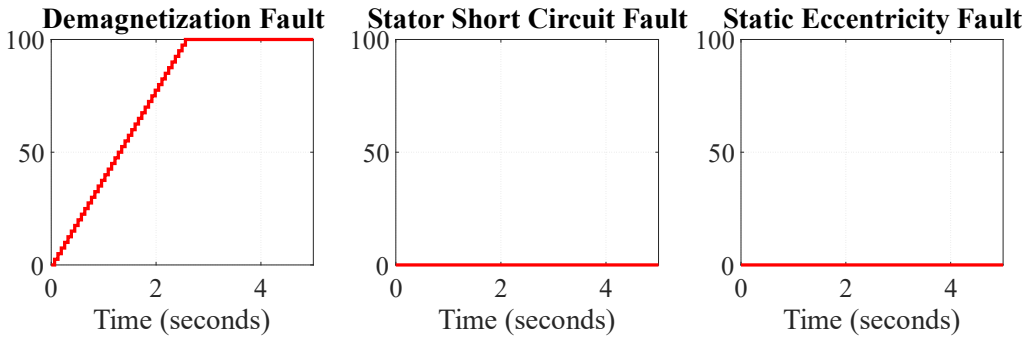

Figure 5.19. CM and FD Results for PMSM with Demagnetization Fault Loaded with 1.2 Nm and Running at 2400 rpm

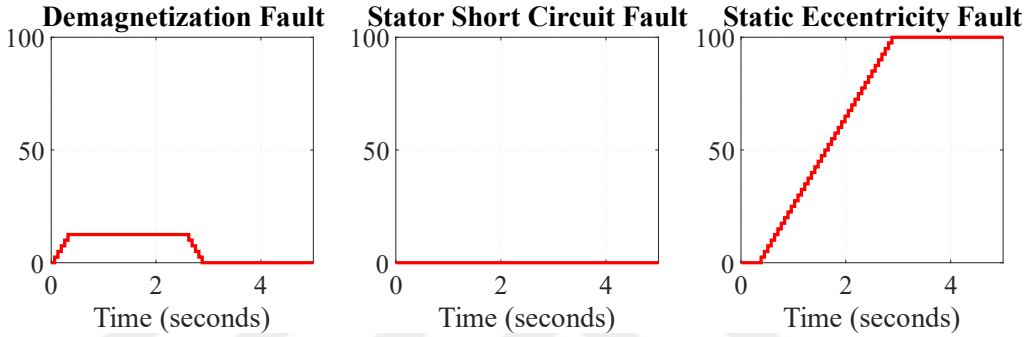

Figure 5.20. CM and FD Results for PMSM with Static Eccentricity Fault Loaded with 1.2 Nm and Running at 2400 rpm

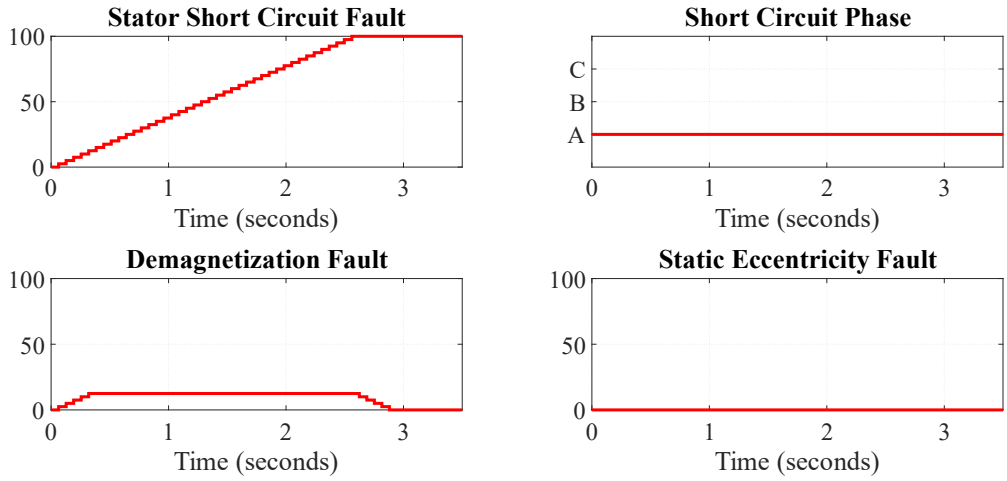

Figure 5.21. CM and FD Results for PMSM with Short Circuit Fault Loaded with 1.2 Nm and Running at 2400 rpm

In Figure 5.10-21, the fault signals at the user end are presented.

- The first three seconds at the beginning of each graph corresponds to the transient state of CM and FD diagnosis algorithm. The buffers are empty and the data is not ready for the computations. Therefore, the fault signals are not true during this interval.
- After three seconds, fault signals become valid. For the healthy PMSMs, all three signals are zero showing that the motor is healthy.
- For the demagnetization and static eccentricity faults, related signals go high showing that the PMSM is faulty. Fault categorization is correct.
- For the short circuit fault, after three seconds, fault signal goes high and another parameter shows the faulty phase, which is A in the experiments. PMSMs with short circuit faults are run for shorter amount of time to prevent overheating of the faulty windings. Therefore, the time axis can only reach to 3.5 seconds in the corresponding figures.

The five wrong decisions given in Table 5.2 were for the cases where motor speed is 600 rpm. At this speed, the fundamental frequencies of the signals become smaller. Therefore, FFT and RMS calculations within the same amount of time yields more noisy results. Then the algorithm may trigger a false alarm. Fortunately, in all other cases, the decisions are correct and the accuracy reaches to 96%.

The advantages of the CM and FD algorithm can be listed as:

- It is implemented in the motor controller software.
- It runs online and gives real-time feedback to the user.
- It does not use any external sensor. Only built-in sensors are used.
- It covers the 75% of the operating conditions (above the 25% of the nominal speed) while maintaining the FD accuracy.

The drawbacks of the algorithm can be listed as:

- It is only valid under stationary conditions. Therefore, it is sensitive to instantaneous speed and load changes.
- It cannot guarantee to make correct decisions under 600 rpm. Therefore, for low speeds, the algorithm needs to be improved.

In Chapter 5, the feature extraction method for fault detection algorithm is selected and algorithm is built by writing equations, assigning fault indicators and determining fault indicator threshold values. First, a Simulink model is built. Then, condition monitoring and fault detection algorithm is combined with servo control software and series of tests are performed on the servo controller. The results show that algorithm works successfully and detects predefined fault conditions accurately. Although it has drawbacks, it forms a practical basis to train the motor controller for learning the PMSM behavior under different conditions and detecting the abnormalities.

CHAPTER 6

CONCLUSIONS AND THE FUTURE WORK

6.1. Summary

An online CM and FD algorithm which runs on a motor drive and uses only internal sensors were built in this study. The objectives of the thesis were given in Chapter 1. Within this scope:

- Stator inter-turn short circuit faults, non-uniform demagnetization faults and rotor static eccentricity faults in PMSMs were examined in this thesis. The failure modes were modeled analytically and verified by simulations. The faults were artificially created on the test motors and experiments were carried on. Theoretical results were verified experimentally.
- Mathematical expressions for the fault indicators were given and the fault threshold values were determined experimentally by comparing the measurements of the faulty and healthy PMSMs.
- The CM and FD algorithm was built on the motor controller software. It has the advantages that;
    - It does not use any external hardware and sensors. It only uses built-in current and position sensors of the servo controller. This was one of the critical objectives and it is achieved.
    - It can detect any of the defined faults and categorize correctly.
    - It does not compromise the proper operation of the motor drive. It works simultaneously and sends the health status of the motor to the user.

    It has the disadvantages that;

- Fault threshold limits are specific to test motor and need to be re-assigned for a new motor.
- Fault diagnosis algorithm is designed for steady-state operation. It may trigger false alarms in speeds lower than 300 rpm and transients. To overcome this disadvantage, the algorithm will only work in higher constant speeds.
- It is applied only on artificially created faults which are very explicit. For more sight faults, threshold limits should be re-assigned so that they do not compromise the normal operation of the motor while it detects slight faults before they evolve and become hazardous to system.

6.2. Contribution to the Field

The CM and FD algorithm will be used in real military systems to get more information on the PMSMs and improve the algorithm. From this point of view:

- This study was a contribution to the reliability and safe operation of the military systems given in Chapter 1.
- The algorithm can be adapted to other systems wherever PMSMs are used.

From the technical point of view, the study is an application on the motor control software.

- Therefore, the proposed method can easily be implemented on any PMSM controller, which has current ad position sensors already.
- The implementation of the algorithm needs handling of the feedback signals, managing data stores and organizing the sequential tasks performed by the digital signal processor. Beginning from the sampling rate of the motor currents and position, the way in which the data is processed determines the resolution and the accuracy of the CM and FD algorithm. Hence, this study is a complete solution from mathematical models of the failure modes to implementation of the algorithm on a real motor drive.

6.3. Future Work

The future work of the thesis is related to the drawbacks and further improvements of the proposed CM and FD algorithm.

- The fault threshold values are specific to test PMSMs and determined experimentally. The automatic determination of the threshold values for an arbitrary motor is left as future work. This can be realized by running a learning algorithm on the drive and track the behavior of healthy motors to understand the pattern by AI algorithms.
- The algorithm can be further improved and integrated to a system identification software to detect slightest faults in PMSMs. CM and FD software is a helpful tool to achieve this goal. In the future, an automatic self-learning CM and FD software is aimed, which is applicable to any system without background information.
- Moreover, the motor drivers at various locations can communicate and share their experience to detect an abnormality in their hardware. The proposed algorithm can be a tool placed in each node of such a network, which extracts information from PMSMs.

REFERENCES

[1] R. Z. Haddad, C. A. Lopez, S. N. Foster, and E. G. Strangas, "A Voltage-Based Approach for Fault Detection and Separation in Permanent Magnet Synchronous Machines," *IEEE Trans. Ind. Appl.*, vol. 53, no. 6, 2017.

[2] F. Cira, M. Arkan, B. Gumus, and T. Goktas, "Analysis of stator inter-turn short-circuit fault signatures for inverter-fed permanent magnet synchronous motors," in *IECON 2016 - 42nd Annual Conference of the IEEE Industrial Electronics Society*, 2016, pp. 1453–1457.

[3] M. Heydarzadeh, M. Zafarani, B. Akin, and M. Nourani, "Automatic fault diagnosis in PMSM using adaptive filtering and wavelet transform," *2017 IEEE Int. Electr. Mach. Drives Conf. IEMDC 2017*, 2017.

[4] A. Usman, B. M. Joshi, and B. S. Rajpurohit, "Review of fault modeling methods for permanent magnet synchronous motors and their comparison," *Proc. 2017 IEEE 11th Int. Symp. Diagnostics Electr. Mach. Power Electron. Drives, SDEMPED 2017*, vol. 2017-Janua, pp. 141–146, 2017.

[5] N. Nakao and K. Akatsu, "Suppressing pulsating torques: Torque ripple control for synchronous motors," *IEEE Ind. Appl. Mag.*, vol. 20, no. 6, pp. 33–44, 2014.

[6] H. Henao *et al.*, "Trends in Fault Diagnosis for Electrical Machines: A Review of Diagnostic Techniques," *IEEE Ind. Electron. Mag.*, vol. 8, no. 2, pp. 31–42, Jun. 2014.

[7] J. Faiz, A. H. Exiri, and H. Nejadi-Koti, "Current-based inter-turn short circuit fault modeling in permanent magnet synchronous machine using magnetic equivalent circuit model," *Proc. - 2016 10th Int. Conf. Compat. Power Electron. Power Eng. CPE-POWERENG 2016*, pp. 265–270, 2016.

[8] S. Hamidizadeh, N. Alatawneh, R. R. Chromik, and D. A. Lowther, "Comparison of Different Demagnetization Models of Permanent Magnet in Machines for Electric Vehicle Application," *IEEE Trans. Magn.*, vol. 52, no. 5, pp. 1–4, 2016.

[9] S. Ruoho and A. Arkkio, "Partial demagnetization of permanent magnets in electrical machines caused by an inclined field," *IEEE Trans. Magn.*, vol. 44, no. 7, pp. 1773–1778, 2008.

[10] P. Zhou, D. Lin, Y. Xiao, N. Lambert, and M. A. Rahman, "Temperature-dependent demagnetization model of permanent magnets for finite element analysis," *IEEE Trans. Magn.*, vol. 48, no. 2, pp. 1031–1034, 2012.

[11] S. Ding, J. Hang, H. Li, and Q. Wang, "Demagnetisation fault detection in

PMSM using zero sequence current components," *Electron. Lett.*, vol. 53, no. 3, pp. 148–150, 2017.

[12] S. Moon, H. Jeong, H. Lee, and S. W. Kim, "Detection and Classification of Demagnetization and Interturn Short Faults of IPMSMs," *IEEE Trans. Ind. Electron.*, vol. 64, no. 12, pp. 9433–9441, 2017.

[13] R. Z. Haddad and E. G. Strangas, "On the Accuracy of Fault Detection and Separation in Permanent Magnet Synchronous Machines Using MCSA/MVSA and LDA," *IEEE Trans. Energy Convers.*, vol. 31, no. 3, pp. 924–934, 2016.

[14] W. Qiao and D. Lu, "A Survey on Wind Turbine Condition Monitoring and Fault Diagnosis - Part I: Components and Subsystems," *IEEE Trans. Ind. Electron.*, vol. 62, no. 10, pp. 6536–6545, 2015.

[15] S. Moon, H. Jeong, H. Lee, and S. W. Kim, "Interturn short fault diagnosis in a PMSM by voltage and current residual analysis with the faulty winding model," *IEEE Trans. Energy Convers.*, vol. 33, no. 1, pp. 190–198, 2018.

[16] M. Ojaghi and V. Bahari, "Rotor Damping Effects in Dynamic Modeling of Three-Phase Synchronous Machines under the Stator Interturn Faults-Winding Function Approach," *IEEE Trans. Ind. Appl.*, vol. 53, no. 3, pp. 3020–3028, 2017.

[17] M. Ben Khader Bouzid, G. Champenois, A. Maalaoui, and S. Tnani, "Efficient Simplified Physical Faulty Model of a Permanent Magnet Synchronous Generator Dedicated to the Stator Fault Diagnosis Part I: Faulty Model Conception," *IEEE Trans. Ind. Appl.*, vol. 53, no. 3, pp. 2752–2761, 2017.

[18] L. Romeral, J. C. Urresty, J.-R. Riba Ruiz, and A. Garcia Espinosa, "Modeling of Surface-Mounted Permanent Magnet Synchronous Motors With Stator Winding Interturn Faults," *IEEE Trans. Ind. Electron.*, vol. 58, no. 5, pp. 1576–1585, May 2011.

[19] B. M. Ebrahimi and J. Faiz, "Feature extraction for short-circuit fault detection in permanent-magnet synchronous motors using stator-current monitoring," *IEEE Trans. Power Electron.*, vol. 25, no. 10, pp. 2673–2682, 2010.

[20] M. Zafarani, E. Bostanci, Y. Qi, T. Goktas, and B. Akin, "Interturn short-circuit faults in permanent magnet synchronous machines: An extended review and comprehensive analysis," *IEEE J. Emerg. Sel. Top. Power Electron.*, vol. 6, no. 4, pp. 2173–2191, 2018.

[21] S. S. Moosavi, Q. Esmaili, A. Djerdir, and Y. A. Amirat, "Inter-Turn Fault Detection in Stator Winding of PMSM Using Wavelet Transform," in *2017 IEEE Vehicle Power and Propulsion Conference (VPPC)*, 2017, pp. 1–5.

[22] H. Jeong, S. Moon, J. Lee, and S. W. Kim, "Inter-turn short fault diagnosis of permanent magnet synchronous machines using negative sequence

components," *Proc. IEEE Int. Conf. Ind. Technol.*, vol. 2016-May, pp. 170–174, 2016.

[23] H. Lee, H. Jeong, and S. W. Kim, "Diagnosis of Interturn Short-Circuit Fault in PMSM by Residual Voltage Analysis," *SPEEDAM 2018 - Proc. Int. Symp. Power Electron. Electr. Drives, Autom. Motion*, pp. 160–164, 2018.

[24] H. Jeong, S. Moon, and S. W. Kim, "An Early Stage Interturn Fault Diagnosis of PMSMs by Using Negative-Sequence Components," *IEEE Trans. Ind. Electron.*, vol. 64, no. 7, pp. 5701–5708, 2017.

[25] L. Otava and L. Buchta, "Permanent magnet synchronous motor stator winding fault detection," *IECON Proc. (Industrial Electron. Conf.*, pp. 1536–1541, 2016.

[26] J. Faiz, A. H. Exiri, and H. Nejadi-Koti, "Simulation of permanent magnet synchronous motors under short circuit fault," *Proc. 18th Mediterr. Electrotech. Conf. Intell. Effic. Technol. Serv. Citizen, MELECON 2016*, no. April, pp. 18–20, 2016.

[27] J. Faiz and H. Nejadi-Koti, "Demagnetization Fault Indexes in Permanent Magnet Synchronous Motors—An Overview," *IEEE Trans. Magn.*, vol. 52, no. 4, 2016.

[28] W. le Roux, R. G. Harley, and T. G. Habetler, "Detecting Rotor Faults in Low Power Permanent Magnet Synchronous Machines," *IEEE Trans. Power Electron.*, vol. 22, no. 1, pp. 322–328, Jan. 2007.

[29] G. Feng, C. Lai, and N. C. Kar, "Particle-Filter-Based Magnet Flux Linkage Estimation for PMSM Magnet Condition Monitoring Using Harmonics in Machine Speed," *IEEE Trans. Ind. Informatics*, vol. 13, no. 3, pp. 1280–1290, 2017.

[30] M. Zhu, W. Hu, and N. C. Kar, "Torque-Ripple-Based Interior Permanent-Magnet Synchronous Machine Rotor Demagnetization Fault Detection and Current Regulation," *IEEE Trans. Ind. Appl.*, vol. 53, no. 3, pp. 2795–2804, 2017.

[31] B. Akin, S. Choi, U. Orguner, and H. A. Toliyat, "A simple real-time fault signature monitoring tool for motor-drive-embedded fault diagnosis systems," *IEEE Trans. Ind. Electron.*, vol. 58, no. 5, pp. 1990–2001, 2011.

[32] T. Goktas, M. Zafarani, and B. Akin, "Discernment of Broken Magnet and Static Eccentricity Faults in Permanent Magnet Synchronous Motors," *IEEE Trans. Energy Convers.*, vol. 31, no. 2, pp. 578–587, 2016.

[33] Z. Liu, J. Huang, and B. Li, "Diagnosing and distinguishing rotor eccentricity from partial demagnetisation of interior PMSM based on fluctuation of high-frequency d-axis inductance and rotor flux," *IET Electr. Power Appl.*, vol. 11,

no. 7, pp. 1265–1275, 2017.

[34] W. G. Zanardelli, E. G. Strangas, and S. Aviyente, “Identification of intermittent electrical and mechanical faults in permanent-magnet AC drives based on time-frequency analysis,” *IEEE Trans. Ind. Appl.*, vol. 43, no. 4, pp. 971–980, 2007.

[35] J. R. Ruiz, J. A. Rosero, A. G. Espinosa, and L. Romeral, “Detection of Demagnetization Faults in Permanent-Magnet Synchronous Motors Under Nonstationary Conditions,” vol. 45, no. 7, pp. 2961–2969, 2009.

[36] J. Faiz and E. Mazaheri-Tehrani, “Demagnetization Modeling and Fault Diagnosing Techniques in Permanent Magnet Machines under Stationary and Nonstationary Conditions: An Overview,” *IEEE Trans. Ind. Appl.*, vol. 53, no. 3, pp. 2772–2785, 2017.

[37] T. Turker, U. Buyukkeles, H. Mese, and F. Bakan, “A discrete-time current controller for permanent magnet synchronous motor drives,” *IECON 2015 - 41st Annu. Conf. IEEE Ind. Electron. Soc.*, pp. 1453–1458, 2015.

[38] W. Roux, R. Harley, and T. Habetler, “Detecting faults in rotors of PM drives,” *IEEE Ind. Appl. Mag.*, vol. 14, no. 2, pp. 23–31, Mar. 2008.